JUSTUS-LIEBIG-
UNIVERSITÄT
GIESSEN

Exploring the Interactions and Functional Implications of Dbp2 and the RSC Complex in *Schizosaccharomyces pombe*

Dissertation

to obtain the academic degree

Doctor rerum naturalium

of the Justus-Liebig-Universität Gießen

submitted by

Jacqueline Böhme

Gießen 2025

This thesis was carried out at the Institute of Biochemistry (Department of Biology and Chemistry) of the Justus-Liebig-Universität in Gießen from December 2019 to March 2024 under the supervision of Dr. Cornelia Kilchert.

Day of submission: 17.11.2025

1. Reviewer: Dr. Cornelia Kilchert

Department of Biology and Chemistry

Institute of Biochemistry

Justus Liebig University Gießen

2. Reviewer: Apl. Prof. Dr. Elena Evguenieva-Hackenberg

Department of Biology and Chemistry

Institute of Microbiology and Molecular Biology

Justus Liebig University Gießen

Contents

Zusammenfassung

Die Transkription ist der fundamentale Prozess, bei dem genetische Information aus der DNA in RNA transkribiert wird und stellt einen essenziellen Schritt in der Genexpression dar. Dieser Prozess wird durch eine Vielzahl von Faktoren reguliert, die sowohl die Aktivität als auch die Zugänglichkeit der DNA beeinflussen. Einer der zentralen Mechanismen, die die Transkription kontrollieren, ist das Chromatin-Remodeling durch spezialisierte Komplexe, die die transkriptionelle Aktivität durch Veränderungen der Chromatinstruktur entweder aktivierend oder repressiv modulieren. Der RSC-Komplex ist an verschiedenen zellulären Prozessen, insbesondere der Transkriptionsregulation, beteiligt. Dbp2, eine RNA-Helikase mit verschiedenen biologischen Funktionen, spielt eine entscheidende Rolle in der mRNA-Prozessierung und anderen RNA-bezogenen Prozessen. Vor dem Hintergrund ihrer potenziellen Wechselwirkungen wurde in dieser Studie die Interaktion zwischen Dbp2 und dem RSC-Komplex in *Schizosaccharomyces pombe* untersucht. Zu diesem Zweck wurde ein modifiziertes Auxin-Depletionssystem erfolgreich etabliert, das eine induzierbare und rasche Depletion der essenziellen Untereinheit Snf21 des RSC-Komplexes ermöglichte. Unsere Ergebnisse deuten auf eine Interaktion zwischen Dbp2 und dem RSC-Komplex im Nukleoplasma hin. Interessanterweise agieren die beiden Komponenten jedoch unabhängig voneinander in Bezug auf ihre Zelllokalisation und Funktion. Besonders hervorzuheben ist, dass der Verlust von Dbp2 zu einer Beeinträchtigung des mRNA-Exports führt, während der Verlust des RSC-Komplexes keine direkten Auswirkungen auf diesen Prozess hat. Zusätzlich wurde der Einfluss des RSC-Komplexes auf die Genexpression eingehend charakterisiert, um seine Rolle in der Transkriptionsregulation aufzuklären und potenzielle Zielgene zu identifizieren. Durch PolII-ChIP-Seq-Experimente identifizierten wir eine überraschend repressive Wirkung des RSC-Komplexes auf eine Vielzahl von Zielgenen, insbesondere solche, die in der Nähe der Telomere lokalisiert sind. Diese Daten liefern neue Erkenntnisse über die Funktion von Chromatin-Remodeling-Komplexen und deren Rolle in der Transkriptionsregulation. Unsere Ergebnisse tragen zur Erweiterung des Verständnisses chromatinbasierter Genomregulation bei und eröffnen neue Perspektiven für die Untersuchung der funktionellen Diversität dieser Komplexe.

Abstract

Transcription is a fundamental process by which genetic information encoded in DNA is transcribed into RNA, representing a crucial step in gene expression. This process is regulated by a variety of factors that influence both the activity and accessibility of DNA. One of the central mechanisms that control transcription is the remodeling of chromatin by dedicated complexes, which modulate transcriptional activity through alterations in chromatin structure, either in an activating or repressive manner. The RSC complex is involved in various cellular processes, particularly transcriptional regulation. Dbp2, an RNA helicase with diverse biological functions, is critical in mRNA processing and other RNA-related processes. In light of their potential interaction, this study investigates the functional connection between Dbp2 and the RSC complex in *Schizosaccharomyces pombe*. To this end, a modified auxin-inducible depletion system was successfully established, enabling inducible and rapid depletion of the RSC complex's essential subunit Snf21. Our results suggest an interaction between Dbp2 and the RSC complex in the nucleoplasm. Interestingly, however, the two components act independently concerning their cellular localization and function. Notably, the loss of Dbp2 results in impaired mRNA export, while the loss of the RSC complex does not directly affect this process. Furthermore, the influence of the RSC complex on gene expression was characterized in greater detail to thoroughly investigate its functional roles in transcriptional regulation and identify potential target genes. Through PolII-ChIP-Seq experiments, we identified a surprising repressive effect of the RSC complex on various target genes, particularly those located near the telomeres. These findings provide new insights into the function of chromatin remodeling complexes and their role in transcriptional regulation. Our results contribute to the broader understanding of chromatin-based genome regulation and open new avenues for exploring the functional diversity of these complexes.

1 Introduction

1.1 Molecular mechanisms of gene expression

Deoxyribonucleic acid (DNA) serves as the repository of genetic information for all living organisms. This information, crucial for cell structure, function, growth, and reproduction, is transcribed into messenger ribonucleic acid (mRNA), a critical step in protein synthesis. This transcription process, the first step in gene expression, is a fundamental process that regulates cellular functions and enables adaptation to environmental conditions. Understanding the molecular mechanisms of transcription has not only deepened our knowledge of cellular signaling pathways and regulatory networks but has also revolutionized biomedical research and the development of new therapeutic approaches.

The transcription of DNA into mRNA, a highly regulated and complex process, involves numerous proteins and regulatory elements to ensure the accurate and timely expression of specific genes. This process can be divided into three stages: initiation, elongation, and termination. In eukaryotes, the key enzyme catalyzing this process is the enzyme RNA polymerase II (Deutschman, 2005), a central player in gene expression.

For transcription initiation, the chromatin must be uncoiled, and the DNA must be exposed (Deutschman, 2005). Together with the transcription factors TFIIB, TFIID, TFIIE, TFIIF, and TFIIH, RNA polymerase II forms the preinitiation complex, in which TFIID is responsible for binding the TATA box in the promoter region (Liu et al., 2013). Depending on the promoter, other sequences, such as cytosine-guanine-rich regions (CpG islands) commonly found near gene promoters, can facilitate RNA polymerase binding in the absence of TATA boxes. These CpG-rich regions often serve as alternative regulatory elements, supporting transcription initiation by providing accessible DNA for binding transcription factors and the transcriptional machinery (Bird, 1986; Cramer, 2019; Deaton and Bird, 2011). RNA polymerase II can only detach from the preinitiation complex and begin RNA synthesis after its C-terminal domain (CTD) is phosphorylated by a specific kinase (Brown, 2002). After 9 to 10 nucleotides have been synthesized (Mohamed et al., 2022), the polymerase leaves the promoter and continues with the elongation phase. This phase, a critical and indispensable part of the transcription process, involves the incorporation of individual nucleotides into the 3' end of the nascent mRNA (Brown, 2002), thereby ensuring the accurate and complete transcription of the genetic information. In the termination phase, RNA polymerase II finally dissociates from the DNA template and the newly synthesized mRNA strand. There are two different models for the termination process. In the allosteric model, termination is triggered by a destabilization or conformational change of the PolII elongation complex after transcription of the poly(A) site. In the torpedo model, endonucleolytic cleavage at the poly(A) enables exonucleases to degrade the remaining RNA in the 5' → 3' direction, resulting in the termination

of PolII (Rosonina et al., 2006). Nowadays, a combined model is widely accepted, particularly the 'sitting duck' model, which suggests that dephosphorylation of the CTD and Spt5 after recognition of the polyadenylation signal slows down RNA polymerase II, making it easier for the torpedo exonuclease to catch up with and terminate transcription (Cortazar et al., 2019; Lopez Martinez and Svejstrup, 2025).

After these processes and already co-transcriptionally, the resulting pre-mRNA is processed. For this purpose, it undergoes 5' capping, splicing, and 3'-end processing. The 5' capping process, crucial for mRNA stability, involves the removal of the γ-phosphate at the 5'-terminal nucleotide by the enzyme triphosphatase. Another enzyme, guanylyltransferase, catalyzes the covalent linkage of guanosine triphosphate (GTP) to the 5'-diphosphate end of the RNA. Finally, the guanine base of the added GTP is methylated by the methyltransferase at position 7 of the guanine ring (Shuman, 2001). This process is particularly important as it prevents degradation by 5' → 3' exonucleases both in the nucleus and in the cytoplasm, thereby ensuring the stability of the mRNA transcript (Hocine et al., 2010). During splicing, non-coding sequences – the introns – are removed, and coding sequences – the exons – are joined together. The splicing is carried out by the spliceosome, a highly dynamic molecular complex formed by the stepwise integration of the small nuclear RNPs U1, U2, U4, U5, and U6, together with many additional proteins (Stark and Lührmann, 2006).

Co-transcriptionally, various yeast proteins, such as Uap56/Sub2, Dbp5, and Mex67, interact with the mature mRNA, which is subsequently transported from the nucleus to the cytoplasm through the nuclear pore complex (Xie and Ren, 2019). The C-terminal domain of Rpb1, the largest subunit of RNA PolII, is crucial for this co-transcriptional recruitment of proteins involved in messenger ribonucleoprotein particle (mRNP) formation because it acts as a recruitment platform during transcription elongation (Meinel and Sträßer, 2015). In the cytoplasm, the mRNA is recognized by ribosomes and translated to synthesize the encoded protein. During translation initiation, the mRNA binds to the small ribosomal subunit, associated with the initiator tRNA and various initiation factors. The large ribosomal subunit then joins, and translation begins. The mRNA sequence is translated into a polypeptide chain as the ribosome interprets the codons of the mRNA and assembles the corresponding amino acids until a stop codon is reached (Korostelev, 2022).

1.2 The RNA helicase Dbp2

Dbp2 (DEAD-box protein 2), the ortholog of the human DDX5/17, is a highly conserved member of the DEAD-box proteins found in all eukaryotes and most prokaryotes (Aubourg et al., 1999; de la Cruz et al., 1999; Rocak and Linder, 2004). These proteins are characterized by the conserved amino acid motif Asp-Glu-Ala-Asp (DEAD) in the Walker B motif (Cordin et al., 2006), which gave the enzyme family its name. In general, helicases are divided into six

superfamilies (Fairman-Williams et al., 2010), whose classification is based on their biochemical function and sequence motifs (Gorbalenya and Koonin, 1993). The superfamilies 3 to 6 form a ring-like structure. In contrast, superfamilies 1 and 2 are monomeric or dimeric, and their catalytic cores exhibit similar folds and robust structural similarity (Singleton et al., 2007). Dbp2 belongs to superfamily 2, one of the two largest helicase superfamilies along with superfamily 1 (Fairman-Williams et al., 2010). Both were initially characterized by the presence of seven conserved helicase motifs (Gorbalenya and Koonin, 1993).

Dbp2 consists of two RecA-like domains typical for DEAD-box proteins (Fig. 1), which include the seven conserved motifs I, Ia, II, III, IV, V, and VI (Gorbalenya and Koonin, 1993). These domains are responsible for ATP binding and hydrolysis, which provides the necessary energy for RNA restructuring activities. Their ability to do so comes from being connected by a flexible linker, forming a distinctive dumbbell-shaped core. During RNA unwinding, the domains adopt a closed conformation made possible by double-stranded RNA and ATP binding. This causes one RNA strand to bend, destabilizing the RNA duplex and releasing the unbent RNA strand (Xing et al., 2019). Motifs III and Va are pivotal for coordinating ATP binding and RNA binding (Ali et al., 2021). The N-terminal and C-terminal regions of Dbp2 contain additional non-conserved motifs and sequences that likely contribute to specific interactions with RNA and other proteins (Fairman-Williams et al., 2010). Additional motifs that are unique to superfamily 2 include the Q-motif, which is necessary for ATP binding and hydrolysis (Tanner et al., 2003), and the TRG-motif, which is attributed a role in the activity of the helicase RecG (Mahdi et al., 2003). The RNA's ribose-phosphate backbone is heavily interacted with, but there are no interactions with the RNA's nucleobases, resulting in a low sequence specificity (Hilbert et al., 2009).

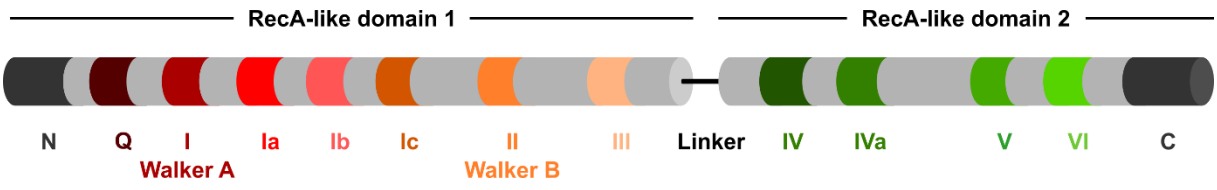

Figure 1 Schematic representation of Dbp2 domains, as an example for superfamily 2 helicases. The helicase core consists of two RecA-like domains (RecA-like domains 1 and 2), which contain the conserved motifs I, Ia, II, III, IV, V, and VI and are connected by a mobile linker.

Dbp2, like many helicases, is involved in various aspects of RNA metabolism. Depending on the organism, these functions can include transcription, chromatin insulation, RNA production, RNA processing, RNA export, and RNA degradation (Xing et al., 2019). Current research

results also show a function in mRNA release after 3'-end formation (Aydin et al., 2024) and possible effects on chromatin (Ma et al., 2016; Cloutier et al., 2012).

Recent structural analyses have shed light on the mechanisms underlying Dbp2 activity. X-ray crystallography of *S. cerevisiae* Dbp2 revealed conformational shifts between open and closed states, with disordered N- and C-terminal tails playing essential roles in RNA binding, ATPase activity, and duplex destabilization (Song et al., 2023). Functionally, genome-wide studies in budding yeast have demonstrated that Dbp2 facilitates transcriptional termination by remodeling RNA-protein complexes, thereby preventing RNA polymerase II accumulation at the 3′-ends of small nucleolar RNAs and mRNAs (Lai et al., 2019). In *S. pombe*, new in vivo data highlight Dbp2 as a key factor in an mRNP-assembly checkpoint at the 3′-end of genes. Dbp2 interacts with polyadenylation factors, localizes to cleavage bodies, and its loss results in the accumulation of polyadenylated transcripts on chromatin and delayed transcription termination (Aydin et al., 2024). Additionally, recent findings suggest that human Dbp2 contributes to genome stability by interacting with DNA repair machinery. It has been shown to associate with protein complexes involved in non-homologous end joining (NHEJ) and nucleotide excision repair (NER) pathways, thereby linking Dbp2 function to DNA replication and damage response (Li et al., 2023). These studies establish Dbp2 not only as an RNA helicase but also as a regulator that coordinates RNA maturation, export, and transcriptome integrity, setting the stage for investigating its interplay with chromatin remodelers, such as the RSC complex.

1.3 Chromatin organization

A key aspect of transcription is its regulation, controlled by various mechanisms to ensure that genes are expressed at the right time, cell type, and amount. Transcription factors, small regulatory RNAs, and chromatin structure can all influence this process. This regulation allows organisms to adapt to changing environmental conditions and control gene expression precisely. Chromosomes represent the highest level of genetic material organization in eukaryotic cells (Fig. 2). Each chromosome consists of chromatids, which become visible during cell division when the DNA is maximally condensed. These chromatids are composed of chromatin, a complex structure of DNA and protein. At a more detailed level, chromatin is organized into nucleosomes, which are DNA wrapped around histone proteins.

Chromatin exists in two primary forms: heterochromatin, which is tightly packed and inaccessible for transcription by RNA polymerase II, and euchromatin, which is less condensed and accessible for transcription (Huisinga et al., 2006). Chromatin-remodeling enzymes and complexes play a crucial role in converting these chromatin states by modifying

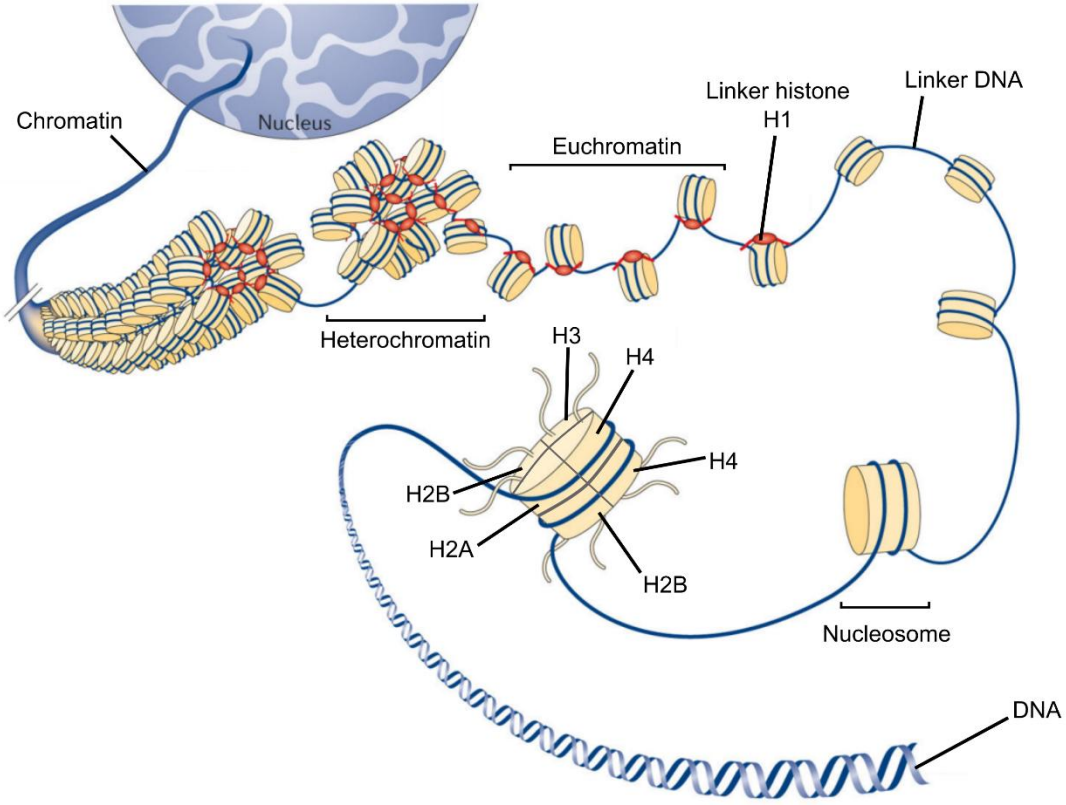

Figure 2 Schematic organization of chromatin in the nucleus. The DNA is wrapped around the histone proteins H2A, H2B, H3, and H4 to form nucleosomes. These nucleosomes are connected by short sequences of linker DNA and are stabilized by the linker histone H1 (adapted from Fyodorov et al., 2018; reproduced with permission from Springer Nature, license number 6285460059432).

the position and composition of nucleosomes. As the basic units of chromatin, the nucleosomes significantly influence its structure. Human nucleosomes comprise about 145 to 147 DNA base pairs, the so-called nucleosome repeat length (NRL), wrapped around a histone octamer in 1.65 turns of a left-handed superhelix, with the octamers containing two copies of the four histone proteins H2A, H2B, H3, and H4 (Dombrowski et al., 2022; Luger et al., 1997). The part of the DNA connecting two nucleosomes is called the linker DNA and is associated with different amounts of the additional histone H1, probably mostly around one per nucleosome (Dombrowski et al., 2022; Bates and Thomas, 1981; Ramachandran et al., 2003). H1 binds to the nucleosome at the site of DNA entry and exit and is thought to be important for nucleosome stabilization; it is not present in actively transcribed genes (Dombrowski et al., 2022; Hergeth and Schneider, 2015). While bulk histones are deposited only during S-phase, so-called histone variants are incorporated into chromatin throughout the cell cycle. These histone paralogs modify nucleosome structure by wrapping varying amounts of DNA or affecting nucleosome stability. They function in DNA repair, chromosome segregation, and transcription regulation (Talbert and Henikoff, 2021). The transcriptionally active euchromatin is typically enriched in acetylated histones H3 and H4 and H3K4 methylation, while

heterochromatin is characterized by hypoacetylation, DNA cytosine methylation, and the association of heterochromatin protein-1, which binds to methylated H3K9 (Tamaru, 2010).

In *S. pombe*, the nucleosome consists of 154 to 156 base pairs in the nucleosome repeat length (Lantermann et al., 2010; Godde and Widom, 1992). Despite having similar genome sizes, *S. pombe* has three large chromosomes (5.7 Mb, 4.6 Mb, and 3.5 Mb), while *S. cerevisiae* has 16 smaller ones. In 2002, the fission yeast genome, with a size of around 13.8 Mb, became the sixth eukaryotic genome to have its sequence published (Wood et al., 2002). Notably, *S. pombe's* smallest chromosome, with 3.5 Mb, is more than twice the size of *S. cerevisiae's* largest 1.5 Mb chromosome (Hoffman et al., 2015). With only around 0.5% of the human genome's size, much of it is constantly open for transcription; yeast chromatin is probably organized differently than human chromatin. While the histones H2A, H2B, H3, and H4 with different histone variants can also be found in *S. pombe*, yeasts lack the linker histone H1 (Takayama and Takahashi, 2007; White et al., 2001; Godde and Widom, 1992). In *S. cerevisiae*, the gene *hho1* encoding a protein similar to linker histones was discovered, and it may function as a linker histone (Landsman, 1996; Patterton et al., 1998). Organisms of yeast, which have an open chromatin structure and lack histone H1, likely organize nucleosomes into higher-order structures distinct from those in higher eukaryotes (White et al., 2001).

1.4 Chromatin remodeling

Eukaryotic cells must balance the compact storage of DNA with its accessibility for essential processes such as transcription, replication, and repair. Therefore, chromatin's flexible structure can be adjusted dynamically, ensuring DNA remains accessible when needed. Chromatin remodeling describes the dynamic restructuring of chromatin in eukaryotic cells. Chromatin regulators are molecules that modify chromatin structure, enabling transcription factors to access their target sites on the DNA strand. Two classes are known to alter chromatin structure in different ways. The first class, histone modifiers, catalyzes modifications at the N-terminal ends of histones, such as acetylation, phosphorylation, and methylation (Jenuwein and Allis, 2001). The second class consists of large multi-subunit complexes that perform ATP-dependent chromatin remodeling by inducing nucleosome sliding, histone exchange, or changes in histone composition. All these changes require energy provided by ATP hydrolysis to disrupt the interaction between DNA and histones (Yamada et al., 2008; Rippe et al., 2007; Clapier and Cairns, 2009; Khorasanizadeh, 2004). For many genes, ATP-dependent chromatin remodeling complexes are required to enable transcription in the presence of nucleosomes (Hirschhorn et al., 1992).

Chromatin remodeling complexes have four leading families, distinguished by their ATPase subunits and specific functional domains: SWI/SNF (switch/sucrose-non-fermenting), ISWI (imitation switch), INO80 (inositol requiring 80) and CHD (chromodomain-helicase-DNA binding), also called Mi-2 (Tyagi et al., 2016; Monahan et al., 2008). SWI/SNF complexes were the first family to be described, with the subunit SWI/SNF giving the name to this family. The second complex in this family is the RSC complex (Tyagi et al., 2016; Monahan et al., 2008). They are known for their ability to shift or remove nucleosomes along the DNA (Mittal and Roberts, 2020). They are known to activate gene transcription by cooperating with histone acetyltransferase complexes but are also involved in gene repression (Roberts and Winston, 1997; Krebs et al., 1999; Trouche et al., 1997). In yeast, the SWI/SNF complex was shown to promote replication initiation and nucleotide excision repair (Flanagan and Peterson, 1999; Hara and Sancar, 2003; Gaillard et al., 2003). In contrast to SWI/SNF complexes, which tend to eject nucleosomes, ISWI remodelers arrange nucleosome arrays, which suggests a possible antagonistic relationship between these remodeling complexes (Parnell et al., 2015). Interestingly, the third family, namely Mi-2, functions in nucleosome remodeling and epigenetic regulation for histone deacetylation and demethylation (Ko et al., 2008; Dege and Hagman, 2014). The INO80 complex mediates several remodeling activities, including the exchange of histone variants, the spacing of nucleosomes at genes, the sliding of nucleosomes, and the eviction of nucleosomes from DNA (Poli et al., 2017).

Yeast, particularly *Schizosaccharomyces pombe*, has proven to be an excellent model organism for studying chromatin organization. In addition to heterochromatin research, *S. pombe* is commonly used to study epigenetic control, chromatin remodeling, and nuclear organization (Allshire and Ekwall, 2015). The simple genetics and the ability to analyze chromatin changes *in vivo* make yeast a valuable system for understanding the underlying mechanisms.

1.5 The RSC complex as a member of the SWI/SNF family

The RSC (remodeling the structure of chromatin) complex is a chromatin remodeler that was first identified in *S. cerevisiae* in 1996 and has since been shown to be highly conserved across higher eukaryotic species (Cairns et al., 1996; Chambers and Downs, 2012). It belongs to the SWI/SNF family of chromatin remodelers and is closely related to the SWI/SNF complex. The two complexes share several common subunits, such as Ssr1, Ssr2, Ssr3, Ssr4, Arp42, and Arp9 in *S. pombe* (Cairns et al., 1996; Monahan et al., 2008). RSC is a very abundant chromatin remodeling complex, with a 10-fold higher abundance than SWI/SNF in yeast cells, and is essential for mitotic growth (Cairns et al. 1996). Unlike SWI/SNF, RSC is critical for cell viability, and its depletion leads to lethality in yeast, highlighting its importance and suggesting different functions for both complexes (Cairns et al., 1996; Asturias et al., 2002). The RSC

complex is crucial in various cellular processes, including transcription regulation, DNA repair, and replication.

1.5.1 Molecular structure of the RSC complex

The structural organization of the RSC complex is central to its function as a chromatin remodeler. The structure of the *S. pombe* RSC complex was determined using electron microscopy as a 4-component complex with a central cavity (Fig. 3A; Asturias et al., 2002). The size and shape of the cavity are well-suited for binding a nucleosome as the nucleosome core fits closely without any interference (Fig. 3B; Asturias et al., 2002). The RSC complex forms a large, multi-protein assembly comprising a varying number of subunits depending on the organism. Some subunits contribute directly to its ATP-dependent chromatin remodeling activity, while others are thought to play supportive structural or regulatory roles (Reyes et al, 2021).

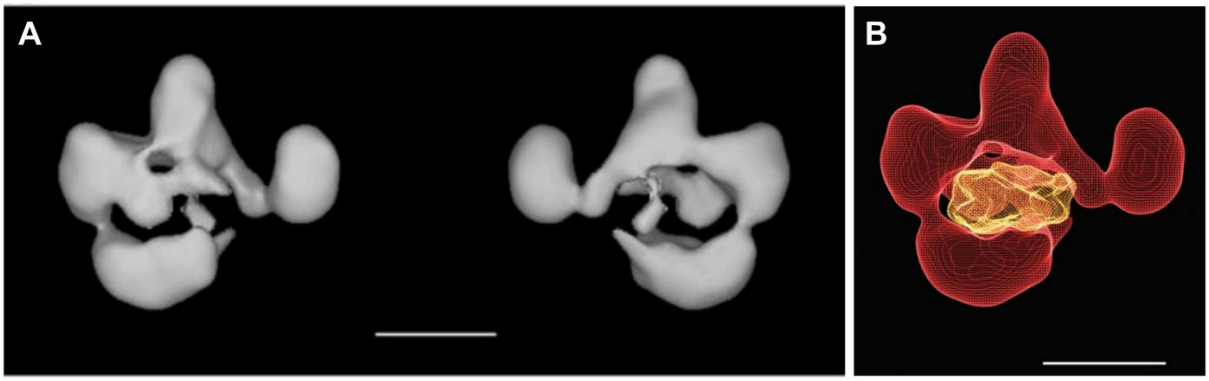

Figure 3 Electron microscopy structure of the *S. pombe* RSC complex. A RSC is composed of four modules that form a central cavity. The structure is displayed from two perspectives. The scale bar corresponds to 100 Å. **B** Possible model for the interaction of the RSC complex and nucleosomes. An X-rax structure of the nucleosome was manually fitted into the RSC cavity. The scale bar corresponds to 100 Å. (Figure modified according to Asturias et al., 2002; copyright (2002) National Academy of Sciences, U.S.A.).

The *S. pombe* RSC complex, distinct from its human counterpart known as the PBAF complex, comprises 13 subunits, six of which are also found in the SWI/SNF complex (Fig. 4). In *S. pombe,* the size of the complex was measured to be approximately 1000 kDa, with subunit sizes below 150 kDa (Cairns et al., 1996). The RSC complex is essential, although not all its subunits are required for cell viability. The RSC-specific subunits Snf21, Sfh1, Rsc9, and Rsc7, as well as four proteins shared with the SWI/SNF complex, namely Ssr1, Ssr2, Ssr3, and Ssr4, are essential. In contrast, unlike in *S. cerevisiae*, the subunits Arp42 and Arp9 are not necessary for viability (Monahan et al., 2008). In *S. pombe*, the catalytically active subunit Snf21 is primarily responsible for the ATP-dependent chromatin remodeling activity of the RSC complex. The essential Snf21 is considered the ortholog of the catalytically active subunit Sth1

in *S. cerevisiae* based on sequence similarity (Yamada et al., 2008; Monahan et al., 2008). In *S. cerevisiae*, RSC appears in at least two forms, depending on the presence of either Rsc1 or Rsc2 bromodomain proteins. In contrast, only the homolog Rsc1 exists in *S. pombe*, suggesting fewer RSC variants. Interestingly, the *S. pombe* RSC complex, like the human PBAF complex, lacks subunits corresponding to the DNA-binding module of the *S. cerevisiae* RSC complex. SMARCB1, the human ortholog of Sfh1 in *S. pombe*, was shown to exhibit DNA-binding activity (Diets et al., 2019), indicating that Sfh1 may also have DNA-binding functions. Overall, the *S. pombe* RSC complex resembles metazoan RSC complexes more closely than the *S. cerevisiae* RSC (Monahan et al., 2008).

S. pombe		***S. cerevisiae***		***H. sapiens***	
RSC	**SWI/SNF**	**RSC**	**SWI/SNF**	**PBAF**	**BAF**
Snf21	Snf22	Sth1	Snf2	BRG1	BRG1 or BRM
	Sol1		Swi1		BAF250
Sfh1	Snf5	Sfh1	Snf5	SNF5	SFN5
Ssr1, Ssr2	Ssr1, Ssr2	Rsc8	Swi3	BAF170, BAF155	BAF170, BAF155
Ssr3	Ssr3	Rsc6	Snf12	BAF60a or BAF60b	BAF60a
Ssr4	Ssr4				
Arp42	Arp42			BAF53	BAF53
Arp9	Arp9	Arp9	Arp9		
		Arp7	Arp7		
				Actin	Actin
	Tfg3		Taf14		
Rsc1		Rsc1 or Rsc2		BAF180	
Rsc4		Rsc4			
Rsc9		Rsc9			
Rsc58		Rsc58			
Rsc7	Snf59	Rsc7	Swp82		
	Snf30				
				BAF57	BAF57
		Rtt102	Rtt102		
			Snf11		
			Snf6		
		Rsc3			
		Rsc30			
		Ldb7			
		Htl1			

ATPase module
Arp module
Arm module
Body module
DNA-interacting module
Scaffold

Figure 4 Composition of ATP-dependent chromatin remodeling complexes SWI/SNF and RSC in *S. pombe*, *S. cerevisiae*, and *H. sapiens* and their association with functional modules. The complexes share several subunits that belong to similar functional modules. Subunits associated with the DNA-interacting module are absent in the RSC complex of *S. pombe*. The subunits of each complex are arranged in columns, with orthologous proteins aligned in rows (Figure based on Monahan et al., 2008; Wagner et al., 2020).

1.5.2 The role of the RSC complex in chromatin remodeling

The RSC complex plays a crucial role in regulating chromatin structure around gene promoters. In addition to nucleosome sliding, RSC is involved in nucleosome eviction and

histone exchange, facilitating access to DNA for essential cellular machinery (Monahan et al., 2008). Given its evolutionary conservation, the fundamental mechanisms of RSC function appear to be preserved across diverse eukaryotic organisms, underscoring its importance in genome dynamics. RSC was found to bind to 700 to 1,400 targets in yeast, predominantly in intergenic regions (Ng et al., 2002; Soutourina et al., 2006). Approximately one-quarter of the RSC-bound sites are located adjacent to genes transcribed by RNA polymerase III, suggesting a role in the transcription of genes that are transcribed by RNA polymerase III (Ng et al., 2002).

The RSC complex is involved in transcriptional activation by making promoter regions accessible and in forming nucleosome-depleted regions (NDRs) that are located upstream of transcription start sites (Fig. 5). Additionally, RSC helps position the nucleosomes adjacent to these NDRs commonly known as the -1 and +1 nucleosomes. The RSC affects both the +1 and −1 nucleosomes. In the case of the -1 nucleosome, DNA exits downstream, whereas the nucleosome itself translocates upstream, in contrast to the +1 nucleosome (Wagner et al., 2020). Biochemical research has revealed that RSC binds to nucleosomes, forming a stable 1:1 complex with an extremely high affinity of around 10^{-8} M (Lorch et al., 1998). When ATP is present, RSC drives the nucleosome into a remodeled state in which the DNA is more exposed and thus more vulnerable to nuclease cleavage (Cairns et al., 1996). In *S. cerevisiae*, RSC facilitates the removal of nucleosomes from promoters by recognizing the orientation of poly(dA:dT) tracts and using it to bias the nucleosome displacement in a specific direction (Krietenstein et al., 2016). In contrast to *S. pombe*, structural analysis of *S. cerevisiae* shows that its RSC consists of five modules: ATPase, ARP, arm, body, and DNA interaction module, with the body module acting as a central scaffold for the others. The DNA-interaction module binds extranucleosomal DNA and plays a role in recognizing promoter elements that influence RSC functionality (Wagner et al., 2020). In *S. cerevisiae*, the body module is composed of the subunits Rsc4, Rsc6, Rsc8, Rsc9, Rsc58, and Htl1, along with the N-terminal region of Sth1, while the C-terminal region of Sth1 extends beyond the helicase-SANT associated (HSA) region, forming the ATPase module. The arm module extends outward from the body and includes subunit Sfh1 and portions of Rsc8, Npl6, and Rsc9. Two structurally distinct copies of Rsc8 closely link the arm and body modules. The N-terminal domains of both Rsc8 copies are located in the arm, while the body contains the SANT domains, one ZZ zinc-finger domain, and the extended C-terminal helices. The ARP module is loosely connected to the body module and includes the HSA region of Sth1, the actin-related proteins Arp7 and Arp9, and Rtt102. (Wagner et al., 2020). This module links ATPase activity to DNA movement and controls remodeling (Clapier et al., 2016; Schubert et al., 2013). The DNA-binding module is important for promoter DNA elements recognition and interacts with extra-nucleosomal DNA (Badis et al., 2008; Kubik et al., 2015; Lorch et al., 2014). In *S. cerevisiae*, RSC features five potential DNA-binding domains, with four exhibiting mobility. Among these are zinc-finger

domains within the Rsc3 and Rsc30 subunits, an RFX domain in Rsc9, and a ZZ zinc-finger domain in one of the two Rsc8 subunits (Wagner et al., 2020). The RSC complex contains six domains that interact with histone tails, including several bromodomains that recognize acetylated lysine residues and mediate interactions with acetylated chromatin. The N-terminal bromodomain in Rsc58 is located on the surface, while five domains are mobile, including a bromodomain in Sth1, two bromodomains in Rsc2, a BAH domain in Rsc2 that binds histone H3, and a tandem bromodomain in Rsc4 that targets acetylated H3 tails, primarily acetylated lysine K14 (Kasten et al., 2004; VanDemark et al., 2007; Wagner et al., 2020). Moreover, yeast RSC may be recruited to its targets by interacting with activators like Hog1 (Mas et al., 2009) and Rpb5, which is a common subunit of all three RNA polymerases (Soutourina et al., 2006). The DNA-interacting module interacts with the DNA exiting the nucleosome (Wagner et al., 2020).

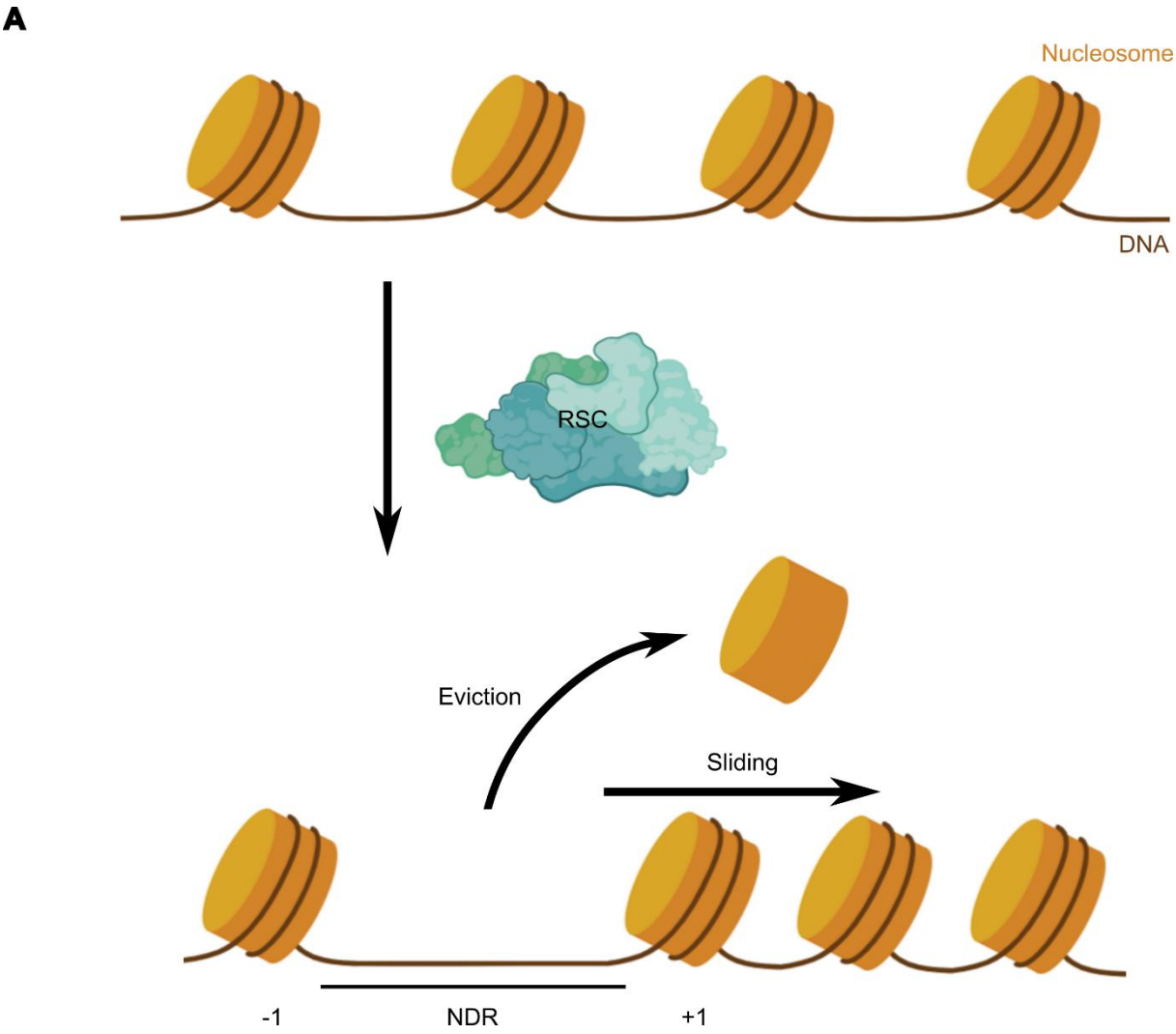

Figure 5 Schematic mechanism of nucleosome remodeling by the RSC complex. The RSC complex facilitates nucleosome repositioning along DNA through nucleosome eviction and sliding. Eviction involves the removal of a nucleosome, creating accessible DNA regions, while sliding shifts nucleosomes along the DNA without removal, altering chromatin accessibility. Created in BioRender. Böhme, J. (2026) https://BioRender.com/y20rpww.

The ATPase and arm modules interact directly with the nucleosome, while the DNA interaction module binds to the DNA as it exits the nucleosome. This arrangement implies that the ATPase motor drives DNA toward the nucleosome's central axis and along the octamer surface in the exit direction during translocation, thereby exposing additional promoter DNA (Wagner et al., 2020). The structure shows that *S. cerevisiae* RSC grips the nucleosome from both sides, sandwiching the histone core. The SnAC domain in Sth1 binds one side, while the arm module binds the other. This interaction, crucial for moving nucleosomes, likely acts as an anchor for histone sliding. The SnAC domain is conserved across species and SWI/SNF complexes, suggesting that this sandwiching interaction is a common feature. The DNA-interacting module helps RSC recognize promoter-enriched DNA elements. For example, the subunits Rsc3 and Rsc30 are involved in identifying a CGCG DNA element located upstream of the transcription start site, likely through their zinc cluster domains (Badis et al., 2008; Kubik et al., 2015; Kubik et al., 2018; Lorch et al., 2014). NDR formation occurs when both neighboring nucleosomes slide away from the center of the NDR. *S. cerevisiae* RSC can only bind to DNA in chromatin where the distance between two nucleosomes is at least 40–50 bp, which may explain its preference for promoter regions, where nucleosomes are less common (Kubik et al., 2015; Wagner et al., 2020).

In summary, the RSC complex is a conserved, ATP-dependent chromatin remodeling complex that plays a pivotal role in regulating gene expression by modulating nucleosome positioning. It predominantly associates with promoters and nucleosome-free regions, enabling dynamic nucleosome placement and structure alterations. This remodeling activity enhances DNA accessibility for transcription factors and the transcriptional machinery. Studies in *Saccharomyces cerevisiae* have demonstrated that loss of RSC function permits increased nucleosome occupancy and impairs access to binding sites for the galactose metabolism regulator Gal4, underscoring RSC's role in maintaining chromatin accessibility at regulatory regions (Floer et al., 2010). In *S. cerevisiae*, RSC regulates transcription mediated by multiple RNA polymerases and contributes to essential cell cycle functions, including kinetochore activity, sister chromatid cohesion, and DNA repair (Monahan et al., 2008). Moreover, RSC-nucleosome complexes are widely distributed across the *S. cerevisiae* genome (Floer et al., 2010). In *S. pombe*, RSC-specific mutants exhibit pleiotropic phenotypes, suggesting that the complex is involved in diverse cellular processes. Genome-wide expression analyses further indicate that RSC in *S. pombe* is critical for regulating gene expression and cellular proliferation (Monahan et al., 2008). Moreover, the *S. pombe* RSC complex controls genes involved in membrane and organelle development (Monahan et al., 2008). Compared to the related SWI/SNF complex, RSC is essential and fulfils a broader role in transcriptional regulation. Notably, cell cycle and chromosome segregation defects observed in some *S. pombe* RSC mutants highlight the utility of this organism as a model system for elucidating the

molecular mechanisms underlying the roles of SWI/SNF-like complexes in cellular transformation and genome stability (Monahan et al., 2008).

1.6 The aim of this thesis

Given the pleiotropic functions of Dbp2, our research group has studied additional possible interaction partners of this helicase. In previous studies, it became clear that proteins of different functional complexes were enriched in a Dbp2 purification (Fig. 6A). Besides already known functions, like mRNA splicing, decay, and maturation (Xing et al., 2019), we were able to show that Dbp2 acts as a crucial DEAD-box ATPase at the 3'-end of genes, serving as a key mRNP remodeling checkpoint that coordinates cleavage factor recycling, ensures proper 3'-end processing, and licenses mRNA export from the nucleus (Aydin et al., 2024). Interestingly, several chromatin remodeling complexes were enriched in Dbp2 purification, suggesting a potential functional link between Dbp2-mediated RNA processing and chromatin remodeling. Within this group and overall, the RSC complex was the most enriched. This strongly suggests a previously unknown interaction between the helicase Dbp2 and the chromatin remodeling complex RSC. Both the helicase and the regulation of chromatin are essential processes in the cell, which is why we investigated a possible interaction of Dbp2 with the essential RSC subunit Snf21 and the non-essential subunit Rsc1 in more detail in the present study. In this respect, the aim was to identify deletion and depletion systems for the different proteins and investigate their interaction concerning localization, occupancy, and mRNA export. Since the RSC complex in *S. pombe* is not yet fully understood, the question of potential target genes of the RSC complex was also addressed.

In addition, the purification of nuclear RNPs via the nuclear cap-binding complex was previously investigated in comparison to an *S. pombe* strain with Dbp2 depletion. Interestingly, in the absence of Dbp2, chromatin remodeling complexes, especially the RSC complex, were highly enriched in the RNP purification (Fig. 6B). In this regard, we hypothesized two scenarios: First, RSC might detach from chromatin after Dbp2 loss and become associated with RNPs. Alternatively, RNPs could be retained at chromatin, thereby increasing the likelihood of interaction with chromatin-bound RSC. Resolving this question was a key objective of this work.

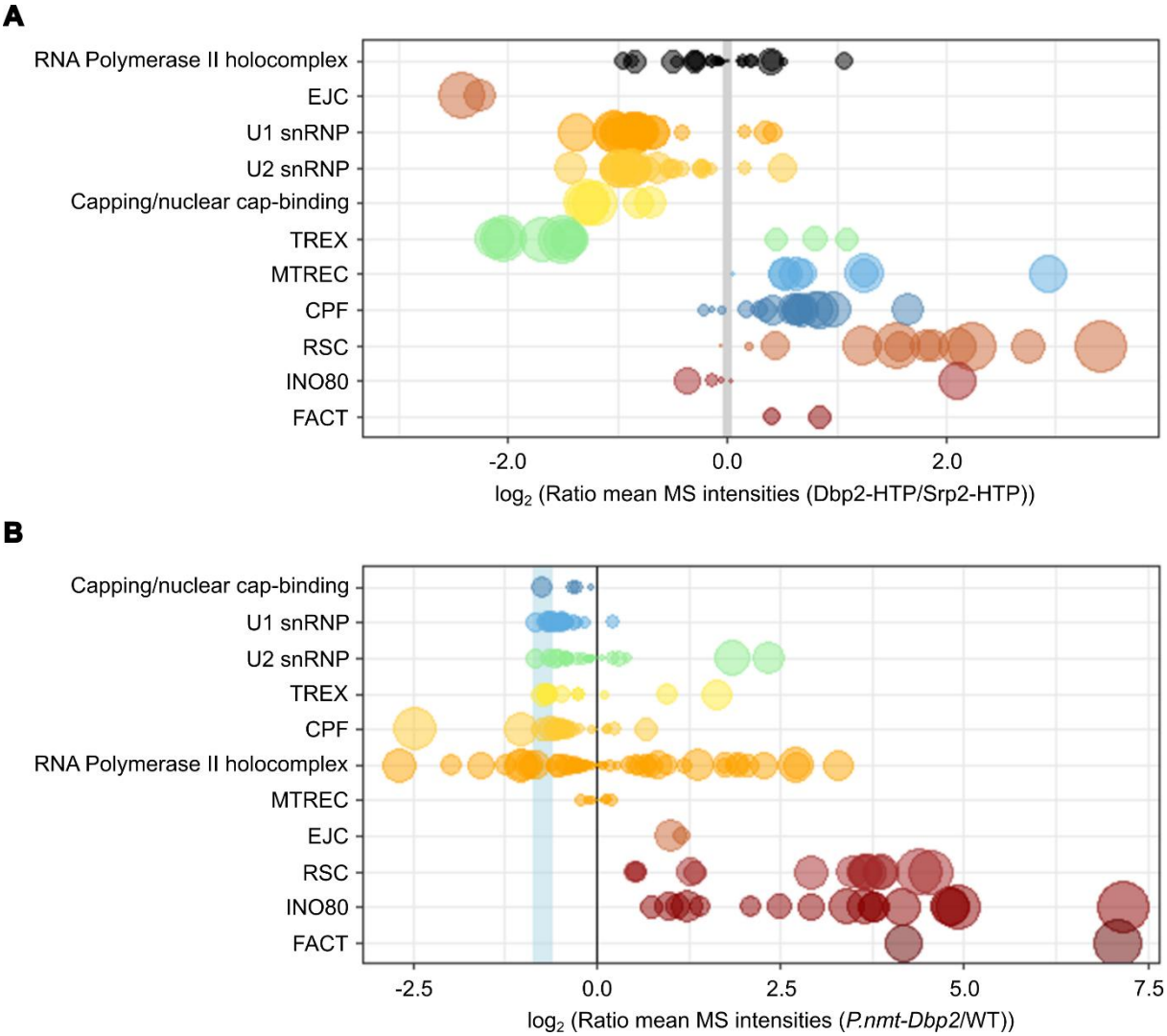

Figure 6 Comparative protein interaction profiling of Dbp2 using liquid chromatography-mass spectrometry. A The RSC complex is enriched in the Dbp2 purification. Relative enrichment of various protein complexes that co-purify with Dbp2 and Srp2, based on mean protein intensities (log2). The size of the circles reflects the p-values (moderated Student's t-test). **B** The RSC complex is enriched in nuclear RNPs in the absence of Dbp2. Relative enrichment of various protein complexes that are enriched after Dbp2 depletion in a Cbc2-HTP purification, based on mean protein intensities (log2). The size of the circles reflects the p-values (moderated Student's t-test). EJC: Exon-Junction Complex. snRNP: small nuclear ribonucleoprotein. TREX: Transcription/Export. MTREC: Mtl1-Red1 nuclear complex. CPF: mRNA cleavage factors complex. RSC: remodeling the structure of chromatin. Ino80: inositol requiring 80. FACT: facilitates chromatin transcription. (Experiment conducted by Ebru Aydin, n = 3).

Overall, a closer examination of the RSC complex is generally of great importance, as nucleosomes are the essential units of chromatin and play a central role in regulating gene expression. Chromatin dysregulation is often associated with diseases such as cancer (Nair and Kumar, 2012; Wolffe, 2001), so it is necessary to understand how nucleosomes are arranged in chromatin. For this purpose, the yeast model organism *Schizosaccharomyces pombe* is used in this study.

S. pombe, or "fission yeast," is a widely adopted model for investigating fundamental molecular and cellular biology processes, including transcription, translation, DNA replication, cell cycle control, and signal transduction pathways. This yeast species, found in diverse natural environments worldwide, is capable of homologous recombination, a feature common to many yeasts. This characteristic allows researchers to construct strains with unique allele combinations by inserting foreign or modified DNA sequences into precise genomic locations, facilitating advanced genetic manipulation (Hoffman et al., 2015). Despite its status as a unicellular eukaryote, *S. pombe* shares several cell cycle characteristics and chromosomal structures that are more similar to those of higher multicellular eukaryotes than other yeast models. This resemblance in chromosomal organization and regulatory mechanisms enhances its relevance in studies related to higher eukaryotic cells (Hoffman et al., 2015; Koyama et al., 2017; Rosas-Murrieta et al., 2015).

2 Materials

2.1 Laboratory equipment

Device	Supplier
Bioruptor UCD-200, Sonication System	Diagenode
Centrifuge 5415 R	Eppendorf
Centrifuge 5425	Eppendorf
ChemoCam Imager ECL HR 16-3200	Intas
DeltaVision Ultra High Resolution Microscope 29206348 / 29254706	Cytiva Life Sciences
Dissection Microscope MSM Manual 100	Singer Instruments
DynaMag-2 Magnet	Thermo Fisher Scientific
Electrophoresis Power Supply – EPS 301	VWR
FastPrep-24 5G	MP Biomedicals
Gel iX20, Transilluminator/gel docu	Intas
KS 4000 ic control	IKA
Megafuge 40R Centrifuge	Thermo Scientific
Milli-Q integral water purification system	Merck
Mini-PROTEAN Tetra Vertical Electrophoresis Cell	Biorad
Mini Trans-Blot Module	Biorad
MyBlock mini dry bath	Benchmark
ND-1000, Spectrophotometer	NanoDrop
Optima XPN-80 UItracentrifuge	Beckmann
Perfection 3200 Photo	Epson
Shaking water bath SW22	Julabo
Stuart rocker & roller mixers	Merck
Sonifier 250	Branson Ultrasonics
T Advance	Biometra
ThermoMixer C	Eppendorf
Type 70 Ti Fixed-Angle Titanium Rotor	Beckmann
QuantStudio 3 Real-Time PCR System	Thermo Fisher Scientific

2.2 Web resources and software

Name	Version
APE	v2.0.30
https://biorender.com	Used until: 2024-02-14

CoralDRAW	24.2.1.446
ImageJ	1.53t
Inkscape	1.1
Integrated Genome Browser	9.1.10
Microsoft Office	2401
RStudio	2023.12.0+369
softWoRx	7.0.0
https://pombase.org	Last updated: 2024-01-02
primer3.ut.ee	4.1.0
QuantStudio Design & Analysis Software	V1.5.2
https://usegalaxy.org	23.2.rc1

Tools from usegalaxy.org	**Version**
bamCoverage	3.3.2.0.0
BAM-to-SAM	2.0.4
Bowtie2	2.5.0+galaxy0
DESeq2	2.11.40.8+galaxy0
FastQC	0.74+galaxy0
Filter FASTQ	1.1.5
FilterSamReads	2.18.2.1
htseq-count	0.9.1+galaxy1
Samtools flagstat	2.0.5
Trimmomatic	0.38.1

2.3 Chemicals and consumables

2.3.1 Chemicals

Chemical	**Supplier catalog number**
Acrylamide 4K solution (30%)	AppliChem (A0951)
Adenine hemisulfate salt	Sigma Aldrich (A9126)
Chloroform	Fisher Scientific (15621290)
Clarity Western ECL Substrate	Biorad (1705060)
Clarity Max Western ECL Substrate	Biorad (1705062)
Dithiothreitol (DTT)	AppliChem (A1101)
Dimethyl sulfoxide (DMSO)	Grüssing (881028231)
Desoxynucleotide Solution Mix (dNTPs)	NEB (N0447)
D-Sorbitol	Carl Roth (6213)

Ethylenediaminetetraacetic acid (EDTA)	Grüssing (103051000)
Formaldehyde solution 37%	Th. Geyer (2137)
GeneRuler 1 kb DNA Ladder	Thermo Fisher Scientific (SM0311)
Geneticin (G418)	Thermo Fisher Scientific (11811)
Glycogen	Sigma Aldrich (G1767)
HDGreen safe DNA dye	Intas (ISII-HDGreen)
HEPES	Fisher Scientific (BP310)
IGEPAL CA-630	Sigma Aldrich (I8896)
L-glutamic acid monosodium salt monate	Sigma Aldrich (49621)
L-histidine	Sigma Aldrich (H8000)
L-leucine	Sigma Aldrich (L8000)
L-Lysin -monohydrochloride	Sigma Aldrich (L5626)
Malt extract	VWR (J873)
Nourseothricin	Jena Bioscience (AB-102)
PageRuler Prestained Protein Ladder	Thermo Fisher Scientific (26616)
Phenylmethane sulfonyl fluoride (PMSF)	Carl Roth (6367)
Poly-L-lysine solution	Sigma Aldrich (P8920)
Potassium hydrogen phthalate	Fisher Scientific (P/5320/60)
Protease inhibitor cocktail (PIC) (10,000x)	Sigma Aldrich (P8215)
Rothi®-Mount FluorCare DAPI	Carl Roth (HP20.1)
ROTI Phenol/Chloroform/Isoamyl alcohol	Carl Roth (A156)
Sodium dodecyl sulfate (SDS)	Carl Roth (CN30)
Sodium phosphate dibasic dihydrate	Sigma Aldrich (71645)
Tetramethylethylendiamin (TEMED)	AppliChem (A1148)
Thiamine hydrochloride	Sigma Aldrich (T4625)
Triton X-100	Sigma Aldrich (93443)
Uracil	Sigma Aldrich (U1128)
Yeast extract	Th. Geyer (9263)
5'a-IAA	TCI (A3390)

2.3.2 Consumables

All non-listed consumables used in this work were purchased from Eppendorf and Sarstedt.

Consumable	**Supplier catalog number**
Blotting Paper	Kobe (4006157)
Bottle-top filters	Fisher Scientific (15953307)

Glass beads	Sigma Aldrich (G8772)
Microscope slides	Fisher Scientific (17224884)
PCR plate half skirt, 96 well, transparent	Sarstedt (72.1981)
Polycarbonate bottle	Beckman (355618)
Precision cover glasses thickness No. 1.5H	Marienfeld (0107032)
Transfer membrane ROTI®PVDF 0.45	Carl Roth (T830.1)
15 ml Bioruptor Plus TPX tubes	Diagenode (C30010009)

2.4 Media, buffers, and stock solutions

The following solutions were prepared with Milli-Q water. Sterilization was accomplished by autoclaving at 121 °C for 20 min, while heat-sensitive solutions were prepared with autoclaved Milli-Q and sterile filtered.

2.4.1 Media and plates

Media	Composition
EMMG medium	3 g/L potassium hydrogen phthalate
	2.76 g/L sodium phosphate dibasic dihydrate
	4.1 g/L L-glutamic acid monosodium salt monohydrate
	225 mg/L adenine hemisulfate
	225 mg/L L-histidine
	225 mg/L L-leucine
	225 mg/L uracil
	225 mg/L lysine hydrochloride
	For plates, 20 g/L agar was added
	After autoclaving, the following components were added:
	1x salt stock
	1x vitamin stock
	1x mineral stock
	3% glucose
ME plates	30 g/L malt extract
	20 g/L agar
	225 mg/L uracil
	225 mg/L leucine
	225 mg/L lysine
	225 mg/L histidine
	pH > 5.5

LB medium	10 g/L tryptone
	5 g/L yeast extract
	5 g/L NaCl
	pH 7.2
	For plates, 20 g/L agar was added
YES medium	5 g/L yeast extract
	30 g/L glucose
	225 mg/L adenine hemisulfate
	225 mg/L L-histidine
	225 mg/L L-leucine
	225 mg/L uracil
	225 mg/L lysine hydrochloride
	For plates 20 g/L agar was added

2.4.2 General buffers

Buffer	Composition
Agarose loading dye (6x)	30% glycerol
	0.03% bromphenol blue
	0.03% xylene cyanol
LiTE buffer	0.1 M LiAc
	1x TE pH 7.5
Lysis buffer	10 mM Tris-HCl pH 8.0
	200 mM KCl
	2.5 mM $MgCl_2$
	0.5 mM EDTA
	0.5% IGEPAL
	Freshly add:
	1 mM DTT
	1x PIC
	1 mM PMSF
Mineral stock (10,000x)	5 g/L boric acid
	10 g/L citric acid
	0.4 g/L molybdic acid
	4 g/L $MnSO_4$
	4 g/L $ZnSO_4 \cdot 7\ H_2O$
	2 g/L $FeCl_3 \cdot 6H_2O$

	1 g/L KI
	0.4 g/L $CuSO_4 \cdot 5H_2O$
PLATE buffer	0.1 M LiAc
	1x TE pH 7.5
	40% PEG
Salt stock (50x)	0.26 M MgCl
	4.99 mM $CaCl_2$
	0.67 M KCl
	14.1 mM Na_2So_4
SDS loading dye (6x)	70% stacking gel buffer
	38% glycerol
	1% SDS
	0.5 M DTT
	1% β-mercaptoethanol
	0.03% bromphenol blue
SDS running buffer	25 mM Tris
	192 mM glycine
	0.1% SDS
Separating gel buffer (4x)	1.5 M Tris-HCl pH 8.8
SSC (20x)	3 M NaCl
	0.3 M $Na_3C_6H_5O_7 \cdot 2H_2O$
	pH 7.0
Stacking gel buffer (4x)	0.5 M Tris/HCl pH 6.8
TBE buffer	100 mM Tris
	100 mM boric acid
	2.5 mM EDTA
	pH 8.3
TBS-T	25 mM Tris
	140 mM NaCl
	0.25 mM KCl
	0.05% Tween-20
	pH 7.4
TE buffer	10 mM Tris-HCl
	1 mM EDTA
	pH 8.0
Transfer buffer (1x)	25 mM Tris
	192 mM glycine

	10% methanol
Vitamin stock (1,000x)	4.2 mM pantothenic acid
	81.2 mM nicotinic acid
	55.5 mM inositol Myo
	40.8 µM biotin

2.4.3 Buffers for Chromatin Immunoprecipitation

Buffer	Composition
Elution buffer	50 mM Tris-HCl pH 7.5
	10 mM EDTA
	1% SDS
Diluent for ChIP	0.143 M NaCl
	1.43 mM EDTA
	71.43 mM HEPES-KOH Ph 7.5
	pH 7.5
FA lysis buffer for ChIP	50 mM HEPES-KOH pH 7.5
	150 mM NaCl
	1 mM EDTA
	1% Triton X-100
	0.1% $C_{24}H_{39}NaO_4$
Glycine buffer for ChIP	3 M glycine
	20 mM Tris
Wash buffer I for ChIP	1x FA lysis buffer
	0.1% SDS
	275 mM NaCl
Wash buffer II for ChIP	1x FA lysis buffer
	0.1% SDS
	500 mM NaCl
Wash buffer III for ChIP	10 mM Tris-HCl pH 8.0
	0.25 M LiCl
	1 mM EDTA
	0.5% IGEPAL
	0.5% $C_{24}H_{39}NaO_4$

2.4.4 Buffers for Co-immunoprecipitation

Buffer	Composition
Stringent wash buffer	10 mM Tris pH 7.5
	500 mM NaCl
	0.5 mM EDTA
	0.05% IGEPAL

2.4.5 Buffers for Fluorescent *in situ* hybridization

Buffer	Composition
Denhardt's solution (50x)	1% polyvinylpyrrolidone (PVP)
	1% bovine serum albumin (BSA)
	1% ficoll-400
Prehybridisation buffer	50% formamide
	10% dextran sulphate
	125 µg/ml *E. coli* tRNA
	500 µg/ml herring sperm DNA
	4x SSC
	1x Denhardt's solution
Wash buffer	1.2 M sorbitol
	100 mM KPO_4 pH 6.4

2.5 Strains

2.5.1 *Schizosaccharomyces pombe* strains

Genotypes were described using nomenclature according to Lera-Ramírez et al. (2023). Strains created in this study were confirmed by colony-PCR and Western blot or microscopy.

Strain	Genotype	Source
Cbc2-GFP	*leu1-32 ura4-D18 ade6-M216 cbc2::cbc2-GFP:kanMX*	Kilchert group
Cbc2-GFP *P.nmt-dbp2*	*leu1-32 ura4D18 ade6-M216 his3-D1? dbp2::ura4:P.nmt1-dbp2 cbc2-GFP:kanR*	Kilchert group
Dbp2-GFP	*leu1-32 ura4D18 ade6-M216 dbp2::dbp2-GFP-HA:KanMX*	This study

Dbp2-HTP	*leu1-32 ura4D18 ade6-M216 dbp2::dbp2-(his6-TEV-proteinA):kanMX*	This study
OsTIR1^{F74A}	*mat1PΔ17 leu1-32 lys1-131 ade6-M216 ura4+::P.adh1-OsTIR1-F47A*	Li-Lin Du (via NBRP)
OsTIR1^{F74A}-Snf21-3xsAID	*mat1PΔ17 leu1-32 lys1-131 ade6-M216 ura4+::P.adh1-OsTIR1-F47A snf21::snf21-3xsAID:kanMX*	This study
OsTIR1^{F74A}-Snf21-3xsAID Dbp2-GFP	*mat1PΔ17 leu1-32 lys1-131 ade6-M216 ura4+::P.adh1-OsTIR1-F47A snf21::snf21-3xsAID:kanMX dbp2::dbp2-GFP-HA:KanMX*	This study
OsTIR1^{F74A}-Snf21-3xsAID Dbp2-HTP	*mat1PΔ17 leu1-32 lys1-131 ade6-M216 ura4+::P.adh1-OsTIR1-F47A snf21::snf21-3xsAID:kanMX dbp2::dbp2-(his6-TEV-proteinA):kanMX*	This study
OsTIR1^{F74A}-Snf21-3xsAID *P.nmt-dbp2*	*mat1PΔ17 leu1-32 lys1-131 ade6-M216 ura4+::P.adh1-OsTIR1-F47A snf21::snf21-3xsAID:kanMX dbp2::ura4:P.nmt1-dbp2*	This study
OsTIR1^{F74A}-Snf21-3xsAID *rscΔ*	*mat1PΔ17 leu1-32 lys1-131 ade6-M216 ura4+::P.adh1-OsTIR1-F47A snf21::snf21-3xsAID:kanMX rsc1Δ::NAT*	This study
pEasy-Snf21-3xsAID	*leu1-32 ura4D81 ade6-M216 snf21-3xsAID::kanMX pEASY-ura4*	This study
pEasy-Snf21-3xsAID Dbp2-HTP	*leu1-32 ura4D18 ade6-M216 dbp2::dbp2-(his6-TEV-proteinA) snf21-3xsAID::kanMX pEASY-ura4*	This study
P.nmt-dbp2	*leu1-32 ura4D18 ade6-M216 his3-D1 dbp2::ura4:P.nmt1-dbp2*	Kilchert group
P.nmt-dbp2 rscΔ	*leu1-32 ura4D18 ade6-M216 dbp2::ura4:P.nmt1-dbp2 rsc1Δ::NAT*	This study
rscΔ	*leu1-32 ura4D18 ade6-M216 rsc1Δ::NAT*	Kilchert group
rsc1Δ Dbp2-GFP	*leu1-32 ura4D18 ade6-M216 dbp2::dbp2-GFP-HA:KanMX rsc1Δ:NAT*	This study
rsc1Δ Dbp2-HTP	*leu1-32 ura4D18 ade6-M216 dbp2::dbp2-(his6-TEV-proteinA):kanMX rsc1Δ:NAT*	This study
Rsc1-GFP	*leu1-32 ura4D18 ade6-M216 rsc1::rsc1-GFP:kanMX*	This study

Rsc1-GFP *P.nmt-dbp2*	*leu1-32 ura4D18 ade6-M216 rsc1::rsc1-GFP::kanMX dbp2::ura4:P.nmt1-dbp2*	This study
Rsc1-HTP	*leu1-32 ura4D18 ade6-M216 rsc1::rsc1-(his6-TEV-proteinA):kanMX*	This study
Rsc1-HTP *P.nmt-dbp2*	*leu1-32 ura4D18 ade6-M216 rsc1::rsc1-(his6-TEV-proteinA):kanMX dbp2::ura4:P.nmt1-dbp2*	This study
Rsc1-tdTomato	*leu1-32 ura4D18 ade6-M216 rsc1::rsc1-tdTomato:kanMX*	This study
Rsc1-tdTomato Dbp2-GFP	*leu1-32 ura4D18 ade6-M216 dbp2::dbp2-GFP-HA:KanMX rsc1::rsc1-tdTomato:kanMX*	This study
Snf21-GFP	*leu1-32 ura4D18 ade6-M216 snf21::snf21-GFP:kanMX*	This study
Snf21-GFP *P.nmt-dbp2*	*leu1-32 ura4D18 ade6-M216 snf21::snf21-GFP::kanMX dbp2::ura4:P.nmt1-dbp2*	This study
Snf21-HTP	*leu1-32 ura4D18 ade6-M216 snf21::snf21-(his6-TEV-protein A):kanMX*	This study
Snf21-HTP *P.nmt-dbp2*	*leu1-32 ura4D18 ade6-M216 snf21::snf21-(his6-TEV-protein A):kanMX dbp2::ura4:P.nmt1-dbp2*	This study
Snf21-tdTomato	*leu1-32 ura4D18 ade6-M216 snf21::snf21-tdTomato:kanMX*	This study
Snf21-tdTomato Dbp2-GFP	*leu1-32 ura4D18 ade6-M216 dbp2::dbp2-GFP-HA:KanMX snf21::snf21-tdTomato:kanMX*	This study
Snf21-tdTomato Rsc1-GFP	*leu1-32 ura4D18 ade6-M216 rsc1::rsc1-GFP::kanMX snf21::snf21-tdTomato:kanMX*	This study
Snf21-3xsAID	*leu1-32 ura4D18 ade6-M216 snf21::snf21-3xsAID:kanMX*	This study
Wild-type	*leu1-32 ura4D18 ade6-M216*	Kilchert group

2.5.2 *Saccharomyces cerevisiae* strains

Strain	Genotype	Source
Spike-in	*met15Δ0*	F. Winston

2.5.3 *Escherichia coli* strains

Strain	Description	Cell type	Source
Padh1-OsTIR1^{F74A}	for optimized auxin-degron-depletion of sAID-tagged proteins	DH5a	Li-Lin Du (via NBRP)
pBS1479 His-TEV-Prot. A KanMX	for C-terminal tagging with His6-TEV-Prot. A in *S. pombe* using kanMX marker	TOP10	Sina Wittmann
pEASY-ura4	pEASY parent vector for Padh1-OsTIR1^{F74A}	DH5a	Li-Lin Du (via NBRP)
pFA6a-kanMX-3xsAID	for C-terminal tagging with 3xsAID as auxin-inducible degron using kanMX marker	DH5a	Li-Lin Du (via NBRP)
TOPO-L3/L6-rrp6-GFP	for C-terminal tagging with GFP using the kanMX marker	DH5a	Kilchert group
TOPO-red1-tdTomato-KanMX	for C-terminal tagging with tdTomato using the kanMX marker	DH5a	Kilchert group

2.6 Oligonucleotides

2.6.1 Oligonucleotides used for genomic integration and colony polymerase chain reaction

Oligo	Sequence (5' → 3')
adh1-promF	CATTGGTC TTCCGCTCCG
dbp2-ex2R	ACCAGAACCCGTAGCTGAAA
dbp2-ex3F	AAGCCAAGCAGGACATTGAT
dbp2-L4-pFA	ttaattaacccggggatccgCCAACGTGAACGCGCAAGGGGGGCAG AATTACT
dbp2-L5-pFA	cgagctcgaattcatcgatGTTCAGTAACCGCTTTCGTAGA
dbp2-promF	CCATAGAATTGATTGTTTTTAGCTCTTTAG
dbp2-RT-R	TTTCAAGCCTCTTCGCTCTT
drsc1-rev	CCGGTCTCAGTATTCCAAAC
HTP-L4	caccatcaccatcaccatgatt
HTP-L5	cctgtttagcttgcctcgtc
KanMX-C2	CGGATCCCCGGGTTAATTAA
KanMX-L5	ATCGATGAATTCGAGCTCG
KanMX-L5-long	ATCGATgaattcgagctcgTTTAAACTGG
rsc1-L3	TCTGGGTCCTTGCAATCCTT

rsc1-L4-GFP	ttaattaacccggggatccgTGGTGGGATCAAAGCATCTGAC
rsc1-L4-HTP	aatcatggtgatggtgatggtgTGGTGGGATCAAAGCATCTGAC
rsc1-L5-GFP	cgagctcgaattcatcgatTGTGATAGATTTGAAGATTTTTAGAACCT
rsc1-L5-HTP	gacgaggcaagctaaacaggTGTGATAGATTTGAAGATTTTTAGAA CCT
rsc1-L6	TAACTTTGCGCCGGATTCAG
snf21-L3	ACCTGAGAAAACCACCGACT
snf21-L4-GFP/sAID	ttaattaacccggggatccgAGCCTCATTTTCAATTCTGTCTTCCAAT TGCGATGT
snf21-L4-HTP	aatcatggtgatggtgatggtgAGCCTCATTTTCAATTCTGTCTTCCAA TTGCGATGT
snf21-L5-GFP/sAID	cgagctcgaattcatcgatTGTGAGATAGAGGATGGGGTG
snf21-L5-HTP	gacgaggcaagctaaacaggTGTGAGATAGAGGATGGGGTG
snf21-L6	TGAAAAGACCGCAAGCTGTC
tdTomato-L4-rc	cggatccccgggttaattAATGTGAGCAAGGGCGAGGAG
TEF-terminator-fw	CAATCGTATGTGAATGCTGGTC
ura4-termRev	GTGATATTGACGAAACTTTTTG

2.6.2 Oligonucleotides used for quantitative polymerase chain reaction on *rps2202*

Oligo	**Sequence (5' → 3')**
Exon-F	TGTCCCATAATGAGGCTCGT
Exon-R	GCCAGCCTTTTCACCGTGA
Fbp1-F	ACTGCGATGAAGTCGAACG
Fbp1-R	CAAGTGACGGCATAGGAACC
GFR-F	GCATCGTTTTTCGCACAATA
GFR-R	CATGGCATGGCATTTTGTTA
Intron-F	ACAAGATGTGAGCGGAAGTC
Intron-R	CGAGAAGCGCGTTAGTTTTC
Promoter-F	CCGTATATGCCCTTCAGGTT
Promoter-R	TGTATCTACAGGAGCAGTCACA
Readthrough1-F	ACTTAGTCTCTGGTTTCGAGCA
Readthrough1-R	TCAACGCCTCTCTCACTTCT
Readthrough2-F	ACTCTGGCACTGTCTGAAGA
Readthrough2-R	TACTCTTCTACGGCGGCATT
Readthrough3-F	CGCTGATATGACTTGTGTACAGT
Readthrough3-R	ACCGATTCCCATTTTGTGCT

5'-F	ACAGAGTGAAAGACCGAGCA
5'-R	TGTAATATTAAGAGATTTTCGACGCA

2.6.3 Probes for fluorescent *in situ* hybridization

Probe	Sequence
Cy3-labelled oligo $d(T)_{50}$ probe	50 x T coupled to Cy3 fluorescent dye

2.7 Antibodies

2.7.1 Antibodies for Western blot

Antibodies for Western blot were diluted in 5% milk in TBS-T.

Antibody	Dilution	Supplier and catalog number
anti-AID, mouse	1:1,000	MBL (M214-3)
anti-GAPDH, mouse	1:3,000	Medimabs (MM-0163-P)
anti-GFP, mouse	1:500	Roche (11814460001)
anti-HA, rabbit	1:1,000	Sigma Aldrich (H6908)
anti-RFP, mouse	1:1,000	Chromotek (6g6)
anti-tubulin,	1:3,000	Sigma Aldrich (T5168)
Peroxidase anti-peroxidase, rabbit	1:3,000	Sigma Aldrich (P1291)
anti-mouse-HRP	1:10,000	Sigma Aldrich (A2304)
anti-rabbit-HRP	1:10,000	Sigma Aldrich (A9169)

2.7.2 Antibodies for Immunoprecipitation

Antibody	Supplier and catalog number
Anti-RNA Polymerase II, mouse	Sigma Aldrich (05-952-I)

2.8 Enzymes and enzyme buffers

Enzyme	Supplier and catalog number
Not I -HF	NEB (R3189)
Phire Hot Start II DNA-Polymerase	Thermo Fisher Scientific (F122)
Q5 Polymerase	NEB (M0491)
Zymolase 100T	Carl Roth (9329)

Enzyme buffer	Supplier and catalog number
rCutSmart Buffer (10x)	NEB (B6004)
Phire Reaction Buffer (5x)	Thermo Fisher Scientific (F-524)
Q5 Reaction Buffer (5x)	NEB (B9027)
Mastermix	**Supplier and catalog number**
PowerUp SYBR Green Mastermix	ThermoFisher Scientific (A25742)

2.9 Beads used for ChIP and Co-IP

Beads	Supplier and catalog number
Dynabeads protein G	Thermo Fisher (10004D)
GFP-Trap magnetic agarose	Chromotek (gtma-20)
Rabbit IgG-agarose	Sigma Aldrich (A2909)
ProteinA magnetic beads	Provided by Prof. Dr. Sträßer, Giessen

2.10 Kits

Kit	Supplier catalog number
BSA Protein Assay Kit	Merck (71285)
NucleoSpin Gel and PCR Clean-up-kit	Macherey-Nagel (740609)
NucleoSpin Plasmid (NoLid)-kit	Macherey-Nagel (740499)

3 Methods

All incubation and centrifugation steps were carried out at room temperature, and autoclaved Milli-Q water was used, except where otherwise indicated.

3.1 Cell biological methods

3.1.1 Cell culture methods

For inoculation, if not stated otherwise, yeast cells were used from glycerol stocks at -80 °C and grown in the respective medium at 30 °C at 180 rpm. *S. pombe* and *S. cerevisiae* strains were grown in yeast extract with supplements (YES) complete medium as standard. Strains containing *P.nmt-dbp2* for repression of *dbp2* transcription were inoculated overnight in Edinburgh minimal medium with glutamate (EMMG). *E. coli* strains were inoculated in LB medium and cultivated at 37 °C at 360 rpm.

3.1.2 Crossing

Mating was induced by mixing strains of different mating types on ME plates at RT to combine the genotypes of two different strains. The formation of tetrads was checked after 4 to 9 days. Tetrads were picked using the Dissection Microscope and incubated for 12 to 24 h at 16 °C. The single tetrads were dissected the next day, and the plates were incubated for 4 to 7 days at 30 °C until colonies formed.

3.1.3 5'adamantyl-IAA treatment

A preculture of the respective *S. pombe* strain was grown overnight in YES medium. For metabolic depletion of Snf21, cells were inoculated at OD_{600} 0.7 and grown for 1 h. Afterward, the respective concentration of 5'adamantyl-indole-3-acetic acid (5'a-IAA) from a 0.5 mM stock in DMSO was added as published before (Watson et al., 2021 and Zhang et al., 2022) and cells were harvested at the relevant times after incubation at 30 °C while shaking.

3.1.4 Thiamine treatment

For Dbp2 depletion, cells were treated with thiamine. *S. pombe* cells were grown overnight to the logarithmic phase in EMMG. For *P.nmt-dbp2* transcription repression, cells were shifted to YES, and 15 µM thiamine was added from a 90 mM stock in water at OD600 0.23, as shown before (Aydin et al., 2024). Cells were incubated at 30 °C and harvested after 5 h.

3.1.5 Live-cell microscopy

Microscopy cover glasses were pre-treated with poly-lysine to increase cell adherence. Therefore, 5 µl poly-lysine solution was spread on each cover glass and dried for 10 min. The coverslips were rinsed with demineralized water and dried overnight.

S. pombe cells were grown in the respective medium overnight to the exponential phase and treated with 5'a-IAA (3.1.3.) or thiamine (3.1.4.). For microscopy analysis, 0.5 to 1 ml of cell suspension was spun down for 10 s and resuspended in 20 µl EMMG. 3 µl of this cell suspension was transferred to a pre-coated poly-lysine slide, covered with a coverslip, and visualized with the DeltaVision Ultra High-Resolution Microscope. Pictures were taken with the softWoRx software and analyzed by using ImageJ.

3.1.6 Fluorescence recovery after photobleaching

Yeast strains were depleted as mentioned before (3.1.2. and 4.1.4.), and fluorescence recovery after photobleaching (FRAP) was performed in collaboration with the Diepold lab (MPI Marburg). A DeltaVision Ultra High-Resolution Microscope was used, and three pictures were taken of each cell before bleaching. After bleaching, 30 images were taken every ~0.3 seconds and analyzed using ImageJ. Each point in time was normalized to the background and the baseline intensity before bleaching. The time required to regain 50% of the maximum intensity was defined and visualized using RStudio. The script for normalization and determination of $t_{50\%}$ was provided by Dr. Thomas Offner.

3.1.7 Preparation of glycerol stocks

To prepare glycerol stocks for long-term storage of *S. pombe* strains, cells were plated in 100 µl water on appropriate agar plates for 3 to 5 days at 30 °C. The dense cell layer was transferred into 800 µl 25% glycerol and stored in cryotubes at -80 °C.

3.1.8 Dot Spots

Dot spot assays were used to compare growth properties between different strains. Therefore, an OD_{600} of 0.1 was inoculated from a preculture and grown for 2 h in YES or 4 h in EMMG. An OD_{600} of 0.2 was pelleted by centrifugation at 3,000 g for 2 min and resuspended in 1 ml water. From this, three 1:10 serial dilutions were made, and 3 µl was spotted on appropriate plates and incubated at 30 °C for 2 to 4 days.

3.2 Molecular biological methods

3.2.1 LiAOc-transformation in *S. pombe*

An efficient LiAOc transformation protocol was used to incorporate foreign DNA into the *S. pombe* genome (Hyun Soo Kim, Keogh lab, AECOM). Cells were grown overnight to log phase OD_{600} 0.5, and 5 ml culture was pelleted by centrifugation at 850 g for 3 min. Washing was done with 1 ml sterile water and centrifugation at 9,400 g for 10 s. The pellet was washed in 500 µl LITE at 9,400 g for 10 s and resuspended in 100 µl LITE. Afterward, 20 µg ssDNA and a total volume of 8 µl of the PCR products or plasmids were added. The cells were mixed by gentle vortexing and incubated at RT for 10 min. After adding 260 µl PLATE, cells were

vortexed again and incubated at 30 °C for 1 h. 43 µl DMSO was added, and a heat shock at 42 °C for 5 min was performed, followed by a short cooling down for 2 min at RT. Cells were pelleted by centrifugation at 3,000 g for 10 s, resuspended in 1 ml YES, and incubated at 30 °C for at least 2 h while shaking. Subsequently, the transformed cells were spun down at 3,000 g for 10 s and plated on selective media plates in 300 µl of water. The plates were incubated at 30 °C for 3 to 5 days until single colonies developed.

3.2.2 Plasmid preparation from *E. coli*

E. coli strains were inoculated in 10 ml LB medium supplemented with the appropriate antibiotic from glycerol stocks and incubated overnight at 37 °C at 230 rpm. The NucleoSpin Plasmid (NoLid)-kit (Macherey-Nagel) was applied according to the manufacturer's protocol for small-scale plasmid preparation. Plasmids were directly used as templates for PCR or linearization or stored at -20 °C.

3.2.3 Plasmid linearization

These plasmids were linearized prior to transformation to enable integration into the genome by homologous recombination. For this purpose, the following reaction was set up:

Component	50 µl Reaction
DNA	1 µg
rCutSmart buffer	5 µl
Not Ⅰ-HF	1 µl
Nuclease-free water	to 50 µl

The reaction was incubated for 1 h at 37 °C, followed by an inactivation step at 65 °C for 20 min. Linearization was verified by loading 3 µl reaction sample in agarose loading dye on a 1% agarose gel. Samples were stored at -20 °C.

3.2.4 Polymerase chain reaction

Polymerase chain reaction (PCR) was performed to produce DNA fragments for genomic integration. The first step was carried out with *S. pombe* gDNA or a plasmid as a template, and a typical reaction for the first step was generated in the following way:

Component	50 µl Reaction
template DNA	1 µl
Q5 Reaction buffer	10 µl
dNTPs [2 mM]	5 µl
Primer fwd. [10 µM]	2.5 µl
Primer rev. [10 µM]	2.5 µl
Q5 Polymerase	0.5 µl
Nuclease-free water	28.5 µl

For the second PCR, the PCR products from the first steps were used as templates, and the following reaction was set up:

Component	50 µl Reaction
template DNA	25 ng each
Q5 Reaction buffer	10 µl
dNTPs [2 mM]	5 µl
Primer fwd. [10 µM]	2.5 µl
Primer rev. [10 µM]	2.5 µl
Q5 Polymerase	0.5 µl
Nuclease-free water	to 50 µl

For amplification, the following temperature profile was used with adjusted annealing temperatures:

Temperature	Time	
98 °C	30 s	
98 °C	10 s	30x
56 - 72 °C	20 s	
72 °C	30 s	
72 °C	2 min	
10 °C	∞	

PCR samples were loaded in agarose loading dye on a 1% agarose gel or stored at -20 °C. For the PCR samples from the first step, a gel extraction step (3.2.7) was performed, while for the second step, a 3 µl sample was analyzed on an agarose gel and used directly for transformation.

3.2.5 Colony polymerase chain reaction

After transformation or crossing, colony-PCR was used to verify a successful genomic integration or deletion. A single colony was picked from an agar plate and used as a template for the following reaction:

Component	25 µl reaction
template DNA	-
Phire Reaction Buffer	5 µl
dNTPs [2 mM]	2.5 µl
Primer fwd. [10 µM]	1.25 µl
Primer rev. [10 µM]	1.25 µl
Nuclease-free water	15 µl

Samples were boiled at 98 °C for 10 to 15 min, spun down, and cooled on ice for 1 to 2 min before 0.5 µl Phire Hot Start II DNA-Polymerase was added per reaction. A PCR with the following temperature profile was performed with ΔR set to 0.6 °C/s :

Temperature	Time	
98 °C	30 s	
98 °C	5 s	35x
58 °C	5 s	
72 °C	1 min 15 s	
72 °C	5 min	
10 °C	∞	

PCR samples were loaded on a 1% agarose gel with a wild-type sample as a control or stored at -20 °C.

3.2.6 Quantitative polymerase chain reaction

Quantitative PCR (qPCR) was used to determine the relative amount of DNA in the sample to be analyzed. In this context, the amplification of DNA by PCR can be monitored in real-time by using a fluorescent dye. The qPCR reaction was set up in technical duplicates with the following components using DNA samples from ChIP (3.2.8.) as templates. The temperature profile shown below includes a melt curve analysis.

Component	15 µl reaction
template DNA	5
PowerUp SYBR Green Mastermix	7.5 µl
Primer fwd. [10 µM]	0.1875 µl
Primer rev. [10 µM]	0.1875 µl
Nuclease-free water	2.125 µl

Temperature	Time	
50 °C	2 min	
95 °C	10 min	
95 °C	5 s	40x
60 °C	30 s	
95 °C	15 s	
60 °C	1 min	
95 °C	15 s	

The qPCR was analyzed by the QuantStudio Design & Analysis Software, and expression levels were determined using the ΔΔCt method. For that purpose, the mean of the analyzed Ct values was calculated for the region of interest and the reference gene. The samples were normalized to a gene-free region on chromosome II (*gfr*) and an input sample to define ΔΔCt. In the final step, the expression was calculated as $2^{-\Delta\Delta Ct}$.

3.2.7 Gel extraction

DNA samples were loaded with 1x agarose loading dye on a 1% agarose gel and analyzed by agarose gel electrophoresis. Samples were extracted from gels using the NucleoSpin Gel and PCR Clean-up kit (Macherey-Nagel) according to the manufacturer's recommendations.

3.2.8 Chromatin immunoprecipitation

Chromatin Immunoprecipitation (ChIP) analysis followed by qPCR was performed to investigate the protein occupancy at different gene regions. The protocol was carried out as published before (Wittmann et al., 2017) with minor changes. *S. pombe* cells were grown overnight, and a 200 ml culture was treated as needed for each experiment. The cells were crosslinked with 20 ml of 11% formaldehyde in diluent incubating for 20 min on a shaker at RT. This reaction was stopped by adding 30 ml of glycine buffer for 5 min while shaking. The cells were washed with 50 ml cold TBS and 10 ml FA lysis buffer/0.1% SDS + 1 mM PMSF and harvested at 3,000 g for 2 min. Pellets were stored at -80 °C.

After thawing on ice, the pellet was resuspended in 1.6 ml FA/lysis buffer/0.5% SDS + PIC and split into two screw cap tubes. The cells were lysed with 300 µl glass beads for 2 x120 s at 6 m/s with a 10 s break in between with the FastPrep-24 at 4 °C. The tubes were punctured with a needle, placed on a falcon tube, and washed four times with 825 µl FA lysis buffer/ 0.1% SDS at 140 g and 4 °C for 2 min. At this step, the lysates from the two screw cap tubes were pooled and transferred to a polycarbonate bottle. The volume was filled to 20 ml with FA lysis buffer/0.1% SDS and pelleted at 22,000 rpm at 4 °C for 30 min using the 70 Ti rotor. The supernatant was discarded, and the transparent halo containing the chromatin was smashed together using a wooden stick. The pellet was resuspended in 750 µl FA lysis buffer/0.1% SDS and transferred to a polycarbonate tube. The polycarbonate bottle was washed with 750 µl FA lysis buffer/0.1% SDS, which was added to the tube. The sample was sonicated in the Bioruptor UCD-200 for 80 min at high energy with a 15 s ON/45 s OFF setting in ice water. The sonicated sample was shifted to two reaction tubes and filled to 1.5 ml with FA lysis buffer/0.1% SDS, followed by centrifugation at 15,000 g for 20 min at 4 °C. The supernatant containing the sheared chromatin was pooled, and concentration was determined using the Nanodrop spectrophotometer. The chromatin aliquots and an input control sample were stored at -80 °C or directly used for Immunoprecipitation.

For HTP-tagged proteins, IgG-agarose beads were prepared by washing 30 µl of 50% slurry beads per sample two times with 1 ml TE buffer at 350 g for 3 min. Beads were resuspended in 200 µl FA lysis buffer/0.1% SDS per sample. To washed beads, 400 µl sheared chromatin, 380 µl FA lysis buffer/0.1% SDS, and 20 µl 5M NaCl was added. The reaction was incubated overnight on a rotating wheel at 4 °C.

Beads were pelleted at 350 g for 3 min and washed twice with 1 ml wash buffer I, followed by two washes with wash buffer II and wash buffer III. Two last washing steps were done by using 1 ml TE buffer. Elution was done in 200 µl elution buffer for 20 min at 65 °C and 300 rpm oh the thermomixer, after which beads were pelleted at 350 g for 2 min to transfer the supernatant to a fresh tube. Another centrifugation step obtained the remaining supernatant at 18,500 g for 2 min. At the same time, an input sample was prepared by adding 150 µl FA lysis buffer/0.1% SDS and 100 µl TE buffer to 50 µl input sample. 30 µl of 20 mg/ml pronase was added and incubated for 1 h at 42 °C, followed by decrosslinking at 65 °C overnight.

After decrosslinking, 50 µl of 4 M LiCl was added, and samples were vortexed. The DNA was extracted with 500 µl phenol/chloroform/isoamyl alcohol and 500 µl chloroform by vortexing, and a centrifugation step at 10,000 g for 10 min at 4 °C. Precipitation was done with 1 µl of 20 mg/ml glycogen and 800 µl 100% ethanol and incubation overnight at -20 °C.

The precipitated sample was pelleted for 30 min at 15,000 g and 4 °C and washed in 1 ml 70% ethanol at 15,000 g for 5 min at 4 °C. The DNA samples from immunoprecipitation were resuspended in 200 µl and DNA input samples in 500 µl water.

3.2.9 Chromatin immunoprecipitation and sequencing

For sequencing (ChIP-Seq), samples were prepared according to the ChIP protocol (3.2.8.) in duplicates with the following adjustments. Additionally, an *S. cerevisiae* strain was harvested at the same OD, and the pellet was split into ten aliquots. A spike-in pellet was added to each *S. pombe* sample before lysis was accomplished. Furthermore, two immunoprecipitations were assembled from each chromatin sample and pooled before washing. For RNAPII-ChIP-Seq, an antibody against RNA PolII subunit Rpb1 was coupled to dynabeads protein G. For that purpose, 20 µl of 50% slurry beads were washed three times in 1 ml TE and 200 µl beads per sample were incubated with 5 µl antibody on a rotating wheel for 2 h at RT. For these beads, all washing steps were done on a magnetic particle collector. After antibody incubation, beads were washed, and IP was performed, as mentioned before. Finally, all samples were resuspended in 20 µl TE buffer and stored at -20 °C. DNA concentrations were measured again, and sequencing was done by Dr. Stefan Günther (MPI, Bad Nauheim).

Galaxy (https://usegalaxy.org) was used to analyze the samples. First, a combination of tools was used for alignment ("Trimmomatic", "Filter FASTQ", "Bowtie2" and "Samtools flagstat"), for which *S. pombe* and *S. cerevisiae* genomes were used. For normalization to the *S. cerevisiae* spike in control, a second set of tools was used ("BAM-to-SAM", "FilterSamReads" and "Samtools flagstat"). Aligned and normalized reads were counted with the tool "htseq-count" and differentially expressed counts were determined by "DESeq2". The integrated genome browser was used for visualization.

3.2.10 Co-immunoprecipitation

Co-immunoprecipitation (Co-IP) was done to investigate possible protein-protein interactions by extracting a protein of interest with a specific antibody. For that purpose, an overnight culture was prepared in YES. The following day, an OD_{600} of 0.3 was inoculated, and cells were incubated for 8 h at 30 °C while shaking. After harvesting at 3,000 g for 2 min at 4 °C, pellets were stored at -80 °C.

Cell lysates were acquired by adding 500 µl lysis buffer and 500 µl glass beads. 10 µl from the lysates were kept for input controls and diluted 1:10 in SDS loading buffer. For IP of GFP-tagged strains, 15 µl of GFP-trap magnetic agarose beads were washed 2x with 1 ml lysis buffer (-DTT, PMSF, PIC) with a magnetic rack, and lysates were incubated with beads for 2 h at 4 °C on a rotating wheel. For HTP-tagged strains, 50 µl protein A magnetic beads were washed 2x with 1 ml lysis buffer (-DTT, PMSF, PIC) at 350 g for 3 min and lysates were

incubated as described before. Beads were washed 2x with lysis buffer (+DTT, PMSF, PIC) and 6x with stringent wash buffer. The liquid was removed, and 40 µl SDS loading buffer was added to the beads. For elution, samples were incubated at 65 °C for 10 min and kept at RT for another 10 min. Lysates were collected with the magnetic rack or centrifugation at 350 g for 3 min and transferred to a new tube. 20 µl of IP and 10 µl of diluted input controls were analyzed using SDS-Page (3.3.3.) and Western blot (3.3.4.).

3.2.11 Fluorescent *in situ* hybridization with oligo d(T)

Fluorescent *in situ* hybridization (FISH) was performed to localize poly(A)-containing RNA in fixed yeast cells (Amberg et al., 1992). Cells with corresponding controls were depleted with 5'a-IAA (3.1.3.) or thiamine (3.1.4.). Double depletion of Snf21 and Dbp2 was done by adding 5'a-IAA after 4.5 h of depletion with thiamine for the last 30 min. For fixation, 8.75 ml cell culture were incubated with 1.25 ml formaldehyde for 1 h on a roller mixer. Heat shock controls were prepared by adding 5.5 ml cells to 3.3 ml pre-warmed YES media with subsequent incubation at 42 °C for 1 h in a water bath. 1.25 ml formaldehyde was added, and cells were fixed at 42 °C in the water bath for 20 min and for 1 h at RT on a roller shaker. After fixation, all samples were harvested at 2,000 g for 5 min and washed with 5 ml of 0.1 M KPO_4 pH 6.4. Cells were transferred to a 1.5 ml tube by resuspending them in 1 ml of 0.1 M KPO_4 pH 6.4, followed by a centrifugation step at 850 g for 5 min. For storage overnight, pellets were resuspended in 1 ml wash buffer and placed at 4 °C.

The following day, samples were spun down at 850 g for 3 min. Cells were incubated in 200 µl wash buffer containing 100 µl zymolase for 1 h at 37 °C. After centrifugation at 350 g for 4 min, pellets were washed once with 1 ml wash buffer, followed by another centrifugation step. Samples were resuspended in 200 µl 2x SSC buffer, incubated at RT for 10 min, and pelletized at 350 g for 4 min. After incubation in 30 µl prehybridization buffer for 1 h at 37 °C, 1 µl of 1 pmol/µl cy3-labeled oligo d(T) probe was added, and samples were incubated at 37 °C overnight under dark conditions.

Cells were collected by centrifugation at 350 g for 4 min and resuspended in 600 µl 0.5x SSC, followed by an incubation step for 30 min on a rotating wheel under dark conditions. Polylysine-coated coverslips were prepared as described before (3.1.5.). After centrifugation at 350 g for 4 min, pellets were resuspended in 60 µl 1x PBS containing 0.1% NaN_3, and 30 µl was transferred on a precoated coverslip. Samples were incubated for 30 min under dark conditions. Next, non-adherent cells were removed by aspiration, and cover glasses were carefully washed with 60 µl 1x PBS containing 0.1% NaN_3. After removal of the liquid, slides were dried for 10 min, and 5 µl ROTIMount FluorCare DAPI was added to an object slide. The object slides were covered with a cover glass, and samples were incubated overnight under dark conditions and analyzed using the DeltaVision Ultra High-Resolution Microscope.

Quantification was conducted with ~200 randomly selected cells, and intensities were determined with ImageJ and plotted with the RStudio software. Semi-automatic cell segmentation was performed using thresholds for the transmitted light channel and DAPI staining. The average intensity of the Z-projections for the nucleus and the cytoplasm were measured. Last, the ratio of the mean fluorescence intensity of the nucleus over the mean fluorescence intensity of the cytoplasm was calculated for each cell. The significance tests for the pairwise comparisons were calculated using the Wilcoxon test.

3.3 Biochemical methods

3.3.1 Preparation of *S. pombe* cell lysates

To analyze proteins using SDS-page, lysates were prepared from cell pellets. The pellets were resuspended in a suitable volume of lysis buffer (+DTT, PMSF, PIC), and glass beads were added. Cells were vortexed for 16 min on high speed for 30 s with 30 s breaks on ice in between. The reaction tube was punctured with a needle, placed on a new tube, and the lysate was collected at 400 g for 2 min at 4 °C. To get rid of cell debris, a centrifugation step at 15,000 g for 5 min at 4 °C was conducted, and the lysate was transferred to a fresh tube. Depending on the following experiment, cell extracts were normalized to equal protein concentration using BSA assay (3.3.2.) and loaded on an SDS-polyacrylamide gel (3.3.3.) for Western blot analysis (3.3.4.).

3.3.2 Determination of protein concentration by BCA assay

BCA assay was done to normalize the protein extract concentrations to equal ones. First, the following standards were pipetted to calculate the sample concentration based on a standard curve.

0	0.5	1	2	4	6	8	Standard [mg/ml]
0 µl	0.25 µl	0.5 µl	1 µl	2 µl	3 µl	4 µl	BSA [10 mg/ml]
5 µl	4.75 µl	4.5 µl	4 µl	3 µl	2 µl	1 µl	Lysis buffer

Additionally, the BCA solution was prepared by adding 20 µl $CuSO_4$ to 1 ml BCA. 5 µl of each, the standard and the protein extract, was mixed with 100 µl BCA solution, and samples were incubated for 30 min at 37 °C. Samples were measured using the "BCA protein" setting of the Nanodrop spectrophotometer. For SDS page, 50 µg of total protein was loaded unless indicated otherwise.

3.3.3 SDS Page

To separate proteins by size difference, the so-called sodium dodecyl sulfate-polyacrylamide gel electrophoresis (SDS-PAGE) was performed (Laemmli, 1970). Gels were prepared using the Mini-PROTEAN tetra vertical electrophoresis cell system by preparing the following gels:

Component	8% separating gel	10% separating gel	4% stacking gel
Water	2.335 ml	2 ml	1.496 ml
Separating gel buffer	1.25 ml	1.25 ml	-
Stacking gel buffer	-	-	625 µl
Acrylamide (30%)	1.333 ml	1.667 ml	334 µl
SDS (10%)	50 µl	50 µl	25 µl
TEMED	7.5 µl	7.5 µl	4.5 µl
APS (10%)	25 µl	25 µl	15.5 µl

Samples were mixed with 1x SDS loading dye and incubated at 65 °C for 10 min. After spinning down, samples were loaded on a gel with the needed percentage with 5 µl protein marker and run at 180 V for 1 h in 1x SDS running buffer. After electrophoretic separation, the polyacrylamide gel was used for immunodetection of the proteins by Western blot (3.3.4.).

3.3.4 Western blot

The transfer of proteins from the polyacrylamide gel to a PVDF membrane was carried out with the mini trans-blot module at 100 V and 4 °C for 70 min (1 gel) or 100 min (2 gels). After transfer, membranes were rinsed with deionized water, washed in TBS-T, and blocked in 5% milk in TBS-T for 1 h. Next, the membrane was incubated with the primary antibody overnight at 4 °C, followed by four washing steps in TBS-T for 10 min on a shaker. The incubation with the secondary antibody was done for 2 h on a shaker. Finally, membranes were rewashed in TBS-T for 10 min four times on a shaker, and chemiluminescence signals were analyzed using the ChemoCam Imager.

4 Results

4.1 Depletion systems for the investigation of the RSC complex and Dbp2

4.1.1 Establishment of the 5'a-IAA depletion system for induced depletion of Snf21

Given our previous data indicating a potential feedback mechanism between the helicase Dbp2 and chromatin remodeling, we investigated a potential functional link between Dbp2 and the RSC complex. To do so, we needed to establish efficient systems for the depletion or deletion of the respective proteins.

For the investigation of the RSC complex, two subunits were selected for strain generation. On the one hand, the gene coding for a non-essential subunit, namely *rsc1,* was deleted; successful deletion was later confirmed by sequencing results (Fig. 16C). On the other hand, for the investigation of essential functions of the complex, the catalytical protein Snf21 was chosen. Because this gene is essential, no deletion was possible for this subunit. Instead, an inducible system for depletion using the auxin analog 5'a-IAA (Watson et al., 2021) was established for Snf21. In this system, the protein of interest is fused to a small auxin-inducible degron (sAID). Under the addition of 5'-IAA, the F-box protein variant OsTIR1^{F74A} binds the AID-tagged endogenous Snf21, which interacts with endogenous Skp1, Cullin, and Rbx1 (Fig. 7A). This complex recruits the ubiquitin-conjugating enzyme E2, which leads to the polyubiquitylation of proteins, targeting them for degradation by the proteasome. To test if this system is working for the depletion of Snf21, an OsTIR1^{F74A}-Snf21-3xsAID depletion strain with corresponding controls was created. Initially, these strains were tested in spot assays on a YES control plate and YES plates containing different concentrations of 5'a-IAA. For the wild-type control, the Snf21-tagged strain in the wild-type background, as well as the untagged version in the OsTIR1^{F74A} background, there was no effect on the growth of the cells by the addition of 5'a-IAA (Fig. 7B). Moreover, a strain where endogenous Snf21 was tagged with sAID in the pEasy background was used, because this background represents the parent vector for OsTIR1^{F74A}. As expected, there was no effect of 5'a-IAA on the growth of this strain. In contrast to that, the Snf21-3xsAID tagged strain in the OsTIR1^{F74A} background showed an apparent growth defect after the addition of 5'a-IAA. This effect occurred with 1 nM 5'a-IAA and became increasingly more robust with higher 5'a-IAA concentrations. Subsequently, we verified depletion of Snf21 on the protein level. For this purpose, cell lysates from different concentrations were prepared in a time course and analyzed by SDS-Page and Western blot. Again, the Snf21-tagged strain in the pEasy background was used as a control strain. As expected, this control showed no effect on Snf21 levels after the addition of 100 nM 5'a-IAA even after two hours (Fig. 7C). Contrary to this, the OsTIR1^{F74A}-Snf21-3xsAID strain showed an apparent reduction of Snf21 levels 15 min after the addition of 1 nM and 10 nM 5'a-IAA.

The depletion of Snf21 with the highest concentration of 100 nM 5'a-IAA led to a complete loss of Snf21 after 15 min.

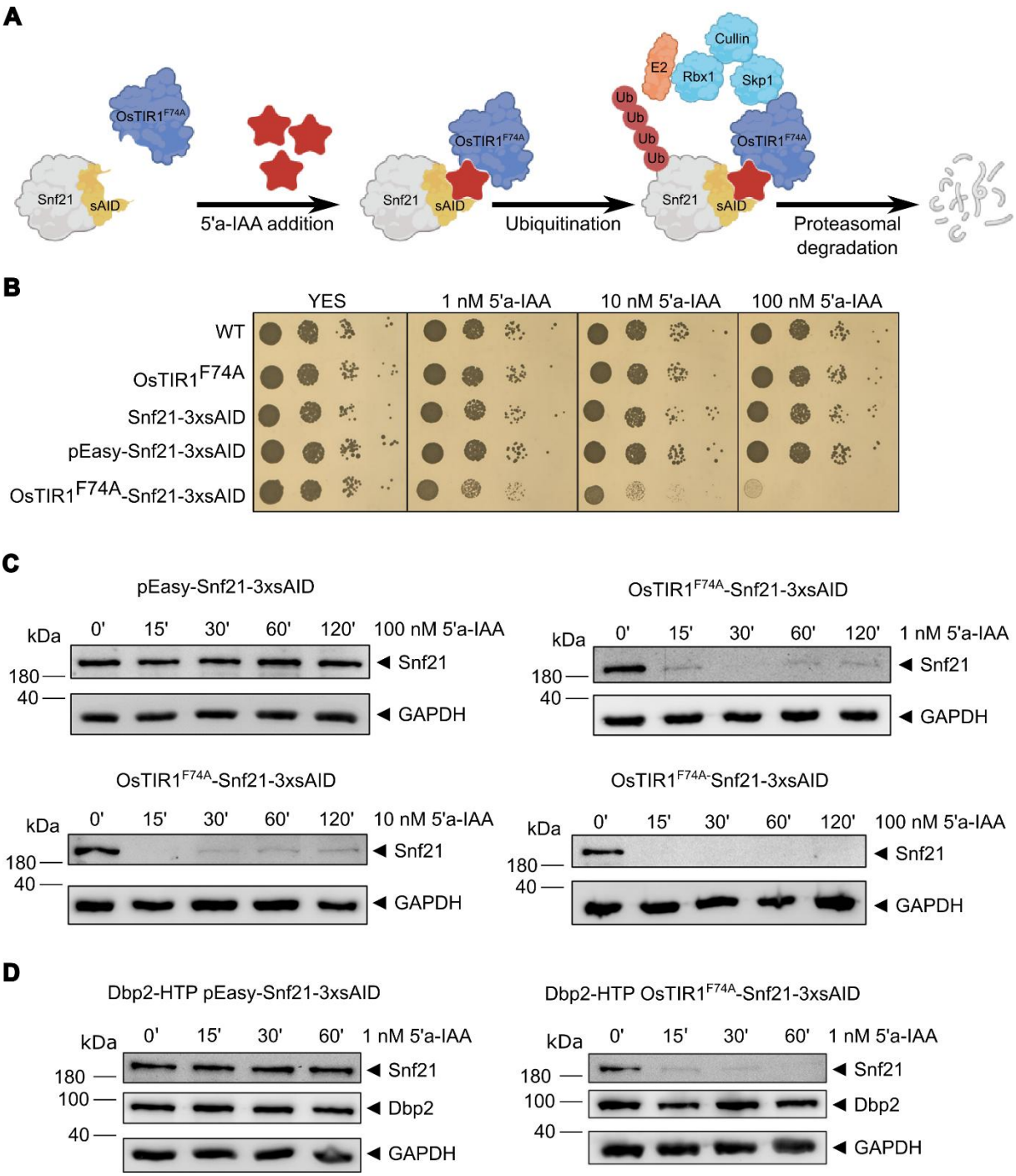

Figure 7 Depletion of the essential RSC subunit Snf21 using 5'a-IAA. A Scheme of the inducible depletion of Snf21 using the auxin analog 5'adamantyl-indole-3-acetic acid (5'a-IAA). After 5'a-IAA addition, the F-box protein OsTIR1^{F74A} recruits Skp1/Cullin/Rbx1 to the sAID-tagged Snf21. E2 is recruited, which leads to polyubiquitylation and degradation by the proteasome. Created in BioRender. Böhme, J. (2026) https://BioRender.com/b7mounq. **B** The indicated strains were grown in YES overnight, serial dilutions were spotted on YES plates and plates containing different concentrations of 5'a-IAA and incubated at 30 °C. The OsTIR1F74A-Snf21-3xsAID strain shows a growth defect by adding 5'a-IAA (n = 3). **C** Lysates of a 5'a-IAA time course for Snf21-3xsAID AID were analyzed by SDS-PAGE and Western blot against AID and GAPDH as a loading control. The addition of 5'a-IAA leads to a reduction of Snf21 levels after 15 min already. **D** Lysates of a 5'a-IAA time course for Snf21-3xsAID AID were analyzed as explained for C with additional Dbp2-HTP tagging. There was no effect of the Snf21 depletion using 5'a-IAA on Dbp2 levels. GAPDH was used as a loading control.

In addition, we wanted to investigate whether the depletion of Snf21 affects other proteins of interest in the context of this project, in this case, Dbp2 . Therefore, we created an Snf21-depletion strain and the corresponding pEasy control with additional tagging of Dbp2 with HTP. There was no effect on Dbp2 levels, while Snf21 depletion worked as efficiently as we have observed before (Fig. 7D).

Taken together, our results demonstrate the inducible depletion of our target protein Snf21 within 15 minutes by using the modified auxin analog 5'a-IAA and the modified F-box protein OsTIR1^{F74A}. Low inducer concentrations between 1 and 100 nM can achieve this depletion, and non-AID-tagged proteins remain unaffected.

4.1.2 Applying the *P.nmt* depletion system to Dbp2

As for Snf21, Dbp2 is an essential protein, which means that an inducible depletion system is needed to investigate the loss of this protein. It was shown before that Dbp2 is resistant to depletion via an auxin-induced degron system (Song et al., 2021). The excellent depletion observed for Snf21 using the modified auxin-degron system nevertheless prompted us to test this modified system as a potential alternative for depleting Dbp2. However, we confirmed that this depletion approach does not work for Dbp2 (Supplement Fig. 2). For this reason, the "no message in thiamine promoter" (*P.nmt)*, which is repressed in the presence of thiamine, was used (Siam et al., 2004). We have shown the application of this promoter system for the effective depletion of Dbp2 within five hours before (Aydin et al., 2024). For this purpose, the endogenous *dbp2* gene is expressed under the *nmt1* promoter, and the presence of thiamine leads to a reduction of *dbp2* gene expression (Fig. 8A). To confirm the successful depletion of Dbp2 in strains where subunits of the RSC complex were additionally tagged, spot assays were performed. The wild-type, as well as the Snf21-GFP or Snf21-HTP-tagged strains, showed no growth defect on EMMG and YES plates (Fig. 8B). However, the strains containing *P.nmt-dbp2* showed impaired growth on YES plates containing thiamine compared to the control EMMG plates. The same effect was observed in *P.nmt-dbp2* strains where the RSC subunit Rsc1 was tagged with GFP or HTP (Fig. 8C). This indicates that on YES plates, which contain thiamine, the *P.nmt* promoter and, therefore, *dbp2* expression is repressed. The loss of this essential protein leads to reduced growth, which can be detected on dot spot plates.

In summary, it can be said that an appropriate method for deletion or depletion was found for both the RSC components and Dbp2. This enables a meaningful investigation of the individual proteins and their interaction with each other.

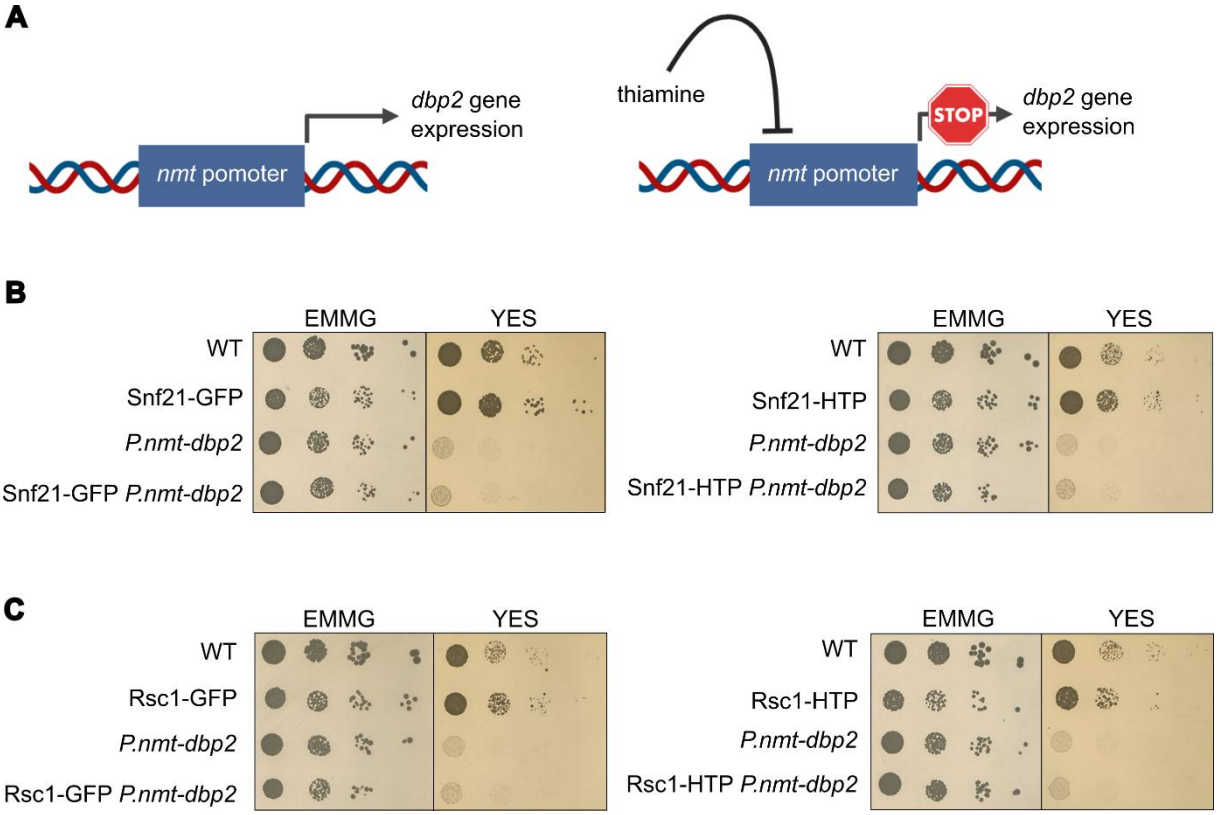

Figure 8 Depletion of the essential RNA helicase Dbp2 using the "no message in thiamine'' promoter. **A** Scheme of the inducible depletion of Dbp2 using the *P.nmt* system. Created in BioRender. Böhme, J. (2026) https://BioRender.com/kquh2j6. **B** The indicated strains were grown in EMMG overnight, serial dilutions were spotted on EMMG control plates, and YES plates containing thiamine, and plates were incubated at 30 °C. The *P.nmt* strains show a growth defect on YES plates (n = 3). **C** The indicated strains were prepared and spotted as shown for B (n = 3).

4.2 The chromatin remodeling complex RSC interacts with the RNP remodeling ATPase Dbp2

Initial purifications from crosslinked cells suggested that there could be an interaction between the RSC complex and the Dbp2 (Fig. 6A). To investigate if this interaction could also be detected under non-crosslinking conditions, Co-IP was performed. Therefore, one tagged protein was precipitated using magnetic beads, and the precipitated protein complexes were analyzed by SDS-Page and Western blot.

We first asked if the RSC subunits Rsc1 and Snf21 co-purify with Dbp2. We analyzed this by purifying Dbp2-GFP-HA using GFP magnetic beads and investigated whether Rsc1-tdTomato and Snf21-tdTomato can also be detected in this purification. We analyzed input samples before precipitation to confirm that Rsc1-tdTomato, Snf21-tdTomato, and Dbp2-GFP could be detected at the expected heights. As anticipated, both proteins were detected in the double-tagged Dbp2-GFP-HA RSC-tdTomato strains (Fig. 9A, left). After precipitation of Dbp2, it is highly enriched compared to the input control, and the washing steps successfully removed

non-associated proteins, such as GAPDH (Fig. 9A, right). In the double-tagged strains, both Rsc1 and Snf21 were purified with Dbp2. However, since Rsc1-tdTomato was also detected in the control Co-IP, this suggests that Rsc1 was only purified unspecifically. In short, the Co-IP indicates an interaction between Dbp2 and the catalytic subunit Snf21. A reverse Co-IP was carried out to corroborate these results. The two RSC subunits, Rsc1 and Snf21, were purified instead of Dbp2 in this experiment. In addition, a different tag was used compared to the previous experiment, namely HTP instead of tdTomato. Once again, detection of the tagged proteins was verified in the input control, and both tags were detected in the double-tagged strains (Fig. 9B, left).

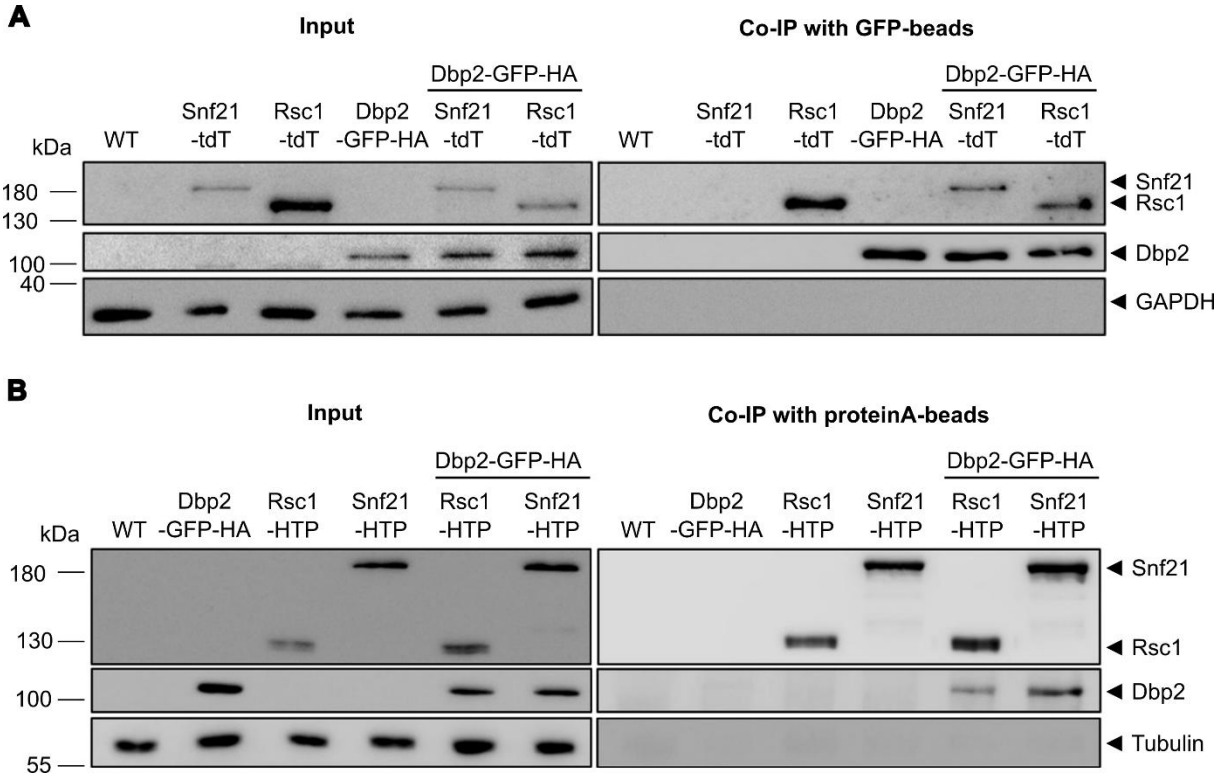

Figure 9 Snf21 and Rsc1 interact with Dbp2. A Input lysates and eluates of a Co-immunoprecipitation with GFP-beads from RSC-tdTomato strains in the presence or absence of Dbp2-GFP and a Dbp2-GFP control were analyzed on SDS-PAGE and by Western blot against GFP and RFP. GAPDH was loaded as a control for sufficient washing. **B** The indicated strains were analyzed as shown for A with *p*rotein A-beads and investigated by Western blot against HA and HTP.

After precipitation with protein A magnetic beads, the bands of all HTP-tagged proteins could be detected as expected. Interestingly, in the RSC-HTP Dbp2-GFP double-tagged strains, Dbp2 was detected by precipitation of both Rsc1 and Snf21. In contrast to using GFP magnetic beads, no Dbp2 was unspecifically co-precipitated in this case. This confirms the previous results of an interaction between Snf21 and Dbp2 and indicates an association of Rsc1 and Dbp2.

In summary, the above results demonstrate a protein-protein interaction between the RSC complex and Dbp2, suggesting a potential intercommunication mechanism between mRNA processing and chromatin remodeling.

4.3 The RSC complex and Dbp2 colocalize in the nucleoplasm

After we demonstrated an interaction between the components of the RSC complex and Dbp2, we asked ourselves where precisely these proteins are localized and in which areas colocalization takes place. For this reason, living cells in which proteins were tagged with different fluorescent proteins were microscopically examined. The localization of the individual proteins within the cell corresponds to the localization determined in later microscopy experiments (Fig. 12 and Fig. 13). In this experiment, we showed that the RSC subunits Rsc1 and Snf21 are localized in a crescent-shaped structure in the nucleoplasm. Dbp2 is also found in the nucleoplasmic region, but the strongest signal for Dbp2 is found in the nucleolus (Fig. 10).

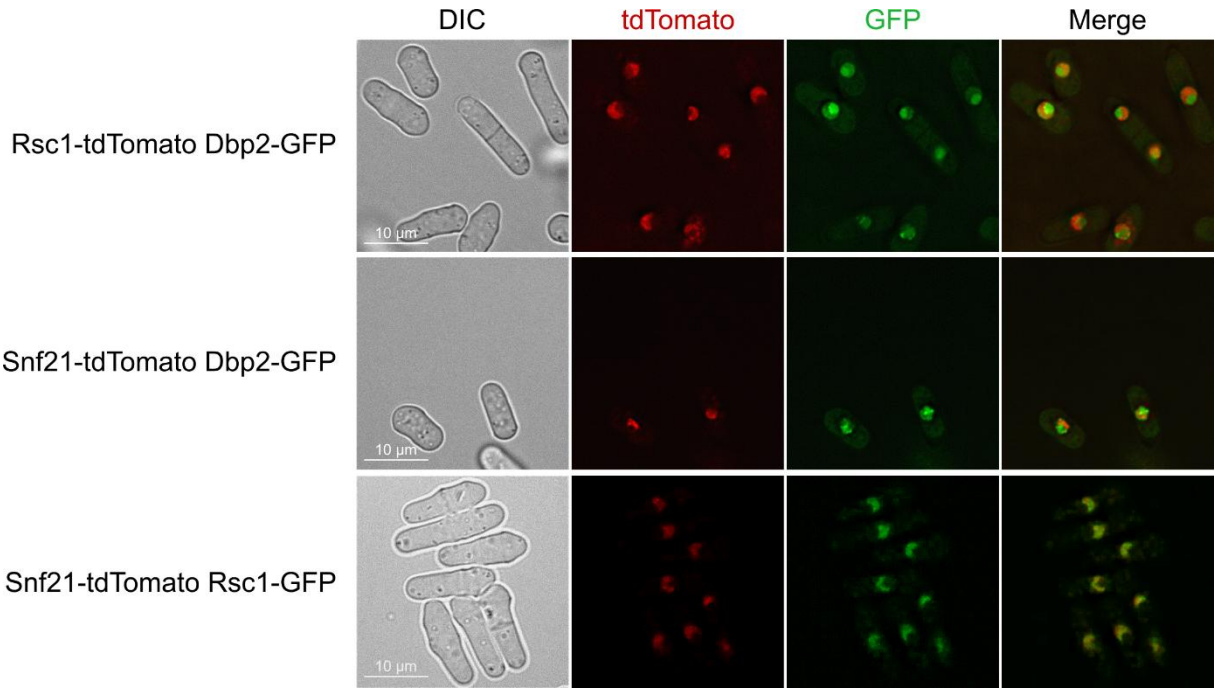

Figure 10 Snf21 and Rsc1 colocalize with Dbp2 in the nucleoplasmic region of the nucleus. Live-cell microscopy of genomically tagged Dbp2 and the RSC subunits Rsc1 and Snf21 as well as Snf21 and Rsc1 together. GFP-tagged proteins are shown in green, and tdTomato-tagged proteins are shown in red. The images shown are representative of three independent biological replicates.

Overall, this suggests that the interaction of Rsc1 and Snf21 with Dbp2 occurs within the nucleoplasm. The fact that the proteins of the RSC complex are found in the DNA-rich structure within the cell nucleus is consistent with its function as a chromatin remodeler. Pleiotropic phenotypes are well known for Dbp2, which is associated with its localization in different

regions. In line with this, it was shown that Dbp2 is associated with transcribing RNA PolII, a process that takes place in the nucleoplasm (Aydin et al., 2024).

4.4 No change in RSC and Dbp2 occupancy on *rps2202* upon loss of the respective other factor

Because we hypothesized a potential feedback mechanism between Dbp2 and the RSC complex that could influence their respective chromatin occupancy, we aimed to investigate changes in protein binding upon loss of the other component. Dbp2 is an RNA helicase involved in RNA processing and surveillance, but it has also been linked to transcriptional regulation through interactions with chromatin and RNA polymerase II. The RSC complex, on the other hand, is a chromatin remodeler that alters nucleosome positioning to regulate transcription. A potential link between Dbp2 and RSC could reflect coordination between chromatin remodeling and RNA processing, ensuring proper gene regulation at multiple levels. Because we hypothesized a potential feedback mechanism between Dbp2 and the RSC complex, which could influence the occupancy of the proteins on the gene, we wanted to investigate possible changes in the occupancy of these proteins after the loss of the other component. We analyzed this by ChIP experiments followed by qPCR on different regions of the ribosomal gene *rps2202*. Primer pairs were used for the 5'-region, the promoter, the intron, the exon, and three regions past the cleavage and polyadenylation site ("readthrough"). In the first experiment, we investigated the differences in the localization of Dbp2 and Rsc1 in the absence of the other protein, and wild-type samples were used as a non-tagged control. Dbp2-HTP showed a higher occupancy in the exon and readthrough region. At the same time, there was no change in Dbp2-HTP occupancy after *rsc1* deletion (Fig. 11A). The RSC subunit Rsc1 could not be detected at levels that exceeded the non-tagged control. We repeated the same experiment looking at Dbp2-HTP occupancy after depletion of the essential RSC subunit Snf21 with either 1 nM or 100 nM 5'a-IAA. As before, Dbp2-HTP occupancy was high in the exon and readthrough regions (Fig. 11B). Like the *rsc1* deletion, the depletion of Snf21 did not affect Dbp2 occupancy. The depletion with the higher concentration of 100 nM appeared to increase Dbp2 occupancy, but this was also observed for the pEasy-Snf21-3xsAID control, which does not deplete Snf21 (Fig. 11C). Similar to Rsc1-HTP, Snf21-HTP did not associate with *rps2202* across the analyzed regions above background levels.

Overall, Dbp2-HTP occupancy did not change with the loss of the RSC subunits, indicating that Dbp2 binding at this locus is independent of these factors. For Rsc1 and Snf21, on the other hand, no chromatin association could be detected under our experimental conditions, neither with depletion of Dbp2 nor without. Due to its function at promoter regions in *S. cerevisiae* (André et al., 2023; Musladin et al., 2014), we assumed to also detect the

S. pombe RSC complex at promoter regions, which we could not show here. This could indicate that the experimental conditions were not suitable for the RSC complex.

4.5 Investigation of RSC and Dbp2 impact on localization

We were able to show that the RSC complex interacts with Dbp2 but that there are no detectable effects on Dbp2 occupancy on chromatin due to the loss of either of the components, at least at one representative gene that we examined. However, since the proteins are all found in the nucleoplasm, we wondered whether this localization depends on the other components, which is why we performed live cell imaging after the deletion or depletion of the individual gene or protein.

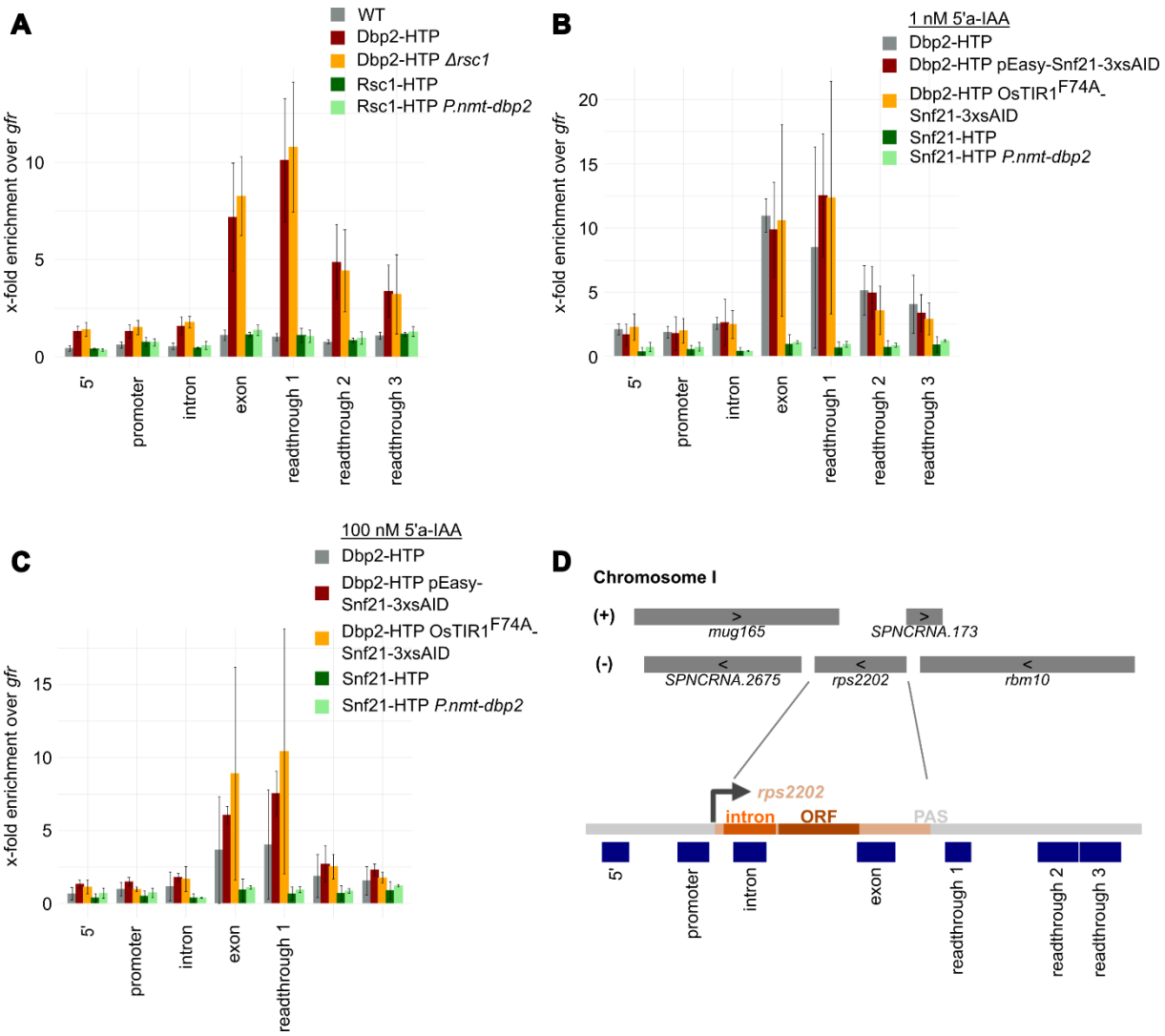

Figure 11 The loss of Rsc1 and Snf21 does not impact Dbp2 occupancy. A ChIP experiments of the indicated strains were performed with subsequent qPCR on the shown regions of *rps2202*. Dbp2 and Rsc1 occupancies with and without depletion or deletion of the other protein or gene are shown (n = 3-7). **B, C** qPCRs were performed as explained for A. The Dbp2 and Snf21 occupancies with and without depletion of Snf21 are shown. Changes in Dbp2 occupancy were tested by Snf21 depletion with both 1 nM (B) and 100 nM (C) 5'a-IAA (n = 3). Bars represent the mean ± standard deviation of independent biological replicates. **D** Schematic representation of the *rps2202* gene showing its position on Chromosome I with (sense (+) and antisense (-) strand, and the locations of the amplicons analyzed.

4.5.1 Dbp2 loss has no impact on RSC localization

First, we investigated the localization of the RSC subunits Rsc1 and Snf21 after the loss of Dbp2, which was induced by treatment with thiamine. In the wild-type background, Snf21-GFP localized to the nucleoplasm as shown before (Fig. 12). Compared to the control, there was no noticeable change in the localization of Snf21-GFP after the depletion of Dbp2 (Fig. 12A). Similar to this, Rsc1-GFP was again shown to localize in the in nucleoplasm, but there was no different localization induced by the loss of Dbp2 (Fig. 12B). In summary, the localization of RSC remains unaffected by the induced depletion of Dbp2.

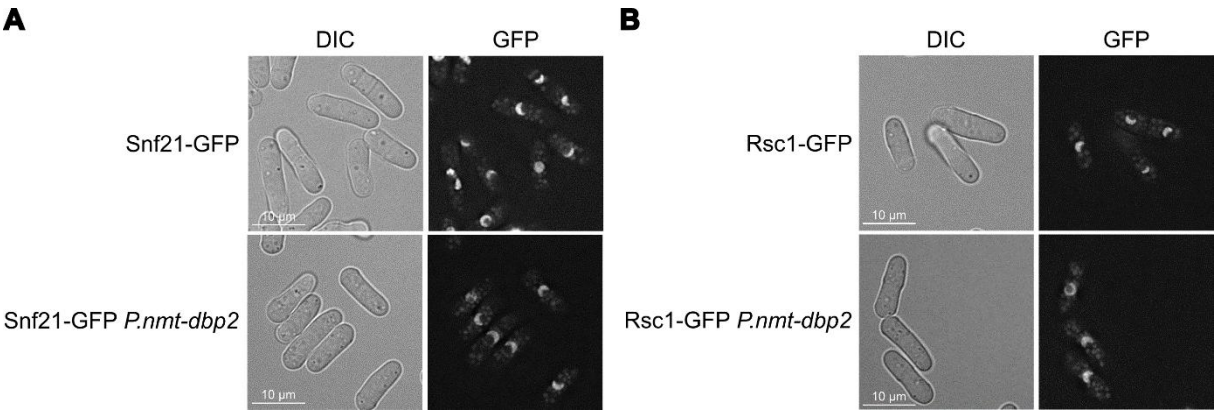

Figure 12 The depletion of Dbp2 does not affect the localization of subunits of the RSC complex. A Live-cell microscopy showing the localization of the Snf21-GFP-tagged subunit of the RSC complex with and without Dbp2 depletion. **B** Live-cell microscopy showing the localization of the Rsc1-GFP-tagged subunit of the RSC complex with and without Dbp2 depletion. The images shown are representative of three independent biological replicates.

4.5.2 RSC loss has no impact on Dbp2 localization

After investigating a possible localization change of the RSC subunits, the inverse experiment was performed for the localization of Dbp2 after the deletion or depletion of *rsc1* and Snf21. This was analyzed by tagging endogenous Dbp2 with GFP and monitoring the localization by live cell imaging. Dbp2 showed the typical localization in the nucleolus and nucleoplasm. The deletion of *rsc1* had no impact on Dbp2-GFP localization (Fig. 13A). Furthermore, the localization of Dbp2-GFP after the loss of Snf21 was investigated. Again, depletion with 1 nM as well as with 100 nM was carried out, and a time course of up to 2 h was monitored. Dbp2-GFP strains with and without the non-depleting control Snf21-3xsAID/pEasy were examined. As expected, treatment with 1 nM 5'a-IAA did not induce a change in the localization of Dbp2-GFP in these strains (Fig. 13B). Notably, the depletion of Snf21 with 1 nM 5'-IAA did also not affect the localization of Dbp2, regardless of the time considered. The same was observed when Snf21 depletion was induced by 100 nM 5'-IAA (Fig. 13C).

In summary, although we could show that Dbp2 and RSC interact with each other and co-localize in the nucleoplasm, no effects on localization were detectable. This suggests that Dbp2 is not essential for RSC localization in the nucleoplasm and vice versa. Their localization is, therefore, independent of each other.

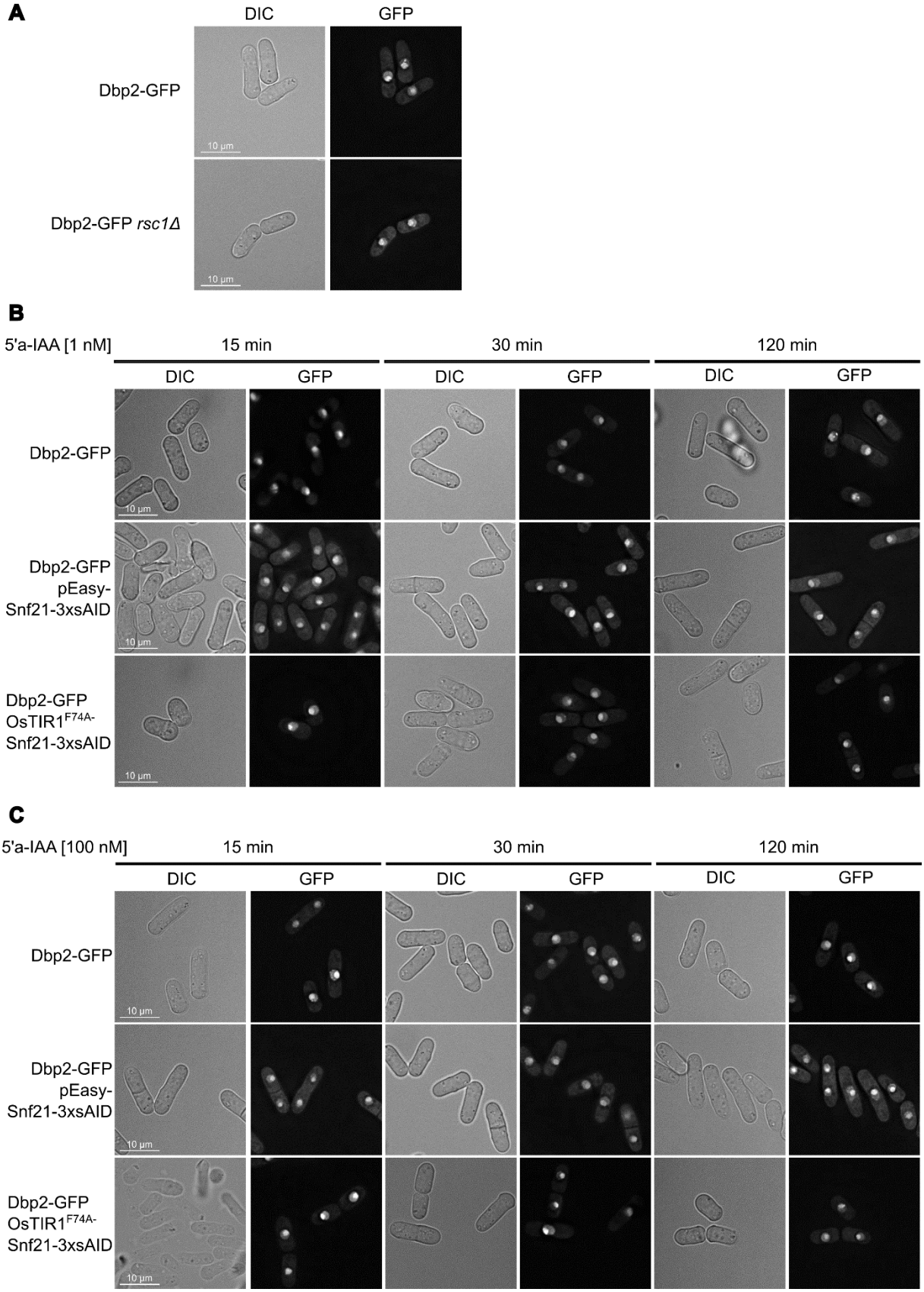

Figure 13 The loss of the RSC complex does not affect the localization of Dbp2. A Live-cell microscopy showing the localization of Dbp2-GFP with and without *rsc1* deletion. **B, C** Live-cell microscopy showing the localization of Dbp2 in Dbp2-GFP and Dbp2-GFP pEasy-Snf21-3xsAID controls and Dbp2-GFP OsTIR1^{F74A}-Snf21-3xsAID depletions using 1 nM 5'a-IAA (B) or 100 nM 5'a-IAA (C) for 15 min, 30 min, and 2 h. The images shown are representative of three independent biological replicates.

4.6 Loss of RSC partially rescues the accumulation of 3'-processed RNA in the nucleus induced by Dbp2 depletion

Dbp2 participates in an essential checkpoint in mRNA processing, and poly(A)+ mRNA accumulates on chromatin in the absence of Dbp2 (Aydin et al., 2024). Therefore, a functional connection between Dbp2 and RSC could imply that depletion of RSC subunits impairs mRNA export. To investigate whether RSC subunits impact mRNA metabolism, we employed fluorescence in situ hybridization (FISH) using a Cy3-labeled oligo(dT) probe to assess nuclear accumulation of poly(A)+ RNA. A wild-type strain was used as a control for the deletion of *rsc1* and the depletion of Dbp2, while the OsTIR1^{F74A} background was chosen as a control for the Snf21 depletion.

As a positive control, we included a heat shock sample, which efficiently obstructs mRNA export in *S. pombe* (Aydin et al., 2024). In our experiment, the heat shock control showed a strong nuclear retention of poly(A)+ mRNA in the nucleus (Fig. 14A). Our wild-type and OsTIR1^{F74A} controls also show a slightly stronger signal in the nucleus than in the cytoplasm, but the mRNA is more evenly distributed overall. The *P.nmt-dbp2* depletion showed a mixed phenotype, with poly(A)+ mRNA still detected in the cytoplasm, but for most of the cells, apparent retention of mRNA in the nucleus was observed. No effect for the single or additional loss of the RSC subunits was visible by eye, so a quantification was carried out to calculate the poly(A)+ signal ratio in the nucleus over the cytoplasm. Here, the heat shock treatment showed strong nuclear retention with a mean ratio of fluorescence intensities of the nucleus over the cytoplasm of 2.8 (Fig. 14B). The quantification revealed the previously observed comparatively even distribution of poly(A)+ mRNA in the cytoplasm and nucleus of wild-type and OsTIR1^{F74A} cells with a ratio of 1.3 and 1.4, respectively.

The observed nuclear retention caused by the loss of Dbp2 was significant, with a ratio of 1.7; at the same time, the high phenotypic variability of this sample became visible in the quantification. Interestingly, the deletion of *rsc1* had the opposite effect, showing a lower ratio compared to the wild-type. Depletion of Snf21 also did not result in mRNA retention. Intriguingly, the additional loss of RSC components partially rescued the mRNA export defect caused by Dbp2 depletion, and the variability in the *P.nmt-dbp2* cells is lost.

In summary, our FISH analysis confirmed the previously reported nuclear retention of mRNA in the absence of Dbp2 (Aydin et al., 2024), whereas depletion of the RSC subunits Rsc1 and Snf21 did not lead to notable nuclear accumulation of polyadenylated transcripts.

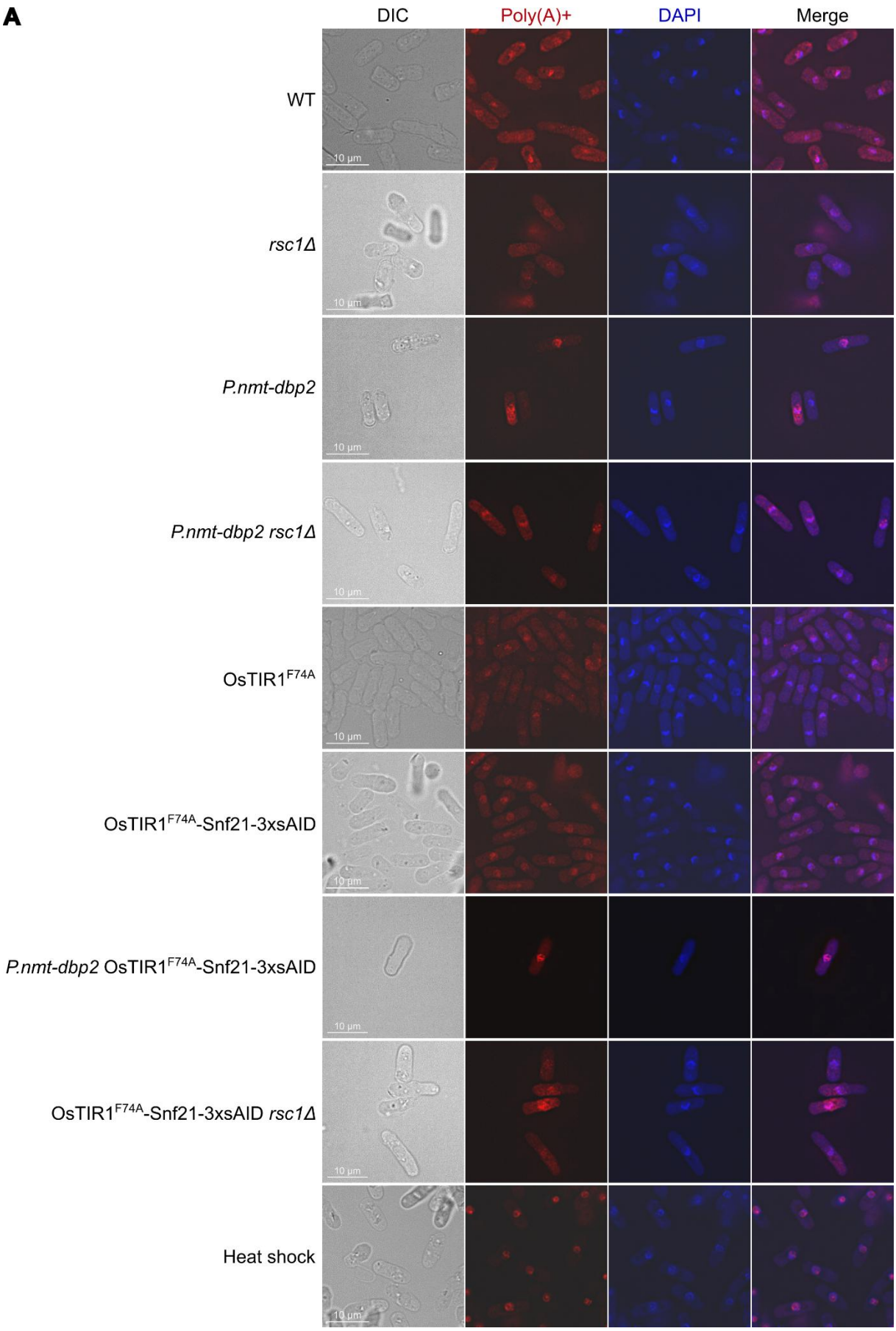
A
DIC
Poly(A)+
DAPI
Merge
WT
rsc1Δ
P.nmt-dbp2
P.nmt-dbp2 rsc1Δ
OsTIR1F74A
OsTIR1F74A-Snf21-3xsAID
P.nmt-dbp2 OsTIR1F74A-Snf21-3xsAID
OsTIR1F74A-Snf21-3xsAID rsc1Δ
Heat shock
10 μm

B

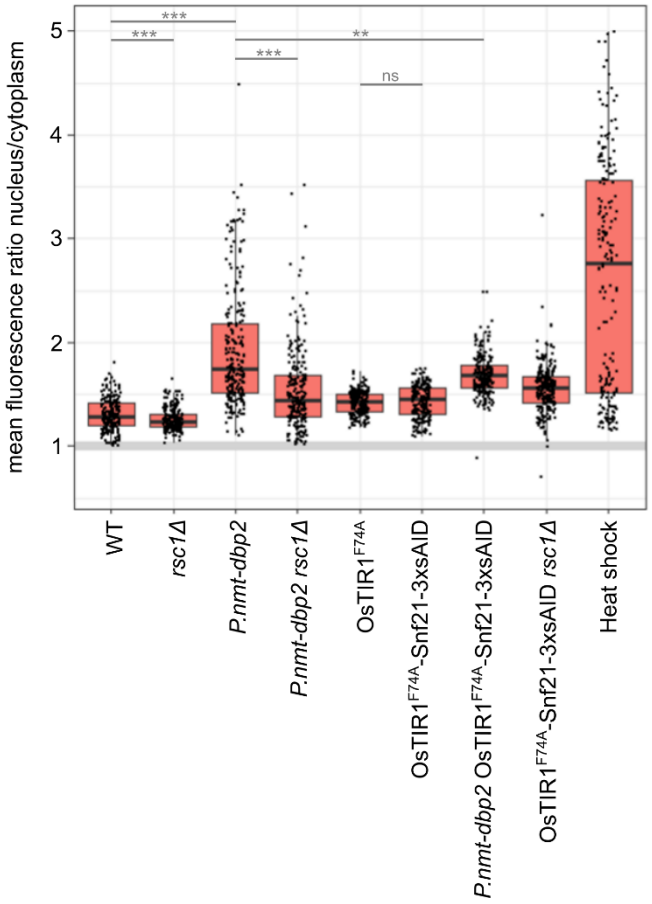

Figure 14 Rsc1 and Snf21 loss partially rescue the mRNA export defect caused by Dbp2 loss. **A** Fluorescence in-situ hybridization against poly(A)+ RNA (red) and DAPI (blue) to stain the DNA. The *P.nmt-dbp2* depletion shows a retention of bulk mRNA, which is slightly rescued by additional loss of Rsc1 and Snf21. The images shown are representative of two independent biological replicates with ~ 100 cells each. **B** Quantification of the nuclear/cytoplasmic fluorescence signal. The black lines show the mean value. The p-values were calculated using the Wilcoxon test with *** $p \leq 0.001$; ** $p \leq 0.01$, and ns = not significant.

4.7 The diffusion rate of Snf21 is independent of Dbp2

We have seen that chromatin remodeling factors appear to be enriched on mRNA in the absence of Dbp2 (Fig. 6B). This finding suggested an increased interaction between mRNA and chromatin in the absence of Dbp2, but the precise nature and directionality of this association remained unclear. To clarify the mechanism, we conducted fluorescence recovery after photobleaching (FRAP) experiments in collaboration with the Diepold lab (MPI Marburg). As the name suggests, in live-cell microscopy of cells with a fluorescently tagged protein, a region of interest is bleached out with a laser. This leads to a loss of fluorescence signal in this region. It can then be observed how long it takes for tagged proteins to diffuse back into this region, and this time can be measured, indicating the underlying kinetics.

Our idea was to investigate whether depletion of Dbp2 led to a change in the kinetics of GFP-tagged Snf21. We hypothesized that Snf21, as a chromatin remodeler subunit, is localized at chromatin and that its diffusion rate is low. If the increased RNA association of Snf21 upon depletion of Dbp2 was accompanied by a dislocation from chromatin, this would then be evident from a change in the diffusion rate. In addition, Cbc2-GFP was used as a marker for mRNA, and the same experiment was carried out. We assumed that Cbc2 has a higher diffusion activity. If the depletion of Dbp2 resulted in slower diffusion, this would provide evidence that Cbc2, as an indicator for mRNA, is attached to chromatin.

Three images were taken before bleaching to be able to normalize to the initial intensity, one of which is shown as an example. The following image represents the bleaching step. We were able to demonstrate that for all strains, the bleaching of a region of interest was successful, as evidenced by a decrease in fluorescence intensity (Fig. 15A). The intensity in the bleached region of interest dropped sharply with bleaching and then steadily recovered (Fig. 15B). For all strains, the bleached region was very quickly restored in shape within seconds, with the intensity not returning to its initial level, as expected. In this respect, no difference in the diffusion rate after depletion of Dbp2 could be identified for Cbc2-GFP and Snf21-GFP. The signal intensity of the GFP-tagged proteins in non-bleached areas also decreased after bleaching. In contrast to the bleached region, however, the fluorescence intensity in this area continues to decline slightly afterward. These two observations show that GFP-tagged proteins diffuse into the bleached region and that this occurs by replacing them with proteins from the non-bleached region. To investigate and compare changes in kinetics, we calculated the time it takes for each cell to reach 50% of the maximum final intensities again. Here, the observation that there is no kinetic difference due to the depletion of Dbp2 for either Cbc2-GFP or Snf21-GFP was confirmed (Fig. 15C). Overall, however, it is important to emphasize that the recovery speed was very high for all samples. The single observation worth pointing out is that the diffusion rate of Snf21-GFP was lower than that of Cbc2-GFP, namely about 6.5 s instead of 4.5 s. This could be related to the function of the RSC complex in chromatin binding.

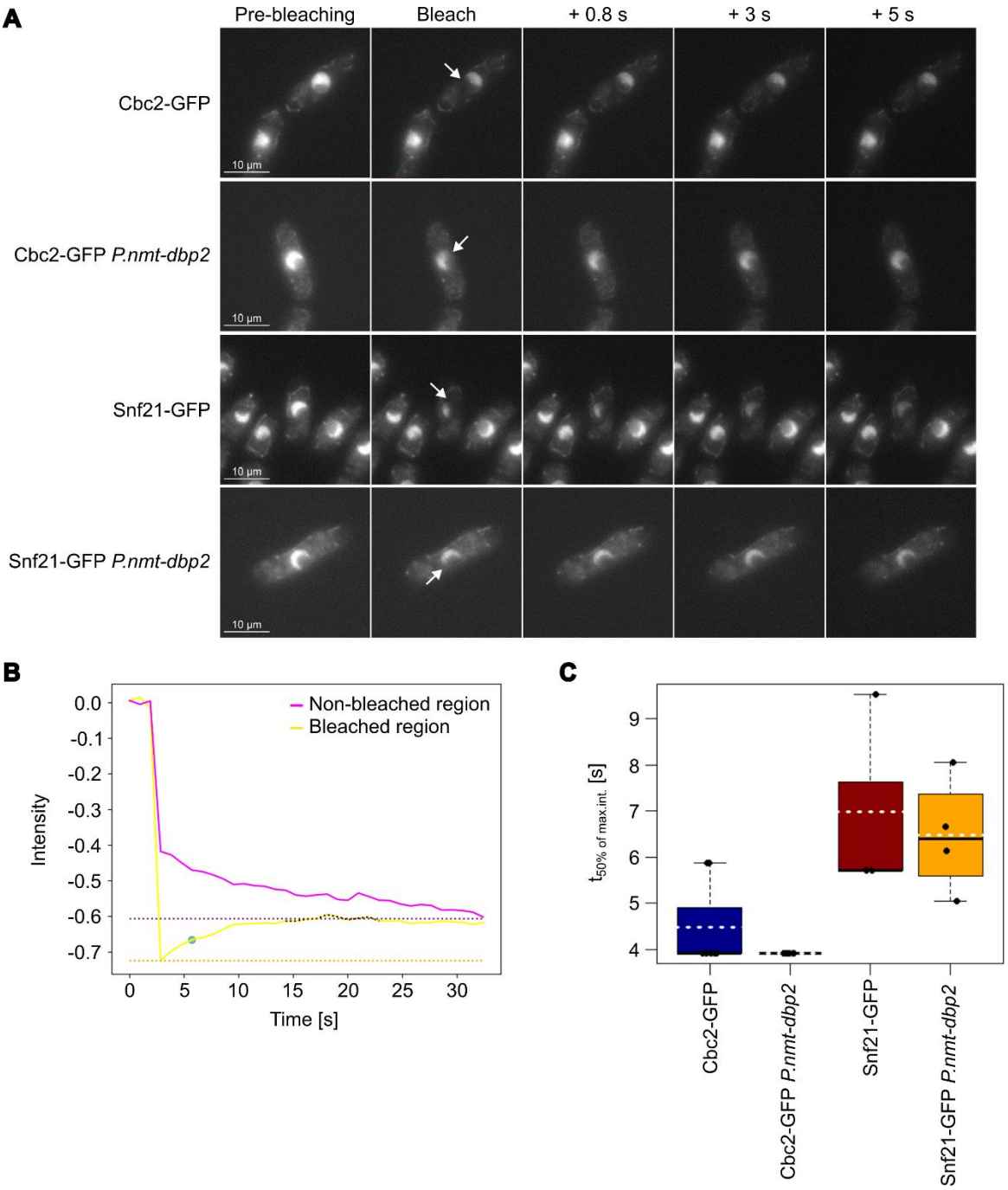

Figure 15 Cbc2 and Snf21 show a fast diffusion rate independent of Dbp2. A Live-cell microscopy of fluorescence recovery after photobleaching experiments on Cbc2-GFP as an indicator for nuclear RNPs and Snf21-GFP as an indicator for the RSC complex with and without Dbp2 depletion. An exemplary picture before bleaching is shown, as well as the time of bleaching and pictures of ~ 0.3 s, 3 s, and 5 s after bleaching. Arrows indicate the bleached region of interest. All samples show a rapid recovery after bleaching. **B** Exemplary representation of the fluorescence intensities within the bleached region (yellow) compared to the non-bleached region (pink) using the example of a Snf21-GFP sample. The dotted lines show the maximum (purple) and minimum intensity (orange). The calculated time for recovery of 50% of the maximum intensity is shown (green dot). **C** Quantification shows the time needed to recover 50% of the maximum final intensities for each cell. The black line represents the median, while the dashed line shows the mean value (n = 3-8).

4.8 Identification of potential RSC target genes

In addition to investigating the interaction between the RSC complex and Dbp2, this study aimed to further characterize the chromatin remodeling complex RSC. To this end, a PolII-ChIP followed by sequencing was carried out to measure the *in vivo* association of RNA polymerase II with chromatin in order to map the actively transcribed genes and compare the transcription levels by quantification. The experiment compared *rsc1Δ* with the wild-type control and the Snf21 depletion strain OsTIR1^{F74A}-Snf21-3xsAID with the corresponding background control strain OsTIR1^{F74A}.

4.8.1 The RSC complex shows gene-specific effects on gene expression

First, we carried out a principal component analysis to show the samples' differences or similarities. As expected, the duplicates behaved very similarly to each other, and both control strains also showed similar patterns (Fig. 16A). In contrast, the *rsc1Δ* strains and the OsTIR1^{F74A}-Snf21-3xsAID strains were very different from one another, and from the respective controls. When analyzing the sequencing results, we first looked at the *rsc1* and *snf21* genes to validate our deletion and gene tagging, respectively. As expected, the *rsc1* gene was similarly present in all input DNA samples, except for the *rsc1Δ* sample, where no reads mapped to the deleted region, confirming the deletion (Fig. 16C). This proves the successful removal of the *rsc1* gene in this strain. We also looked at the *snf21* gene. Since, in this case, the gene is not deleted, but merely the protein is depleted, gene transcription in the OsTIR1^{F74A}-Snf21-3xsAID strain was similar to that in the other samples (Fig. 16D). In cells where *snf21* is C-terminally tagged with 3xAID, we observed an apparent drop in signal over the modified region in both the input and IP samples. This likely reflects the genomic alteration introduced by the tag, which replaces a portion of the original sequence. The apparent gap corresponds to the genomic sequence replaced during integration of the tagging cassette. Moreover, during depletion conditions, *snf21* transcription appears to be upregulated, possibly reflecting a compensatory response. Overall, we demonstrated the successful implementation of the ChIP-Seq protocol and confirmed the loss of the RSC subunits.

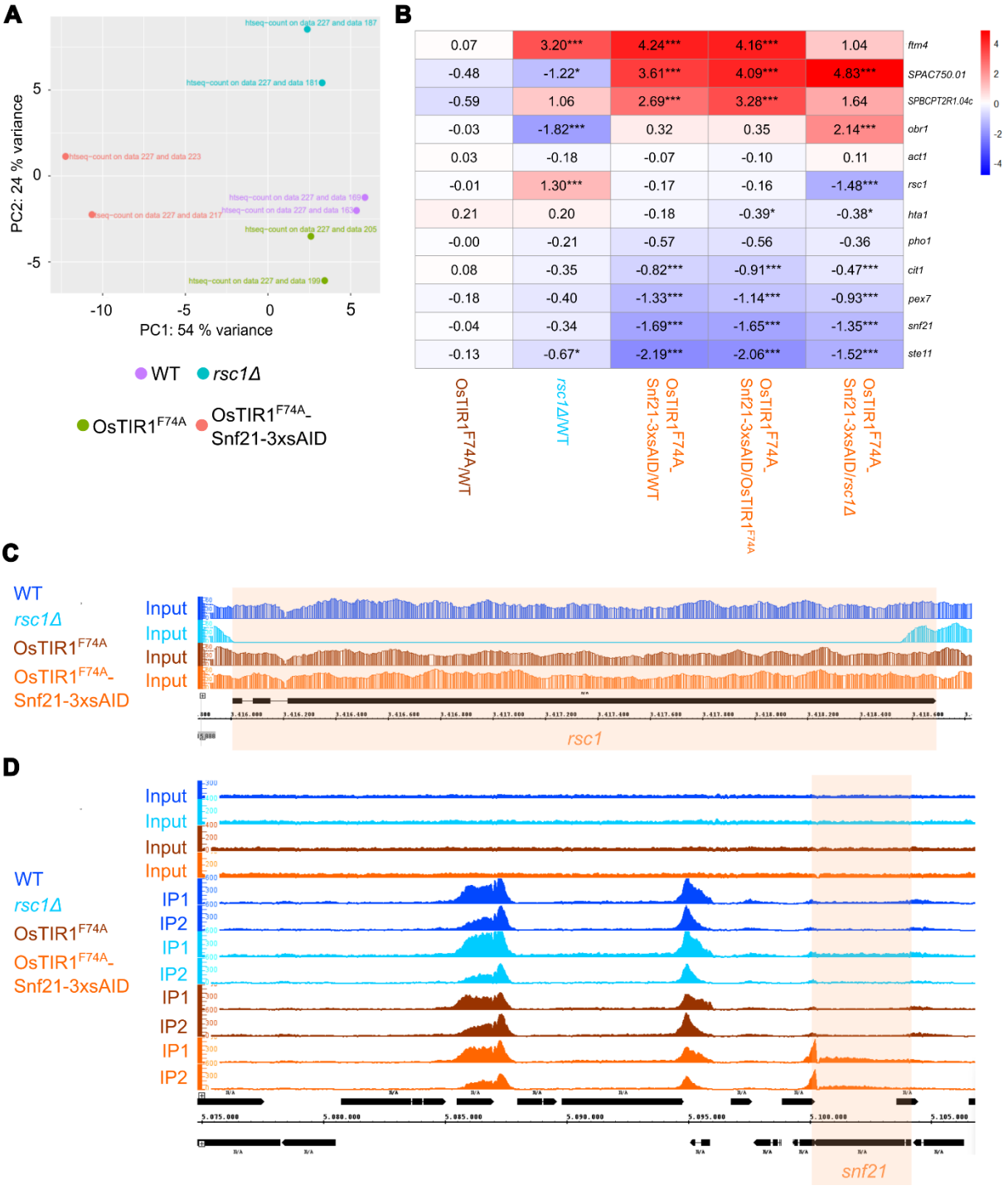

Figure 16 Verification of the deletion of *rsc1* and depletion of Snf21. A The principal component analysis after PolII-ChIP-Seq shows the comparability of the duplicates and the difference between the RSC-deficient samples and their respective controls. **B** Log_2 fold changes of the analyzed genes for Pol Ⅱ binding across multiple strains relative to the specified reference strain, as determined by DESeq2. Statistical significance is indicated by asterisks based on the false discovery rate (FDR): * FDR < 0.05, *** FDR < 0.001. **C** In contrast to all other strains, there is no transcription activity of the *rsc1* gene (highlighted region) in the *rsc1Δ* samples. **D** Validation of the *rsc1* gene (highlighted region) deletion in the *rsc1Δ* samples. **D** There is a difference in transcription in the C-terminal region of *snf21* (highlighted region) in the Snf21-3xsAID-tagged strains.

We then asked which potential target genes have been previously identified for the RSC complex and whether we can verify them using our data. Previous studies showed that the transcription factor *ste11* is a target gene of the RSC complex in *S. pombe* (Materne et al.,

2016). Their conclusion was based on chromatin immunoprecipitation followed by quantitative PCR, which demonstrated direct binding of RSC components to the *ste11* promoter region, as well as gene expression analyses indicating that RSC is required for *ste11* activation. In contrast, our approach examines changes in transcriptional activity via PolII occupancy following the loss of RSC subunits Rsc1 and Snf21. We observed an increase in transcriptional activity at the *ste11* locus upon deletion of these subunits (Fig. 17A). The previous study compared inducing versus non-induced conditions and observed reduced induction in the absence of RSC, leading to the conclusion that RSC is required for *ste11* activation (Materne et al., 2016). In contrast, we compared non-induced RSC mutants to non-induced wild-type cells and observed elevated basal transcription of *ste11*. This suggests that, under non-inducing conditions, RSC normally represses *ste11*, and that its absence leads to derepression or constitutive activation rather than a failure to activate. Consequently, the observed differences primarily reflect altered basal transcription, while the relative fold increase upon induction would be expected to be similar. Another published target gene of the RSC complex in *S. cerevisiae* is the histone-encoding gene *hta1* (Libuda and Winston, 2006), as it was shown that the RSC interaction with the *hta1* promoter depends on corepressors and is related to the repression of transcription (Ng et al., 2002). In our *S. pombe* data, we could not detect any differences in *hta1* transcriptional activity after deletion of *rsc1* or depletion of Snf21 compared to controls (Fig. 17B). Thus, in contrast to results in budding yeast, the fission yeast RSC complex does not seem to play a role in *hta1* activation or repression. In addition to *hta1*, the publication also identified *cit1* as a target gene of the RSC complex (Ng et al., 2002), which encodes a protein involved in citrate metabolism (Lee et al., 2007). In our data sets, differential expression analysis revealed a modest increase in transcription of almost 2-fold after depletion of Snf21 (Fig. 16B), which implies that the RSC complex is somewhat responsible for the repression of the gene in *S. pombe* as well. The same group also identified *act1*, which encodes the essential cytoskeletal protein actin (Wertman et al., 1992), as a gene not associated with the RSC complex (Ng et al., 2002). In *S. pombe*, we could not detect any differences in the transcriptional activity of this gene after loss of the RSC subunits compared to their controls; suggesting that *act1* expression is not regulated by the RSC complex in either yeast species.

Overall, our sequencing results have so far confirmed a previously published target gene of the RSC complex, namely *ste11*, although we found opposing functions in terms of activation or repression. Surprisingly, for an essential chromatin remodeler that has been reported to be required to keep promoters nucleosome-depleted, the RSC complex shows very few global effects on transcription but appears to act in a very gene-specific manner (Fig. 16B).

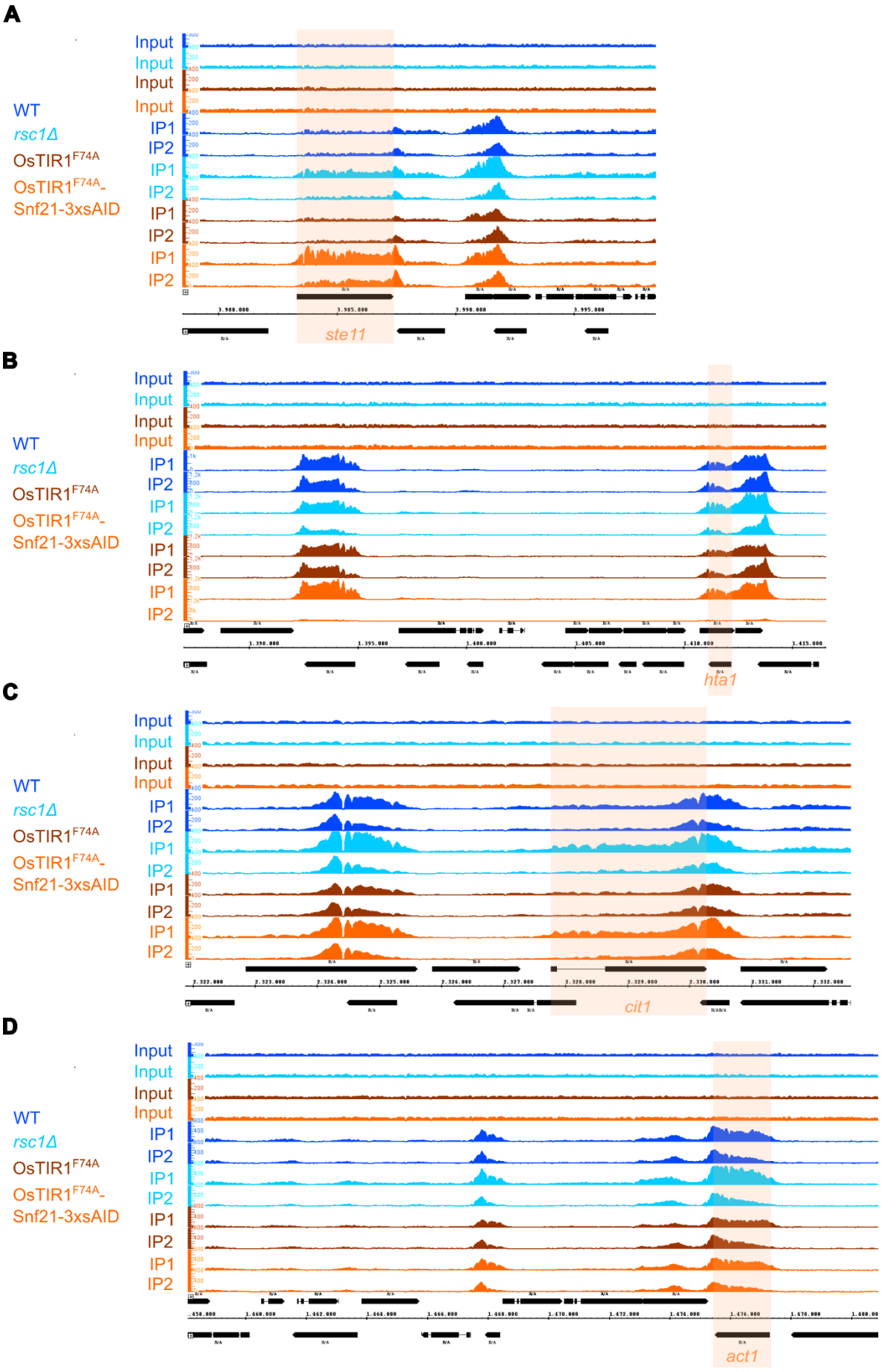
A
WT
rsc1Δ
OsTIR1F74A
OsTIR1F74A-Snf21-3xsAID
Input
Input
Input
Input
IP1
IP2
IP1
IP2
IP1
IP2
IP1
IP2
ste11
B
WT
rsc1Δ
OsTIR1F74A
OsTIR1F74A-Snf21-3xsAID
Input
Input
Input
Input
IP1
IP2
IP1
IP2
IP1
IP2
IP1
IP2
hta1
C
WT
rsc1Δ
OsTIR1F74A
OsTIR1F74A-Snf21-3xsAID
Input
Input
Input
Input
IP1
IP2
IP1
IP2
IP1
IP2
IP1
IP2
cit1
D
WT
rsc1Δ
OsTIR1F74A
OsTIR1F74A-Snf21-3xsAID
Input
Input
Input
Input
IP1
IP2
IP1
IP2
IP1
IP2
IP1
IP2
act1

Figure 17 Identification of potential target genes of the RSC complex. A Rsc1 and Snf21 are necessary to repress *ste11* (highlighted region). **B** The transcription activity of *hta1* (highlighted region) is independent of Rsc1 and Snf21. **C** Rsc1 and Snf21 are needed for the repression of *cit1* (highlighted region). **D** The transcription activity of *act1* (highlighted region) is independent of Rsc1 and Snf21.

4.8.2 The RSC complex shares several target genes with the SWI/SNF complex, having the opposite regulatory effect

Since the RSC and SWI/SNF complexes belong to the same family, we asked whether these complexes also share target genes. Therefore, we compared different published target genes of the SWI/SNF complex in *S. pombe* with our sequencing data. First, we looked at the gene *obr1*, which encodes a protein with oxidoreductase function, whose physiological role is not yet fully understood, and where the SWI/SNF complex has been shown to be necessary for the activation of gene expression (Monahan et al., 2008). Most interestingly, our data revealed different outcomes after loss of Rsc1 and Snf21. For example, transcriptional activity increased strongly after deletion of *rsc1*, whereas after depletion of Snf21, it showed no difference to the already low transcriptional activity in the control (Fig. 18A). This suggests that Rsc1 is required for repression of the gene, whereas the essential subunit Snf21 has no function for *obr1*. The gene *pex7*, which codes for a peroxisomal assembly protein, was also identified as a target gene on whose expression the SWI/SNF complex has an activating effect (Monahan et al., 2008). In contrast to *obr1*, removing both subunits of the RSC complex had the same effect, which was significantly stronger for Snf21 than for Rsc1. After the loss of both Rsc1 and Snf21, *pex7* expression levels increased compared to controls (Fig. 18B), indicating that the RSC subunits target *pex7* but act as repressors of the gene.

As the last known target gene of the SWI/SNF complex, we considered *pho1*, which encodes a protein with hydrolysis activity and whose transcriptional activity is likewise activated by the RSC complex (Monahan et al., 2008). In contrast to the previously investigated genes, our data showed no difference after the deletion of *rsc1* and depletion of Snf21 on the transcription of *pho1,* although we find the neighbouring gene, *pho84*, upregulated in both RSC mutants (Fig. 18C). This suggests that *pho1* is a target of the SWI/SNF complex but not a target gene of the RSC complex.

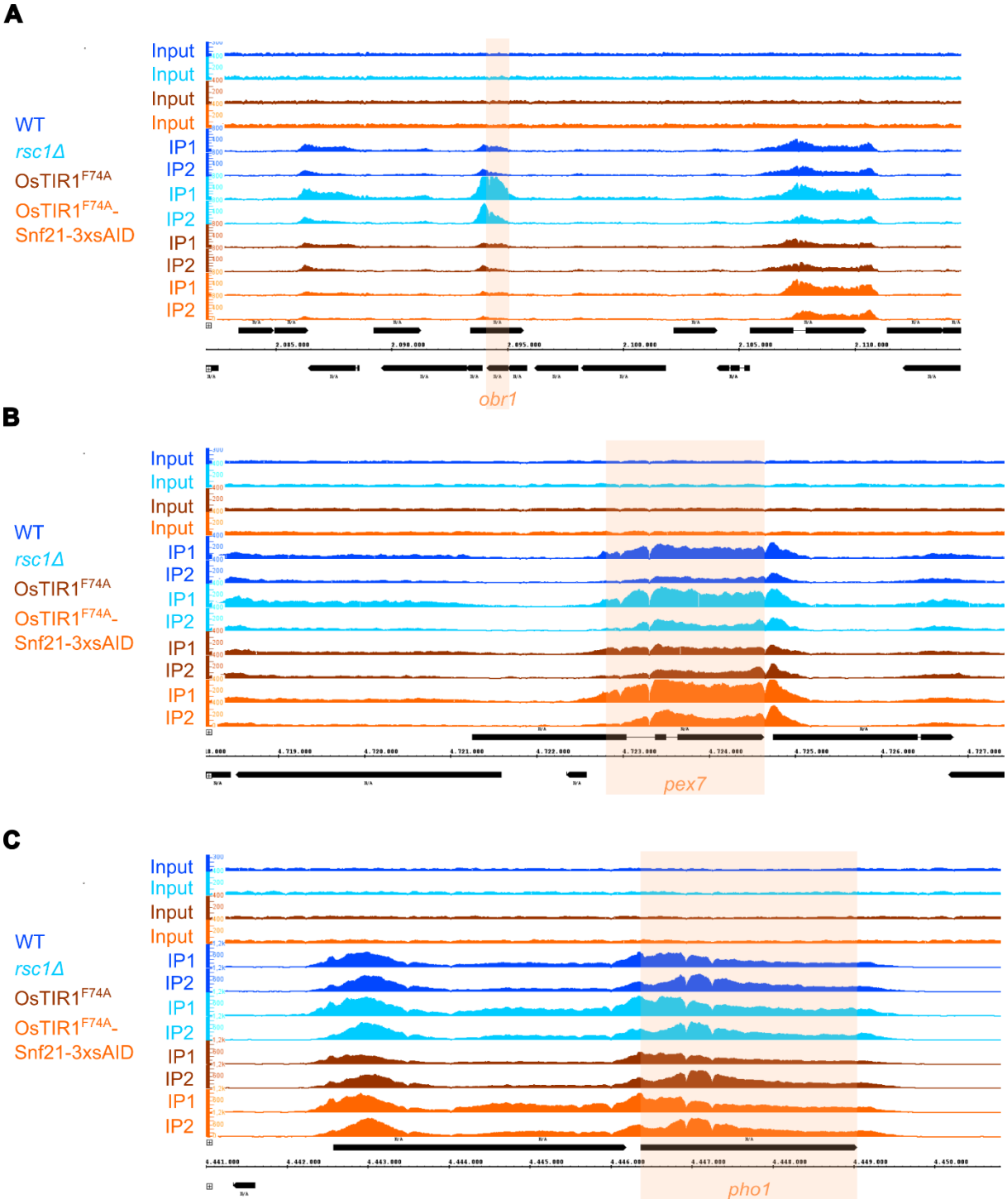

Figure 18 Rsc1 and Snf21 share target genes with the SWI/SNF complex, on which they have the opposite regulatory function. A Rsc1 but not Snf21 is necessary for *obr1* (highlighted region) repression. **B** *pex7* (highlighted region) is a target gene for repression by Rsc1 and Snf21. **C** The transcription activity of *pho1* (highlighted region) is independent of Rsc1 and Snf21.

In summary, we were able to show that RSC appears to share a few target genes with SWI/SNF, namely *obr1* and *pho1*, and some target genes are unique targets of the SWI/SNF complex, particularly *pex7*. In addition, the RSC subunits show partial contrary effects on the

activation or repression of the gene, and, in general, the RSC seems to act in opposition to the SWI/SNF complex.

4.8.3 Subtelomeric regions are targets of the RSC complex

After we had shown that the RSC complex has surprisingly few global effects but relatively gene-specific ones with a rather repressive effect, we asked ourselves which genes are targets for an activating role of the complex. Looking at the PolII-ChIP sequencing results, we noticed that particularly the subtelomeric regions of the chromosomes contained gene segments that showed a decrease in transcriptional activity after the loss of Rsc1 and Snf21. In the subtelomeric region of chromosome I, there were once again genes that showed different effects after loss of Rsc1 and Snf21. Thus, in *SPAC750.01*, there is more robust activity after the loss of Rsc1 and reduced transcriptional activity after the loss of Snf21 (Fig. 19A). This shows that this gene is a target of the RSC complex and is mainly activated by the essential subunit Snf21. Similarly, the transcription of *ftm4* is also activated by the RSC complex, as a significant decrease in PolII activity is detectable in the absence of the RSC complex, which becomes even more evident by looking at the transcription in detail (Fig. 19C). Similar effects can also be seen in the subtelomeric regions of chromosome II. The gene *SPBPB2B2.19c* also appears to require the RSC complex for transcriptional activation, as both the deletion of *rsc1* and the depletion of Snf21 result in a substantial drop in gene expression (Fig. 19B). Interestingly, some genes react differently to the loss of the two subunits, for example *SPBCPT2R1.04c*. In this case, *rsc1Δ* causes no change, while Snf21 appears crucial for transcription.

In summary, we were able to show that target genes for the activating effect of the RSC complex are mainly located in the sub-telomeric region of chromosome I and chromosome II. Even though the RSC subunits also showed different effects here, the overall effect is more activating compared to the previously analyzed genes.

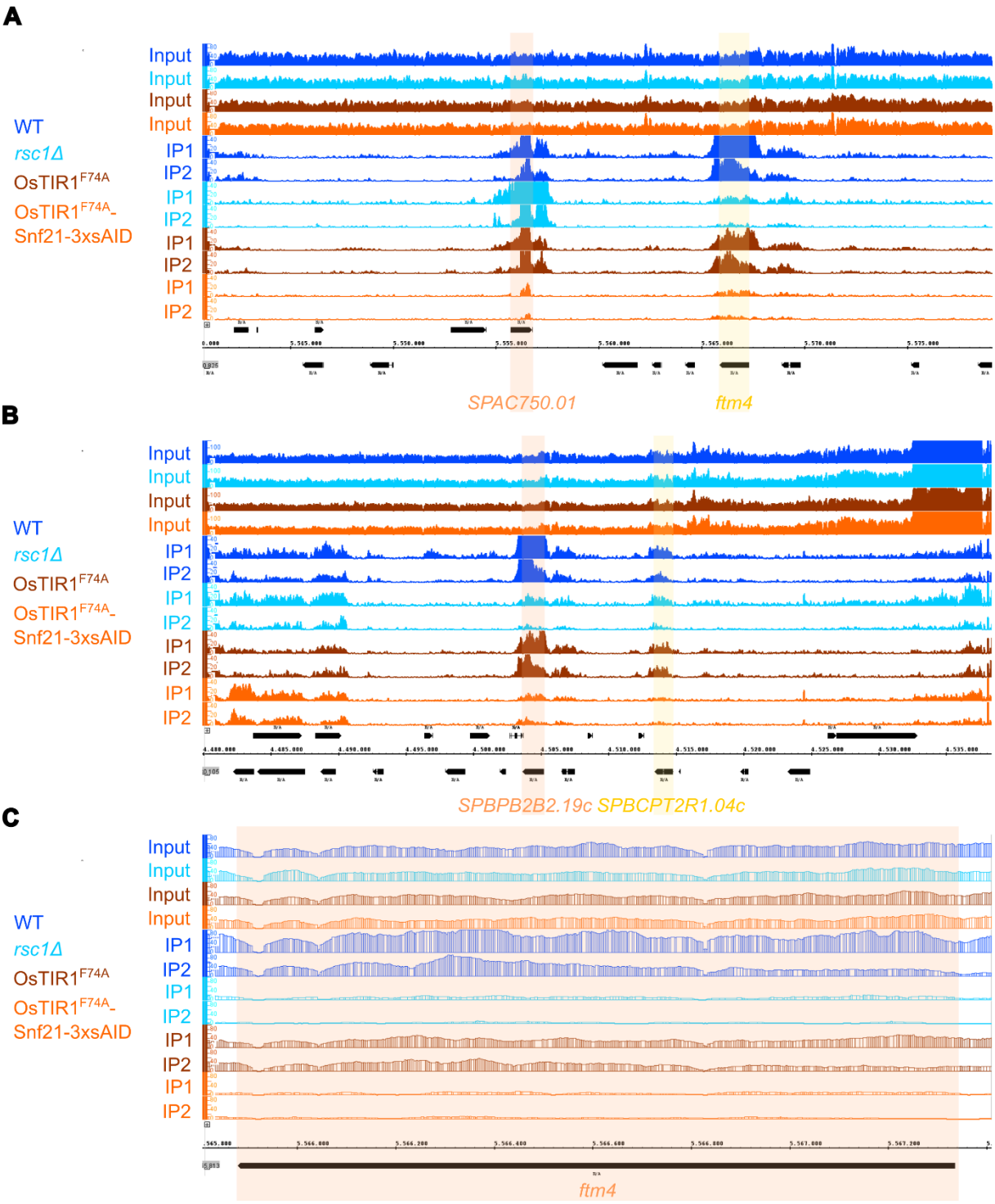

Figure 19 Target genes of the RSC complex are primarily located in the subtelomeric regions of chromosomes I and II. A Target genes on chromosome I show an activating (*ftm4*, yellow) or divergent (SPAC750.01, orange) function of the RSC complex on gene transcription. **B** The target genes *SPBPB2B2.19c* and *SPBCPT2R1.04c* on chromosome II show an activating function of the RSC complex on gene transcription. **C** Detailed transcription activity of *ftm4* from A.

5 Discussion

5.1 The optimized 5'a-IAA depletion system efficiently induces loss of the essential RSC subunit Snf21

Depletion systems are a valuable and frequently employed tool for investigating proteins. In recent years, the CRISPR/Cas9 system has become increasingly popular for introducing a genetic deletion or mutation (Yang et al., 2021). In contrast, transient expression systems can also be used, in which the stability of a target protein can be influenced by the overexpression of inhibitors (Gaykema et al., 2022). Particularly to examine the effect of losing an essential protein, systems with inducible depletion of the target protein must be applied, as genetically stable deletion of a crucial gene would lead to non-viable cells. One of the most prominent depletion systems nowadays is the so-called Auxin-Inducible Degron (AID) system, where the plant hormone auxin triggers the degradation of an AID-tagged protein by the E3 ubiquitin ligase Skp1-Cullin 1-F-box (SCF) complex. A major advantage of this system is the rapid induction of protein loss, which allows the temporal course of cellular processes to be analyzed. In addition, depletion can be controlled precisely, and protein expression can resume after removing the auxin to restore normal function. In addition to the ability to deplete vital proteins, another advantage is that the in vivo study of dynamic processes such as cell differentiation, cell cycle, and genome organization becomes feasible. However, this depletion system also has disadvantages. In particular, a high auxin concentration and long exposure time can have a cytotoxic effect, and there is the possibility of off-target effects, which makes the use of controls important. This Auxin-inducible Degron system has recently been further developed and optimized using a combination of 5-adamantyl indole-3-acetic acid (5'a-IAA) instead of auxin with the binding pocket mutant $TIR1^{F79A}$ to accommodate the bulky auxin analogue. This provides much higher binding stability, the use of a modest concentration, the possibility of employing a tiny tag, and the utilization of endogenous proteins that trigger depletion (Yesbolatova et al., 2020).

The present study investigated the loss of the RSC subunits Rsc1 and Snf21 and the loss of the RNA helicase Dbp2. Since Rsc1 is not an essential protein in *S. pombe*, the gene encoding Rsc1 was deleted. In addition to metabolic depletion using auxin, depletion using thiamine was also used, where thiamine inhibits a target promoter, leading to a halt in its gene expression and thus resulting in the loss of the target protein (Siam et al., 2004). We have successfully used this system for Dbp2 depletion before (Aydin et al., 2024). Thus, it was also employed in the current study to induce Dbp2 loss. First, we sought to identify successful conditions for depletion of our proteins of interest. Therefore, initially, the standard method of depletion using NAA (Nishimura et al., 2009) was compared with the modified usage of 5'a-IAA (Watson et al., 2021, and Zhang et al., 2022) and adjusted to our protein of interest. For a previously examined

essential protein, namely Dbp5, both systems were compared and investigated with their respective controls in a plate-based growth assay. It became evident that both depletion systems induced a growth defect (Supplement Fig. 1A, Supplement Fig. 1C). Depletion was also monitored at the protein level, revealing that only the optimized usage of the auxin analog 5'a-IAA led to a depletion of the target protein under the parameters used. In contrast, with the conventional method using the unmodified F-box protein OsTIR1, no decrease in protein levels was observed with either 50 µM or 500 µM NAA (Supplement Fig. 1B, Supplement Fig. 1D). Compared to a control strain, a reduction in Dbp5 protein levels was achieved with 100 nM 5'a-IAA after only 15 minutes, with nearly complete depletion observed after 30 minutes. Thus, depletion could only be achieved using the modified 5'a-IAA system, even with a modest concentration and in a short period. Since the adapted 5'a-IAA depletion system showed the most promising results in these previous experiments, a potential depletion of the target protein of this study, namely Snf21, was also examined using this system. For this purpose, a depletion strain in which Snf21 was tagged with three copies of a small AID tag was generated in the OsTIR1^{F74A} background. Additionally, various controls were examined to exclude that any observed depletion was solely due to using 5'a-IAA, the OsTIR1^{F74A} background, or the sAID tag itself. Successful Snf21 depletion was demonstrated with 1 nM and 100 nM 5'a-IAA after only 15 minutes (Fig. 7).

To recapitulate, the initial part of this study outlined several depletion systems for analyzing target proteins. Of particular interest is the previously established inducible 5'a-IAA system with constitutive expression of OsTIR1^{F74A} (Zhang et al., 2022) in *S. pombe*. This system enables the study of the loss of essential proteins that cannot be degraded by conventional auxin depletion or other depletion systems. Additionally, a modest concentration is sufficient, and no side effects on controls are observed. In contrast, high NAA concentrations were shown to impact control strains (Kanke et al., 2011). Another significant advantage is the short timeframe required for depletion. Since this has already been demonstrated for Snf21 and Dbp5, it is plausible that the low concentration and short duration may also be sufficient for other proteins. Switching to the system shown here may be advantageous for proteins that can be depleted using other systems, as many depletion systems require high concentrations or a much more extended treatment period (Aydin et al., 2024).). In the present system, only the F-box protein OsTIR1^{F74A} is introduced into the organism. At the same time, other auxin systems may require the additional introduction of Skp1 proteins, which can lead to higher toxicity and other side effects (Kanke et al., 2011). Furthermore, the depletion of the target protein persists for several hours, even after a single administration, without any observed reappearance of the protein.

5.2 The chromatin remodeler RSC interacts with the RNA helicase Dbp2

In our Co-IP experiments, Snf21 and Dbp2 were found to co-purify, indicating an association between these proteins. However, this does not necessarily reflect a direct physical interaction, as co-purification could be mediated by other proteins or nucleic acids. Nuclease treatment could be used to test whether RNA or DNA contributes to the observed association. Based on fluorescence microscopy, both Dbp2 and RSC subunits are present in the nucleoplasm, making it a plausible compartment for the interaction. Interestingly, the association is somewhat unexpected given their canonical genomic localization: RSC is primarily associated with promoter regions (Monahan et al., 2008), whereas Dbp2 is associated with transcribed genes, with a tendency for enrichment toward the 3′ ends (Aydin et al., 2024). This suggests that additional mechanisms may facilitate their encounter *in vivo*.

The reliability of Co-IP results is frequently debated due to concerns regarding contaminants and false positive interactions (Dwane and Kiely, 2011). To counteract this and strengthen the confidence in the results, a second, reverse Co-IP was carried out in which the RSC components were purified instead of Dbp2. This purification was additionally carried out using a different tag, namely HTP, and thus also with other beads. Again, detecting the corresponding tags in the single and double-tagged strains was confirmed for the input controls (Fig. 9B, left). In this case, the purification was conducted with protein A beads, which can be seen by an increase in the strength of the HTP signal after purification (Fig. 9B, right). The successful loss of non-specific binding was also evidenced here by the washing out of tubulin. It should be emphasized that the interactor Dbp2 could be detected together with Snf21 as well as together with Rsc1. This confirms the result of the previous Co-IP and provides further confidence in the result that Snf21 interacts with Dbp2. Although no statement on the interaction between Rsc1 and Dbp2 could be made in the previous Co-IP, the second Co-IP suggests that Dbp2 interacts with both RSC components, Snf21 and Rsc1. This discrepancy may reflect differences in the sensitivity or specificity of the purification methods used. The initial Co-IP relying on GFP-tag purification might have missed a weaker or more transient interaction with Rsc1, while the use of the HTP tag and protein A beads in the second Co-IP could capture such interactions more effectively. Alternatively, the interaction between Dbp2 and Rsc1 could be indirect or mediated through other components of the RSC complex, resulting in variable detectability depending on experimental conditions. These possibilities highlight the complexity of protein interactions within chromatin remodeling complexes and underscore the importance of using complementary approaches to validate such interactions.

After we successfully showed that Dbp2 interacts with components of the RSC complex, we asked ourselves which cell compartments the individual proteins are located in and in which area of the cell the interaction between them occurs. This could be directly addressed in future

studies using a split-YFP system, which allows visualization of protein–protein interactions in living cells (Hu et al., 2002). We showed that Rsc1 and Snf21 are localized in a crescent-shaped area that corresponds to the DNA-containing nucleoplasm in *S. pombe* (Matsuda et al., 2015; Sakai et al., 2021). Localization of Snf21 to the nucleus has previously been reported (Yamada et al., 2008). Here, we further clarify that both Rsc1 and Snf21 localize to the nucleoplasm, which aligns with the RSC complex's function in maintaining the nucleosome-free regions in promoter areas of genes (Ye et al., 2019). In contrast, Dbp2 is distributed throughout the nucleus, with significant accumulation in the nucleolus (Fig. 10), as has been previously reported (Aydin et al., 2024; Matsuyama et al., 2006). The localization of Dbp2 in the nucleoplasm reflects its function in transcription, splicing, and nuclear mRNA export, while the enrichment in the nucleolus may be due to its function in ribosomal RNA biogenesis (Xing et al., 2019). The overlapping localization of both RSC and Dbp2 in the nucleoplasm suggests that this is where they interact. This spatial co-localization strongly supports the notion that the functional interaction between Dbp2 and the RSC complex takes place within the nucleoplasm, highlighting the nucleoplasm as the critical cellular environment for their coordinated role in chromatin remodeling and RNA-related processes.

In *S. cerevisiae,* it has been shown that Dbp2 is recruited to chromatin co-transcriptionally via nascent RNA (Ma et al., 2016) and that it functions at the interface between RNA surveillance and chromatin architecture, acting as a critical component in transcriptome quality control (Cloutier et al., 2012). In *S. pombe*, Dbp2 has similarly been shown to localize to RNA PolII-transcribed loci (Aydin et al., 2024), supporting a conserved role in coordinating transcriptional and post-transcriptional processes. Furthermore, it is known that the RSC complex can interact with mediators to regulate NDRs and transcription (André et al., 2023). Combined with our findings, these data raise the possibility that Dbp2 and RSC might cooperatively regulate gene expression by linking chromatin remodeling with RNA processing. For example, Dbp2 may be recruited to actively transcribed chromatin regions by RSC, where it could modulate RNA maturation or surveillance processes in a chromatin-context-dependent manner. This suggests a model in which the two factors coordinate transcription initiation or elongation with co-transcriptional RNA processing, thereby ensuring transcriptome integrity. However, the precise molecular mechanism underlying their cooperation remains unclear. It is possible that their interaction is either direct or mediated through additional regulatory factors. They may function sequentially or in parallel at common genomic loci to coordinate chromatin remodeling with RNA processing. Further studies using chromatin immunoprecipitation in combination with functional assays of RNA output will be necessary to clarify the dynamics and regulatory consequences of this interaction.

In conclusion, two independent Co-IPs confirmed the interaction between Dbp2 and the RSC complex previously observed in a crosslinking purification. While this does not constitute

definitive proof of a direct interaction, it provides additional supporting evidence under physiological conditions. It is important to emphasize that the use of both negative and positive controls for the interaction is incredibly important to increase confidence in the results and prevent false positives. Negative controls are also essential to verify the successful removal of non-specific interactors during the wash steps. Based on localization, we consider the nucleoplasm the most likely place for the interaction. Overall, we demonstrate through two independent Co-immunoprecipitation approaches that Dbp2 interacts with components of the RSC chromatin remodeling complex in *S. pombe*. This interaction likely occurs within the nucleoplasmic region of the nucleus, where both proteins are colocalized. While the precise molecular mechanism of this interaction remains to be clarified, our findings suggest a potential functional link between chromatin remodeling and RNA metabolic processes. The identification of this interaction is significant because it adds to the growing understanding of how chromatin structure and RNA processing may be coordinated. Given the established roles of RSC in maintaining nucleosome-free regions and of Dbp2 in RNA surveillance and processing, their cooperation could represent a conserved regulatory mechanism for transcriptome quality control. Future research should aim to define the functional consequences of this interaction in more detail. For instance, genome-wide binding studies combined with transcriptomic analyses could reveal whether Dbp2 recruitment to specific loci depends on RSC activity. Additionally, dissecting the temporal dynamics of their interaction during transcription could provide further insights into how chromatin state influences RNA fate.

5.3 Effects of RSC on Dbp2 and vice versa

We could show that the RSC complex and Dbp2 interact with each other. In addition, a previous project has already demonstrated that the RSC components are increasingly associated with nuclear mRNPs after Dbp2 depletion (Fig. 6B), suggesting that Dbp2 may regulate the association of RSC components with mRNA, which hints at a functional interplay at the RNA level. This raises the question of how exactly the respective proteins affect each other at different molecular levels, such as chromatin occupancy and subcellular localization. Individual proteins were depleted or deleted to investigate the effect of the loss of one protein in more detail, and the impact on the occupancy and cellular localization of the other protein was examined. Firstly, a ChIP followed by qPCR was performed to investigate whether the loss of Rsc1 affects Dbp2 occupancy and vice versa. For Dbp2, recruitment to the gene body with a prominent enrichment in the 3' region as well as downstream of the transcription termination site – consistent with previous ChIP-Seq experiments (Aydin et al., 2024) – was detected, without the deletion of *rsc1* having an effect (Fig. 11A). This occupancy observed for Dbp2 contrasts with observations in *S. cerevisiae*, where Dbp2 was shown to be evenly distributed across coding regions (Ma et al., 2016). We were unable to detect association of Rsc1 with chromatin above background level, so no statement can be made about its

occupancy. This suggests either genuinely low occupancy levels or technical limitations of ChIP-qPCR in detecting Rsc1 binding at this locus. The Dbp2 results were reproducible even in the absence of Snf21, as its depletion had no effect (Fig. 11B, C). Unfortunately, we were also unable to detect chromatin association of Snf21. Since the RSC complex is mainly responsible for maintaining nucleosome-depleted regions in the promoter area (Lorch and Kornberg, 2017), we had expected an increased occupancy of the RSC components in this area. For the RSC complex, we could not present any results on occupancy using ChIP followed by qPCR, which could be because this is not a suitable method for analyzing occupancy for chromatin remodelers, and an alternative method is required for this investigation. A suitable alternative for chromatin isolation could be the high-resolution CUT&RUN method, where no crosslinking is needed, and nuclei are extracted with magnetic beads, followed by calcium-induced DNA cleavage by the endo-exonuclease micrococcal nuclease (MNase), after which fragments diffuse out of the nucleus (Skene and Henikoff, 2017). Another recently published method, CheC-seq2, uses DNA-bound proteins directly fused to MNase, leading to DNA cleavage after permeabilization and calcium treatment (VanBelzen et al., 2024). Additionally, the possibility that transient or weak interactions of chromatin remodelers with DNA are below the detection limit of ChIP-qPCR should be considered. This is particularly relevant for the RSC complex, as it dynamically interacts with chromatin to remodel nucleosomes, often binding only briefly or with low affinity, which can make it challenging to capture these interactions using conventional ChIP methods. Moreover, the analysis was limited to the single gene *rps2202*, which constrains the generalizability of the findings. Future studies employing genome-wide approaches such as ChIP-Seq, CUT&RUN, or CUT&Tag could provide more insights. RNA-protein interaction techniques like CLIP-Seq might further clarify potential interactions between Dbp2, the RSC complex, and RNA molecules. In summary, it could be shown that RSC subunits do not influence the preferential binding of Dbp2 to the 3'-ends of genes.

In addition, we wanted to investigate whether the proteins play a role in the cellular localization of each other and whether the loss of one protein influences the localization of the other protein. However, neither did the loss of RSC affect the localization to Dbp2, nor vice versa (Fig. 12, Fig. 13). This finding suggests that the subcellular distribution of Dbp2 and the RSC complex is independent of each other, despite their physical interaction.

In conclusion, we were able to show that Dbp2 and the RSC complex are independent of each other in both their chromatin occupancy and their cellular localization, despite their interaction in the nucleoplasm. This suggests that the interaction between Dbp2 and RSC may reflect a specialized or transient function that does not broadly impact chromatin occupancy or subcellular distribution. Moreover, it could be due to the fact that the interaction of both components is based on a different function that was not investigated here. This other function

could also be very specific so that no general effect of the loss can be detected in the experiments carried out here.

5.4 Dbp2, but not the RSC complex, is indispensable for efficient mRNA export

Our findings, particularly the enrichment of the RSC complex in a Dbp2 purification and the subsequent discovery that the RSC complex is increasingly associated with nuclear mRNPs after Dbp2 depletion, are of significant importance. This observation can be interpreted in two plausible ways. First, previous work from the lab demonstrated that loss of Dbp2 results in increased retention of RNA at chromatin (Aydin et al., 2024), raising the possibility that these retained RNAs might engage more frequently with the RSC complex. This raises the question of whether such RNA interactions affect RSC function. It is conceivable that RSC senses RNA accumulation as an indicator of export defects and adapts its activity accordingly, potentially leading to reduced transcription. However, the relatively mild impact of Snf21 depletion on RNA Polymerase II occupancy argues against widespread transcriptional repression via this mechanism. Second, although chromatin remodelers like RSC are typically considered DNA-binding proteins, there is growing evidence that many chromatin-associated proteins also bind RNA in a competitive or mutually exclusive manner with DNA. These RNA interactions can have diverse outcomes, such as chromatin eviction or the formation of RNA-dependent condensates concentrating regulatory factors at target sites (Hendrickson et al., 2016; Keller et al., 2012; Ullah et al., 2022). Therefore, it is also conceivable that the RSC complex interacts with RNA under specific conditions, adding complexity to its role in chromatin regulation.

It has already been shown that Dbp2 plays a role in many steps of mRNA processing and is also required for successful mRNA export. Therefore, we asked ourselves whether the loss of the RSC complex also plays a role in mRNA export and how a simultaneous loss of both components affects it. In contrast to Dbp2, loss of the RSC complex did not affect the mRNA export capacity of the cell, consistent with its established role as a chromatin remodeler acting primarily on DNA (Fig. 14). However, additional loss of the RSC complex seems to reduce the export defect associated with Dbp2 depletion. The mechanism behind this remains unclear, but this unexpected partial rescue might suggest compensatory mechanisms or altered RNA processing pathways upon double depletion, indicating a complex interplay between Dbp2 and the RSC complex in regulating mRNA export under certain conditions. However, this function is not yet known, and our observation could also be an indirect effect of the double depletion and deletion in this experimental setup without corresponding to a natural biological effect. These unknown aspects open up new avenues for further exploration and research in this field.

5.5 Depletion of Dbp2 has no measurable impact on the diffusion rates of Snf21 or Cbc2

To assess whether Snf21 was displaced from chromatin in the absence of Dbp2, we performed Fluorescence Recovery After Photobleaching (FRAP), bleaching GFP-labelled Snf21 in a defined area in the nucleoplasm with a laser. By measuring how long the diffusion of the protein back into this area takes, this technique allowed us to study the dynamics of protein diffusion and its interaction with chromatin. An increased diffusion rate of Snf21 after the loss of Dbp2 could be indicative of decreased association with chromatin. In addition, we monitored diffusion of Cbc2, which is associated with nuclear RNPs, in the presence and absence of Dbp2. A decreased diffusion rate could have provided direct evidence that Cbc2 and, thus, the mRNA, is increasingly bound to chromatin. In wild-type cells, Snf21 diffused at a comparatively slow rate (Fig. 15C), which fits with its capacity for DNA binding. In contrast, Cbc2, a subunit of the nuclear cap-binding protein complex (CBC), is known to remain bound to the mRNA during nuclear RNA processing and then assists in mRNA export to the cytoplasm (Qiu et al., 2012). Since the mobility of RNA is higher than the mobility of DNA, our results here reflect the known biological processes. However, there were no detectable differences in diffusion rate after depletion of Dbp2 for either Snf21 or Cbc2.

Overall, it can be said that we were unable to show any results to support our hypotheses here, but an expected biological trend is emerging. As this experiment was only carried out once with a small number of cells, it underscores the need for further repetitions with a higher number of cells to be able to make a clear statement. This would improve statistical significance and help account for biological variability that might mask subtle effects. In addition, it is not known to what extent Snf21 and Cbc2 are present in a bound or soluble form. The effect to be investigated could only be shown if Snf21 is primarily bound to chromatin. If a large proportion is present in soluble form, this would explain why the Dbp2 loss shows no effect, and a difference in the lower bound proportion would not be apparent in comparison. Future studies could clarify the distribution of bound versus soluble forms using biochemical fractionation or advanced imaging techniques.

5.6 RSC depletion has no global effects on transcription

In contrast to the human system, where BAF, the SWI/SNF orthologue, is more abundant than the RSC orthologue PBAF (Yan et al., 2005), the yeast RSC complex is about ten times more abundant than the SWI/SNF complex (Monahan et al., 2008). Nevertheless, relatively little is known about the detailed chromatin binding of RSC, and its target genes remain unidentified. To gain insights into DNA binding and the functional roles of RSC, the difference in depletion of Snf21 and deletion of *rsc1* compared to non-depleted and non-deleted controls was analyzed with PolII-ChIP-Seq. In this experiment, the genome-wide distribution of RNA

polymerase II is visualized, showing which genes are being transcribed. In addition to whether Snf21 and Rsc1 regulate the transcription of specific genes and thus the identification of RSC target genes, this experiment can also be used to address other questions. For example, regulatory mechanisms by which proteins influence transcription or direct versus indirect interactions can also be investigated. Since it has been reported that the RSC complex binds to promoter regions in *S. cerevisiae* to maintain their accessibility for transcription (André et al., 2023; Musladin et al., 2014), we hypothesized that a similar mechanism might be present in *S. pombe*. Therefore, we analyzed PolII-ChIP-seq data to infer changes in transcriptional activity at promoters upon RSC subunit loss. However, PolII occupancy does not directly measure RSC binding or chromatin accessibility, so our experiments cannot conclusively determine whether RSC binds to promoters in *S. pombe*. Future experiments to directly assess chromatin accessibility or RSC-specific ChIP-Seq to map its binding sites would provide more insights into the role of RSC in promoter regulation and chromatin structure in *S. pombe*.

First, we were able to show that the controls for Snf21 depletion and *rsc1* deletion behaved very similarly to each other. At the same time, the depletion and deletion were both distinct and significantly different from the controls (Fig. 16A). The replicates also showed high consistency, increasing confidence in the results and indicating that the experiment was not particularly susceptible to handling variability. Since *rsc1* was deleted, protein-level analyses similar to those performed for Snf21 were not feasible previously. In this experiment, however, the successful deletion of *rsc1* was confirmed using sequencing data (Fig. 16C). This absence of genomic *rsc1* sequences confirmed the successful deletion. For *snf21*, deletion of a segment of the endogenous 3'-UTR, which is replaced with a cassette carrying the tag and the resistance marker upon tagging, could also be verified. In addition, we observed increased transcription of the tagged gene upon depletion of its protein. This could reflect a compensatory mechanism or, alternatively, may be due to the known potential of sequence alterations of affecting transcription (Kilpinen et al., 2013).

When analyzing the effect of RSC depletion on previously reported target genes, we were able to reconfirm that the RSC complex regulates the expression of *ste11* and *cit1* (Fig. 17). The fact that *ste11* was previously identified as a target gene of the activating RSC function (Materne et al., 2016) can be explained by the different methodology used in the study. In that study, RT-qPCR was used to quantify gene expression, with normalization typically performed against reference genes assumed to remain stable across conditions. This approach reflects steady-state mRNA levels but does not capture dynamic transcriptional regulation directly. In contrast, our data are based on PolII-ChIP-Seq, which reflects active transcription through RNA PolII occupancy. Thus, the apparent discrepancy between studies may stem from both the different levels of gene regulation being measured and from how the data were normalized. Overall, the combination of protein depletion and PolII-ChIP-Seq

provides a powerful strategy to investigate the role of a protein in regulating gene expression at a genome-wide level. Combining multiple complementary methods could provide an even more comprehensive understanding of gene regulation and the multifaceted roles of the RSC complex.

In addition, we were able to show that the RSC complex shares some target genes with the SWI/SNF complex (Fig. 18). In this regard, it was exciting that the RSC complex had the opposite function on the expression of these genes. Although both complexes are chromatin remodelers and share common subunits (Monahan et al., 2008), both can have activating and repressive effects (Ng et al., 2002; Martens and Winston, 2002). These differences may be due to the specific composition. They could have an essential regulatory function so that both complexes act as antagonists despite their similar structure and enable rapid and effective gene regulation. It has already been shown that the SWI/SNF and RSC complex exhibit partially overlapping but not identical functions at heat shock gene promoters (Erkina et al., 2010) and distinct roles in promoting nucleotide excision repair across the genome (Bohm et al., 2021), which fits with the results observed here. Most interestingly, our data revealed different outcomes after loss of Rsc1 and Snf21 for *obr1* (Fig. 18A). The increase in transcription following the loss of Rsc1 suggests a robust repressive role of Rsc1 at the *obr1* locus that is not easily compensated. In contrast, the short-term depletion of Snf21 may not have fully disrupted transcriptional regulation within the limited experimental timeframe, or Snf21 may not be directly required for repression at this locus.

After discovering that the RSC complex repressed gene expression, especially in opposition to the SWI/SNF complex, we aimed to identify target genes that the RSC complex activates. For the *S. cerevisiae* RSC complex, genetic analysis showed a localization across the genome with potentially around 700 target genes (Ng et al., 2002; Soutourina et al., 2006), suggesting many different roles in, for example, stress response, metabolism, mitochondrial function, regulation of transcription and chromosome segregation (Angus-Hill et al., 2001; Chai et al., 2002; Damelin et al., 2002; Du et al., 1998; Moreira and Holmberg, 1999; Ng et al., 2002; Hsu et al., 2003). In contrast, we found very few genes that were repressed in the absence of RSC in the genome-wide analysis of *S. pombe*. Very striking and surprising was the fact that such genes were most often localized in the subtelomeres of the chromosomes (Fig. 19). Telomeres are unique structures consisting of repeated DNA sequences and associated proteins. They are located at the ends of the linear chromosomes of eukaryotic cells and have several essential functions, such as ensuring the faithful replication of genetic material and protecting against DNA damage signaling, thus protecting the stability and integrity of the genome (Lu et al., 2013). For other chromatin remodeling complexes, such as INO80, a function in the regulation of telomere structures has already been demonstrated, and regulation of telomere length via relevant genes by the RSC complex has also been assumed (Recht et al., 2016; Yu

et al., 2007). In *S. cerevisiae*, Rsc2 is associated with telomere shortening (Shim et al., 2005), and the RSC complex is thought to play a role in maintaining the regulation of telomere formation and structure (Recht et al., 2016). Most interestingly, Dbp2 is also believed to prevent the accumulation of R-loops at the telomeric regions of chromatin due to its RNA-DNA hybrid unwinding activity (Pérez-Martínez et al., 2022), which would allow an interaction of both complexes in these chromatin regions.

Overall, the combination of protein depletion and Pol Ⅱ-ChIP-Seq provides a powerful strategy to investigate the role of a protein in regulating gene expression at a genome-wide level. Notably, the loss of RSC subunits resulted in relatively few global effects on transcription (Fig. 16B), highlighting the complexity of its regulatory roles. Integrative approaches combining chromatin accessibility analyses, proteomics, and other omics techniques could further deepen our understanding of RSC functions and gene regulation in future studies.

5.7 Conclusion and outlook

Our study investigated the interaction between Dbp2 and the RSC complex and their respective roles in cell biology and mRNA processing. Despite their interaction within the nucleoplasm, we demonstrated that Dbp2 and the RSC complex carry out many of their functions independently. This independence underscores their distinct molecular functions and suggests that they operate through separate regulatory mechanisms within the nucleus.

Our PolⅡ-ChIP-Seq analysis of transcriptional regulation revealed that the RSC complex unexpectedly represses a broad set of target genes, challenging the previously assumed role of the RSC complex as a transcriptional activator. This finding has significant implications for our understanding of gene regulation and the roles of chromatin remodeling complexes.

The functional interplay between Dbp2 and the RSC complex, particularly regarding their interaction during mRNA processing, could be further explored through additional experiments. For instance, the potential RNA-binding activity of the RSC complex could be investigated using CLIP-Seq and RIP-Seq methodologies. Furthermore, Co-immunoprecipitation under RNase treatment could help determine whether the interaction between Dbp2 and the RSC complex is RNA-dependent. The RSC complex itself could be characterized in greater detail through experiments such as ChIP-Seq at various depletion time points, enabling a deeper understanding of the temporal dynamics of its function, its influence on chromatin structure, and its role in transcriptional regulation.

In conclusion, this study provides critical new insights into the interaction between Dbp2 and the RSC complex. It highlights Dbp2's pivotal role in mRNA export and the RSC complex’s multifaceted role in gene transcription. These findings open new avenues for further research

to dissect the molecular mechanisms underlying these components' functional specialization and interplay. Moving forward, integrative and multidisciplinary approaches combining genomics, proteomics, and advanced imaging techniques will be crucial to fully unravel the complex regulatory networks involving Dbp2 and the RSC complex.

6 References

Ali, M. A. M. (2021): The DEAD-box protein family of RNA helicases: sentinels for various cellular functions with emerging roles in tumorigenesis. *International journal of clinical oncology* 26, S. 795–825.

Allshire, R. C. and Ekwall, K. (2015): Epigenetic Regulation of Chromatin States in Schizosaccharomyces pombe. *Cold Spring Harbor Perspectives in Biology* 7.

Amberg, D. C., Goldstein, A. L., Cole, C. N. (1992): Isolation and characterization of RAT1: an essential gene of Saccharomyces cerevisiae required for the efficient nucleocytoplasmic trafficking of mRNA. *Genes & development* 6, S. 1173-1189.

André, K. M., Giordanengo A. N., Martinez-Fernandez, V., Zeitler, L., Alberti, A., Goldar, A., Werner, M., Denby Wilkes, C., Soutourina, J. (2023): Functional interplay between Mediator and RSC chromatin remodeling complex controls nucleosome-depleted region maintenance at promoters. *Cell reports* 42, 112465.

Angus-Hill, M. L., Schlichter, A., Roberts, D., Erdjument-Bromage, H., Tempst, P., Cairns, B. R. (2001): A Rsc3/Rsc30 zinc cluster dimer reveals novel roles for the chromatin remodeler RSC in gene expression and cell cycle control. *Molecular cell* 7, S. 741–751.

Asturias, F. J., Chung, W.-H., Kornberg, R. D., Lorch, Y. (2002): Structural analysis of the RSC chromatin-remodeling complex. *Proceedings of the National Academy of Sciences of the United States of America* 99, S. 13477–13480.

Aubourg, S.; Kreis, M.; Lecharny, A. (1999): The DEAD box RNA helicase family in Arabidopsis thaliana. *Nucleic acids research* 27, S. 628–636.

Aydin, E.; Schreiner, S.; Boehme, J.; Keil, B.; Weber, J.; Žunar, B.; Glatter, T.; Kilchert, C. (2024): DEAD-box ATPase Dbp2 is the key enzyme in an mRNP assembly checkpoint at the 3'-end of genes and involved in the recycling of cleavage factors. *Nature communications* 15, S. 6829.

Badis, G., Chan, E. T., van Bakel, H., Pena-Castillo, L., Tlo, D., Tsui, K., Carlson, C. D., Gossett, A. J., Hasinoff, M. J., Warren, C. L., Gebbia, M., Talukder, S., Yang, A., Mnaimneh, S., Terterov, D., Coburn, D., Li Yeo, A., Yeo, Z. X., Clarke, N. D., Lieb, J. D., Ansari, A. Z., Nislow, C., Hughes, T. R. (2008): A library of yeast transcription factor motifs reveals a widespread function for Rsc3 in targeting nucleosome exclusion at promoters. *Molecular cell* 32, S. 878–887.

Bates, D. L. and Thomas, J. O. (1981): Histones H1 and H5: one or two molecules per nucleosome? *Nucleic acids research* 9, S. 5883–5894.

Bird, A. P. (1986): CpG-rich islands and the function of DNA methylation. *Nature* 321, S. 209–213.

Bohm, K. A., Hodges, A. J., Czaja, W., Selvam, K., Smerdon, M. J., Mao, P., Wyrick, J. J. (2021): Distinct roles for RSC and SWI/SNF chromatin remodelers in genomic excision repair. *Genome research* 31, S. 1047–1059.

Brown, T. A. (2002): Genomes. 2. ed. New York, NY: Wiley-Liss.

Cairns, B. R., Lorch, Y., Li, Y., Zhang, M., Lacomis, L., Erdjument-Bromage, H., Tempst, P., Du, J., Laurent, B., Kornberg, R. D. (1996): RSC, an Essential, Abundant Chromatin-Remodeling Complex. *Cell* 87, S. 1249–1260.

Chai, B., Hsu, J.-M., Du, J., Laurent, B. C. (2002): Yeast RSC function is required to organize the cellular cytoskeleton via an alternative PKC1 pathway. *Genetics* 161, S. 575–584.

Chambers, A. L. and Downs, J. A. (2012): The RSC and INO80 chromatin-remodeling complexes in DNA double-strand break repair. *Progress in molecular biology and translational science* 110, S. 229–261.

Clapier, C. R. and Cairns, B. R. (2009): The biology of chromatin remodeling complexes. *Annual review of biochemistry* 78, S. 273–304.

Clapier, C. R., Kasten, M. M., Parnell, T. J., Viswanathan, R., Szerlong, H., Sirinakis, G., Zhang, Y., Cairns, B. R. (2016): Regulation of DNA Translocation Efficiency within the Chromatin Remodeler RSC/Sth1 Potentiates Nucleosome Sliding and Ejection. *Molecular cell* 62, S. 453–461.

Cloutier, S. C., Ma, W. K., Nguyen, L. T., Tran, E. J. (2012): The DEAD-box RNA helicase Dbp2 connects RNA quality control with repression of aberrant transcription. *The Journal of biological chemistry* 287, S. 26155–26166.

Cordin, O., Banroques, J., Tanner, N. K., Linder, P. (2006): The DEAD-box protein family of RNA helicases. *Gene* 367, S. 17–37.

Cortazar, M. A., Sheridan, R. M., Erickson, B., Fong, N., Glover-Cutter, K., Brannan, K., Bentley, D. L. (2019): Control of RNA Pol II Speed by PNUTS-PP1 and Spt5 Dephosphorylation Facilitates Termination by a "Sitting Duck Torpedo" Mechanism. *Molecular cell* 76, S. 896–908.

Cramer, Patrick (2019): Organization and regulation of gene transcription. *Nature* 573, S. 45-54.

de la Cruz, J., Kressler, D., Linder, P. (1999): Unwinding RNA in Saccharomyces cerevisiae: DEAD-box proteins and related families. *Trends in biochemical sciences* 24, S. 192–198.

Deaton, A. M. and Bird, A. (2011): CpG islands and the regulation of transcription. *Genes & development* 25, S. 1010–1022.

Dege, C. and Hagman, J. (2014): Mi-2/NuRD chromatin remodeling complexes regulate B and T-lymphocyte development and function. *Immunological reviews* 261, S. 126–140.

Deutschman, C. S. (2005): Transcription. *Critical care medicine* 33, S 400–3.

Diets, I. J., Prescott, T., Champaigne, N. L.; Mancini, G. M. S., Krossnes, B., Frič, R., Kocsis, K., Jongmans, M. C. J., Kleefstra, T. (2019): A recurrent de novo missense pathogenic variant in SMARCB1 causes severe intellectual disability and choroid plexus hyperplasia with resultant hydrocephalus. *Genetics in medicine : official journal of the American College of Medical Genetics* 21, S. 572–579.

Dombrowski, M., Engeholm, M., Dienemann, C., Dodonova, S., Cramer, P. (2022): Histone H1 binding to nucleosome arrays depends on linker DNA length and trajectory. *Nature structural & molecular biology* 29, S. 493–501.

Domelen, M., Simon, I., Moy, T. I., Wilson, B., Komili, S., Tempst, P., Roth, F. P., Young, R. A., Cairns, B. R., Silver, P. A. (2002): The genome-wide localization of Rsc9, a component of the RSC chromatin-remodeling complex, changes in response to stress. *Molecular cell* 9, S. 563–573.

Du, J., Nasir, I., Benton, B. K., Kladde, M. P., Laurent, B. C. (1998): Sth1p, a Saccharomyces cerevisiae Snf2p/Swi2p homolog, is an essential ATPase in RSC and differs from Snf/Swi in its interactions with histones and chromatin-associated proteins. *Genetics* 150, S. 987–1005.

Dwane, S. and Kiely, P. A. (2011): Tools used to study how protein complexes are assembled in signaling cascades. *Bioengineered bugs* 2, S. 247–259.

Erkina, T. Y., Zou, Y., Freeling, S., Vorobyev, V. I., Erkine, A. M. (2010): Functional interplay between chromatin remodeling complexes RSC, SWI/SNF and ISWI in regulation of yeast heat shock genes. *Nucleic acids research* 38, S. 1441–1449.

Fairman-Williams, M. E., Guenther, U.-P., Jankowsky, E. (2010): SF1 and SF2 helicases: family matters. *Current opinion in structural biology* 20, S. 313–324.

Flanagan, J. F. and Peterson, C. L. (1999): A role for the yeast SWI/SNF complex in DNA replication. *Nucleic acids research* 27, S. 2022–2028.

Floer, M., Wang, X., Prabhu, V., Berrozpe, G., Narayan, S., Spagna, D., Alvarez, D., Kendall, J., Krasnitz, A., Stepansky, A., Hicks, J., Bryant, G. O., Ptashne, M. (2010): A RSC/nucleosome complex determines chromatin architecture and facilitates activator binding. *Cell* 141, S. 407–418.

Fyodorov, D. V., Zhou, B.-R., Skoultchi, A. I., Bai, Y. (2018): Emerging roles of linker histones in regulating chromatin structure and function. *Nature reviews. Molecular cell biology* 19, S. 192–206.

G Hendrickson, D., Kelley, D. R., Tenen, D., Bernstein, B., Rinn, J. L. (2016): Widespread RNA binding by chromatin-associated proteins. *Genome biology* 17, S. 28.

Gaillard, H., Fitzgerald, D. J.; Smith, C. L., Peterson, C. L., Richmond, T. J.; Thoma, F. (2003): Chromatin remodeling activities act on UV-damaged nucleosomes and modulate DNA damage accessibility to photolyase. *The Journal of biological chemistry* 278, S. 17655–17663.

Gaykema, L. H., van Nieuwland, R. Y., Dekkers, M. C., van Essen, M. F., Heidt, S., Zaldumbide, A., van den Berg, C. W., Rabelink, T. J., van Kooten, C. (2022): Inhibition of complement activation by CD55 overexpression in human induced pluripotent stem cell derived kidney organoids. *Frontiers in Immunology* 13, S. 1058763.

Godde, J. S. and Widom, J. (1992): Chromatin structure of Schizosaccharomyces pombe. A nucleosome repeat length that is shorter than the chromatosomal DNA length. *Journal of molecular biology* 226, S. 1009–1025.

Gorbalenya, A. E. and Koonin, E. V. (1993): Helicases: amino acid sequence comparisons and structure-function relationships. *Current opinion in structural biology* 3, S. 419–429.

Hara, R., and Sancar, A. (2003): Effect of damage type on stimulation of human excision nuclease by SWI/SNF chromatin remodeling factor. *Molecular and cellular biology* 23, S. 4121–4125.

Hergeth, S. P., and Schneider, R. (2015): The H1 linker histones: multifunctional proteins beyond the nucleosomal core particle. *EMBO reports* 16, S. 1439–1453.

Hilbert, M., Karow, A. R., Klostermeier, D. (2009): The mechanism of ATP-dependent RNA unwinding by DEAD box proteins. *Biological chemistry* 390, S. 1237–1250.

Hirschhorn, J. N., Brown, S. A., Clark, C. D., Winston, F. (1992): Evidence that SNF2/SWI2 and SNF5 activate transcription in yeast by altering chromatin structure. *Genes & development* 6, S. 2288–2298.

Hocine, S., Singer, R. H., Grünwald, D. (2010): RNA Processing and Export. *Cold Spring Harbor Perspectives in Biology* 2.

Hoffman, C. S., Wood, V., Fantes, P. A. (2015): An Ancient Yeast for Young Geneticists: A Primer on the Schizosaccharomyces pombe Model System. *Genetics* 201, S. 403–423.

Hsu, J.-M., Huang, J., Meluh, P. B., Laurent, B. C. (2003): The yeast RSC chromatin-remodeling complex is required for kinetochore function in chromosome segregation. *Molecular and cellular biology* 23, S. 3202–3215.

Hu C.D., Chinenov Y, Kerppola TK (2002). Visualization of interactions among bZIP and Rel family proteins in living cells using bimolecular fluorescence complementation. *Mol Cell.* S. 789–98.

Huisinga, K. L., Brower-Toland, B., Elgin, S. C. R. (2006): The contradictory definitions of heterochromatin: transcription and silencing. *Chromosoma* 115, S. 110–122.

Jenuwein, T. and Allis, C. D. (2001): Translating the histone code. *Science (New York, N.Y.)* 293, S. 1074–1080.

Kanke, M., Nishimura, K., Kanemaki, M., Kakimoto, T., Takahashi, T.S., Nakagawa, T., Masukata, H. (2011): Auxin-inducible protein depletion system in fission yeast. *BMC cell biology* 12, S. 8.

Kasten, M., Szerlong, H., Erdjument-Bromage, H., Tempst, P., Werner, M., Cairns, B. R. (2004): Tandem bromodomains in the chromatin remodeler RSC recognize acetylated histone H3 Lys14. *The EMBO Journal* 23, S. 1348–1359.

Keller, C., Adaixo, R., Stunnenberg, R., Woolcock, K. J., Hiller, S., Bühler, M. (2012): HP1(Swi6) mediates the recognition and destruction of heterochromatic RNA transcripts. *Molecular cell* 47, S. 215–227.

Kilpinen, H., Waszak, S. M., Gschwind, A. R., Raghav, S. K., Witwicki, R. M., Orioli, A., Migliavacca, E., Wiederkehr, M., Gutierrez-Arcelus, M., Panousis, N. I., Yurovsky, A., Lappalainen, T., Romano-Palumbo, L., Planchon, A., Bielser, D., Bryois, J., Padioleau, I., Udin, G., Thurnheer, S., Hacker, D., Core, L. J., Lis, J. T., Hernandez, N., Reymond, A., Deplancke, B., Dermitzakis, E. T. (2013): Coordinated effects of sequence variation on DNA binding, chromatin structure, and transcription. *Science* 342, S. 744–747.

Khorasanizadeh, S. (2004): The nucleosome: from genomic organization to genomic regulation. *Cell* 116, S. 259–272.

Ko, M., Sohn, D. H., Chung, H., Seong, R. H. (2008): Chromatin remodeling, development and disease. *Mutation research* 647, S. 59–67.

Korostelev, A. A. (2022): The Structural Dynamics of Translation. *Annual review of biochemistry* 91, S. 245–267.

Koyama, M., Nagakura, W., Tanaka, H., Kujirai, T., Chikashige, Y., Haraguchi, T., Hiraoka, Y., Kurumizaka, H. (2017): In vitro reconstitution and biochemical analyses of the Schizosaccharomyces pombe nucleosome. *Biochemical and biophysical research communications* 482, S. 896–901.

Krebs, J. E., Kuo, M. H., Allis, C. D., Peterson, C. L. (1999): Cell cycle-regulated histone acetylation required for expression of the yeast HO gene. *Genes & development* 13, S. 1412–1421.

Krietenstein, N., Wal, M., Watanabe, S., Park, B., Peterson, C. L., Pugh, B. F., Korber, P. (2016): Genomic Nucleosome Organization Reconstituted with Pure Proteins. *Cell* 167, S. 709-721.

Kubik, S., Bruzzone, M. J., Jacquet, P., Falcone, J.-L., Rougemont, J., Shore, D. (2015): Nucleosome Stability Distinguishes Two Different Promoter Types at All Protein-Coding Genes in Yeast. *Molecular cell* 60, S. 422–434.

Kubik, S., O'Duibhir, E., de Jonge, W. J., Mattarocci, S., Albert, B., Falcone, J.-L., Bruzzone, M. J., Holstege, F. C. P., Shore, D. (2018): Sequence-Directed Action of RSC Remodeler and General Regulatory Factors Modulates +1 Nucleosome Position to Facilitate Transcription. *Molecular cell* 71, S. 89–102.

Laemmli, U. K. (1970): Cleavage of structural proteins during the assembly of the head of bacteriophage T4. *Nature* 227, S. 680–685.

Lai, Y.-H., Choudhary, K., Cloutier, S. C., Xing, Z., Aviran, S., Tran, E. J. (2019): Genome-Wide Discovery of DEAD-Box RNA Helicase Targets Reveals RNA Structural Remodeling in Transcription Termination. *Genetics* 212, S. 153–174.

Landsman, D. (1996): Histone H1 in Saccharomyces cerevisiae: a double mystery solved? *Trends in biochemical sciences* 21, S. 287–288.

Lantermann, A. B., Straub, T., Strålfors, A., Yuan, G.-C., Ekwall, K., Korber, P. (2010): Schizosaccharomyces pombe genome-wide nucleosome mapping reveals positioning mechanisms distinct from those of Saccharomyces cerevisiae. *Nature structural & molecular biology* 17, S. 251–257.

Lee, Y. J., Hoe, K. L., Maeng, P. J. (2007): Yeast cells lacking the CIT1-encoded mitochondrial citrate synthase are hypersusceptible to heat- or aging-induced apoptosis. *Molecular biology of the cell* 18, S. 3556–3567.

Lera-Ramírez, M., Bähler, J., Mata, J., Rutherford, K., Hoffman, C. S., Lambert, S., Oliferenko, S., Martin, S. G., Gould, K. L., Du, L-L., Sabatinos, S. A., Forsburg, S. L.,

Nielsen, O., Nurse, P., Wood, V. (2023): Revised fission yeast gene and allele nomenclature guidelines for machine readability. *Genetics* 225.

Leschziner, A. E. (2011): Electron microscopy studies of nucleosome remodelers. *Current opinion in structural biology* 21, S. 709–718.

Li, F., Ling, X., Chakraborty, S., Fountzilas, C., Wang, J., Jamroze, A., Liu, X., Kalinski, P., Tang, D. G.(2023): Role of the DEAD-box RNA helicase DDX5 (p68) in cancer DNA repair, immune suppression, cancer metabolic control, virus infection promotion, and human microbiome (microbiota) negative influence. *Journal of experimental & clinical cancer research* 42, S. 213.

Libuda, D. E. and Winston, F. (2006): Amplification of histone genes by circular chromosome formation in Saccharomyces cerevisiae. *Nature* 443, S. 1003–1007.

Liu, Xin; Bushnell, David A.; Kornberg, Roger D. (2013): RNA polymerase II transcription: structure and mechanism. *Biochimica et biophysica acta* 1829, S. 2–8.

Lopez Martinez, D., and Svejstrup, J. Q. (2025): Mechanisms of RNA Polymerase II Termination at the 3'-End of Genes. *Journal of molecular biology* 437, S. 168735.

Lorch, Y. and Kornberg, R. D. (2017): Chromatin-remodeling for transcription. *Quarterly reviews of biophysics* 50.

Lorch, Y., Cairns, B. R., Zhang, M., Kornberg, R. D. (1998): Activated RSC-nucleosome complex and persistently altered form of the nucleosome. *Cell* 94, S. 29–34.

Lorch, Y., Maier-Davis, B., Kornberg, R. D. (2014): Role of DNA sequence in chromatin remodeling and the formation of nucleosome-free regions. *Genes & development* 28, S. 2492–2497.

Lu, W., Zhang, Y., Liu, D., Songyang, Z., Wan, M. (2013): Telomeres-structure, function, and regulation. *Experimental cell research* 319, S. 133–141.

Luger, K., Mäder, A. W., Richmond, R. K., Sargent, D. F., Richmond, T. J. (1997): Crystal structure of the nucleosome core particle at 2.8 A resolution. *Nature* 389, S. 251–260.

Ma, W. K., Paudel, B. P., Xing, Z., Sabath, I. G., Rueda, D., Tran, E. J. (2016): Recruitment, Duplex Unwinding and Protein-Mediated Inhibition of the Dead-Box RNA Helicase Dbp2 at Actively Transcribed Chromatin. *Journal of molecular biology* 428, S. 1091–1106.

Mahdi, A. A., Briggs, G. S., Sharples, G. J., Wen, Q., Lloyd, R. G. (2003): A model for dsDNA translocation revealed by a structural motif common to RecG and Mfd proteins. *The EMBO Journal* 22, S. 724–734.

Martens, J. A., Winston, F. (2002): Evidence that Swi/Snf directly represses transcription in S. cerevisiae. *Genes & development* 16, S. 2231–2236.

Mas, G., de Nadal, E., Dechant, R., Rodríguez de La Concepción, M. L., Logie, C., Jimeno-González, S., Chávez, S., Ammerer, G., Posas, F. (2009): Recruitment of a chromatin remodeling complex by the Hog1 MAP kinase to stress genes. *The EMBO Journal* 28, S. 326–336.

Materne, P., Vázquez, E., Sánchez, M., Yague-Sanz, C., Anandhakumar, J., Migeot, V., Antequera, F., Hermand, D. (2016): Histone H2B ubiquitylation represses gametogenesis by opposing RSC-dependent chromatin remodeling at the ste11 master regulator locus. *eLife* 5.

Matsuda, A., Chikashige, Y., Ding, D.-Q., Ohtsuki, C., Mori, C., Asakawa, H., Kimura, H., Haraguchi, T., Hiraoka, Y. (2015): Highly condensed chromatins are formed adjacent to subtelomeric and decondensed silent chromatin in fission yeast. *Nature communications* 6, S. 7753.

Matsuyama, A., Arai, R., Yashiroda, Y., Shirai, A., Kamata, A., Sekido, S., Kobayashi, Y., Hashimoto, A., Hamamoto, M., Hiraoka, Y., Horinouchi, S., Yoshida, M. (2006): ORFeome cloning and global analysis of protein localization in the fission yeast Schizosaccharomyces pombe. *Nature biotechnology* 24, S. 841–847.

Meinel, D. M. and Sträßer, K. (2015): Co-transcriptional mRNP formation is coordinated within a molecular mRNP packaging station in S. cerevisiae. *BioEssays : news and reviews in molecular, cellular and developmental biology* 37, S. 666–677.

Mittal, P., Roberts, C. W. M. (2020): The SWI/SNF complex in cancer - biology, biomarkers and therapy. *Nature reviews. Clinical oncology* 17, S. 435–448.

Mohamed, A. A., Vazquez Nunez, R., Vos, S. M. (2022): Structural advances in transcription elongation. *Current opinion in structural biology* 75, S. 102422.

Monahan, B. J., Villén, J., Marguerat, S., Bähler, J., Gygi, S. P., Winston, F. (2008): Fission yeast SWI/SNF and RSC complexes show compositional and functional differences from budding yeast. *Nature structural & molecular biology* 15, S. 873–880.

Moreira, J. M. and Holmberg, S. (1999): Transcriptional repression of the yeast CHA1 gene requires the chromatin-remodeling complex RSC. *The EMBO Journal* 18, S. 2836–2844.

Musladin, S., Krietenstein, N., Korber, P., Barbaric, Slobodan (2014): The RSC chromatin remodeling complex has a crucial role in the complete remodeler set for yeast PHO5 promoter opening. *Nucleic acids research* 42, S. 4270–4282.

Nair, S. S. and Kumar, R. (2012): Chromatin remodeling in cancer: a gateway to regulate gene transcription. *Molecular oncology* 6, S. 611–619.

Ng, H. H., Robert, F., Young, R. A., Struhl, K. (2002): Genome-wide location and regulated recruitment of the RSC nucleosome-remodeling complex. *Genes & development* 16, S. 806–819.

Nishimura, K., Fukagawa, T., Takisawa, H., Kakimoto, T., Kanemaki, M. (2009): An auxin-based degron system for the rapid depletion of proteins in nonplant cells. *Nature methods* 6, S. 917–922.

Parnell, T. J., Schlichter, A., Wilson, B. G., Cairns, B. R. (2015): The chromatin remodelers RSC and ISW1 display functional and chromatin-based promoter antagonism. *eLife* 4.

Patterton, H. G., Landel, C. C., Landsman, D., Peterson, C. L., Simpson, R. T. (1998): The biochemical and phenotypic characterization of Hho1p, the putative linker histone H1 of Saccharomyces cerevisiae. *The Journal of biological chemistry* 273, S. 7268–7276.

Pérez-Martínez, L., Wagner, T., Luke, B. (2022): Telomere Interacting Proteins and TERRA Regulation. *Frontiers in genetics* 13, S. 872636.

Poli, J., Gasser, S. M.; Papamichos-Chronakis, M. (2017): The INO80 remodeller in transcription, replication and repair. *Philosophical transactions of the Royal Society of London. Series B, Biological sciences* 372.

Qiu, Z. R., Chico, L., Chang, J., Shuman, S., Schwer, B. (2012): Genetic interactions of hypomorphic mutations in the m7G cap-binding pocket of yeast nuclear cap binding complex: an essential role for Cbc2 in meiosis via splicing of MER3 pre-mRNA. *RNA* 18, S. 1996–2011.

Ramachandran, A., Omar, M., Cheslock, P., Schnitzler, G. R. (2003): Linker histone H1 modulates nucleosome remodeling by human SWI/SNF. *The Journal of biological chemistry* 278, S. 48590–48601.

Recht, J., Ratnakumar, K., Wong, L., Laurent, B. C. (2016): Rsc2 protects from telomere fusions caused by loss of Rap1 (not submitted or peer-reviewed).

Reyes, A. A., Marcum, R. D., He, Y. (2021): Structure and Function of Chromatin Remodelers. *Journal of molecular biology* 433, S. 166929.

Rippe, K., Schrader, A., Riede, P., Strohner, R., Lehmann, E., Längst, G. (2007): DNA sequence- and conformation-directed positioning of nucleosomes by chromatin-remodeling complexes. *Proceedings of the National Academy of Sciences of the United States of America* 104, S. 15635–15640.

Roberts, S. M. and Winston, F. (1997): Essential functional interactions of SAGA, a Saccharomyces cerevisiae complex of Spt, Ada, and Gcn5 proteins, with the Snf/Swi and Srb/mediator complexes. *Genetics* 147, S. 451–465.

Rocak, S. and Linder, P. (2004): DEAD-box proteins: the driving forces behind RNA metabolism. *Nature reviews*. Molecular cell biology 5, S. 232–241.

Rosas-Murrieta, N. H., Rojas-Sánchez, G., Reyes-Carmona, S. R., Martínez-Contreras, R. D., Martínez-Montiel, N., Millán-Pérez-Peña, L., Herrera-Camacho, I. P. (2015): Study of Cellular Processes in Higher Eukaryotes Using the Yeast Schizosaccharomyces pombe as a Model. *Microbiology in Agriculture and Human Health: InTech.*

Rosonina, E., Kaneko, S., Manley, J. L. (2006): Terminating the transcript: breaking up is hard to do. *Genes & development* 20, S. 1050–1056.

Sakai, K., Kondo, Y., Fujioka, H., Kamiya, M., Aoki, K., Goto, Y. (2021): Near-infrared imaging in fission yeast using a genetically encoded phycocyanobilin biosynthesis system. *Journal of cell science* 134.

Schubert, H. L., Wittmeyer, J., Kasten, M. M., Hinata, K., Rawling, D. C., Héroux, A., Cairns, B. R., Hill, C. P. (2013): Structure of an actin-related subcomplex of the SWI/SNF chromatin remodeler. *Proceedings of the National Academy of Sciences of the United States of America* 110, S. 3345–3350.

Shim, E. Y., Ma, J.-L., Oum, J.-H., Yanez, Y., Lee, S. E (2005): The yeast chromatin remodeler RSC complex facilitates end joining repair of DNA double-strand breaks. *Molecular and cellular biology* 25, S. 3934–3944.

Shuman, S. (2001): Structure, mechanism, and evolution of the mRNA capping apparatus. Progress in nucleic acid research and molecular biology 66, S. 1–40.

Siam, R., Dolan, W. P., Forsburg, S. L. (2004): Choosing and using Schizosaccharomyces pombe plasmids. *Methods* 33, S. 189–198.

Singleton, M. R., Dillingham, M. S., Wigley, D. B. (2007): Structure and mechanism of helicases and nucleic acid translocases. *Annual review of biochemistry* 76, S. 23–50.

Skene, P. J. and Henikoff, S. (2017): An efficient targeted nuclease strategy for high-resolution mapping of DNA binding sites. *eLife* 6.

Song, Q.-X., Liu, N.-N., Liu, Z.-X., Zhang, Y.-Z., Rety, S., Hou, X.-M., Xi, X.-G. (2023): Nonstructural N- and C-tails of Dbp2 confer the protein full helicase activities. *The Journal of biological chemistry* 299, S. 104592.

Song, X., Xu, R., Sugiyama, T. (2021): Two plasmid modules for introducing the auxin-inducible degron into the fission yeast Schizosaccharomyces pombe by PCR-based gene targeting. *MicroPublication Biology*.

Soutourina, J., Bordas-Le Floch, V., Gendrel, G., Flores, A., Ducrot, C., Dumay-Odelot, H., Soularue, P., Navarro, F., Cairns, B. R., Lefebvre, O., Werner, M. (2006): Rsc4 connects the chromatin remodeler RSC to RNA polymerases. *Molecular and cellular biology* 26, S. 4920–4933.

Stark, H. and Lührmann, R. (2006): Cryo-electron microscopy of spliceosomal components. *Annual review of biophysics and biomolecular* structure 35, S. 435–457.

Sugimoto, A., Iino, Y., Maeda, T., Watanabe, Y., Yamamoto, M. (1991): Schizosaccharomyces pombe ste11+ encodes a transcription factor with an HMG motif that is a critical regulator of sexual development. *Genes & development* 5, S. 1990–1999.

Takayama, Y. and Takahashi, K. (2007): Differential regulation of repeated histone genes during the fission yeast cell cycle. *Nucleic acids research* 35, S. 3223–3237.

Talbert, P. B. and Henikoff, S. (2021): Histone variants at a glance. *Journal of cell science*.

Tamaru, Hisashi (2010): Confining euchromatin/heterochromatin territory: jumonji crosses the line. *Genes & development* 24, S. 1465–1478.

Tan, K. and Wong, K. H. (2019): RNA polymerase II ChIP-seq-a powerful and highly affordable method for studying fungal genomics and physiology. *Biophysical reviews* 11, S. 79–82.

Tang, Y., Wang, J., Lian, Y., Fan, C., Zhang, P., Wu, Y., Li, X., Xiong, F., Li, X., Li, G., Xiong, W., Zeng, Z. (2017): Linking long non-coding RNAs and SWI/SNF complexes to chromatin remodeling in cancer. *Molecular cancer* 16, S. 42.

Tanner, N. K., Cordin, O., Banroques, J., Doère, M., Linder, P. (2003): The Q motif: a newly identified motif in DEAD box helicases may regulate ATP binding and hydrolysis. *Molecular cell* 11, S. 127–138.

Trouche, D., Le Chalony, C., Muchardt, C., Yaniv, M., Kouzarides, T. (1997): RB and hbrm cooperate to repress the activation functions of E2F1. *Proceedings of the National Academy of Sciences of the United States of America* 94, S. 11268–11273.

Tyagi, M., Imam, N., Verma, K., Patel, A. K. (2016): Chromatin remodelers: We are the drivers!! *Nucleus (Austin, Tex.)* 7, S. 388–404.

Ullah, I., Thölken, C., Zhong, Y., John, M., Rossbach, O., Lenz, J., Gößringer, M., Nist, A., Albert, L., Stiewe, T., Hartmann, R., Vázquez, O., Chung, H-R., Mackay, J.l P., Brehm, A. (2022): RNA inhibits dMi-2/CHD4 chromatin binding and nucleosome remodeling. *Cell reports* 39, S. 110895.

VanBelzen, J., Duan, C., Brickner, D. G., Brickner, J. H. (2024): ChEC-seq2: an improved chromatin endogenous cleavage sequencing method and bioinformatic analysis pipeline for mapping in vivo protein-DNA interactions. *NAR genomics and bioinformatics* 6.

VanDemark, A. P., Kasten, M. M., Ferris, E., Heroux, A., Hill, C. P., Cairns, B. R. (2007): Autoregulation of the rsc4 tandem bromodomain by gcn5 acetylation. *Molecular cell* 27, S. 817–828.

Wagner, F. R., Dienemann, C., Wang, H., Stützer, A., Tegunov, D., Urlaub, H., Cramer, P. (2020): Structure of SWI/SNF chromatin remodeller RSC bound to a nucleosome. *Nature* 579, S. 448–451.

Wang, L., Yu, J., Yu, Z., Wang, Q., Li, W., Ren, Y., Chen, Z., He, S., Xu, Y. (2022): Structure of nucleosome-bound human PBAF complex. *Nature communications* 13, S. 7644.

Watson, A. T., Hassell-Hart, S., Spencer, J., Carr, A. M. (2021): Rice (Oryza sativa) TIR1 and 5′adamantyl-IAA Significantly Improve the Auxin-Inducible Degron System in Schizosaccharomyces pombe. *Genes* 12.

Wertman, K. F., Drubin, D. G., Botstein, D. (1992): Systematic mutational analysis of the yeast ACT1 gene. *Genetics* 132, S. 337–350.

White, C. L., Suto, R. K., Luger, K. (2001): Structure of the yeast nucleosome core particle reveals fundamental changes in internucleosome interactions. *The EMBO Journal* 20, S. 5207–5218.

Wittmann, S., Renner, M., Watts, B. R., Adams, O., Huseyin, M., Baejen, C., El Omari, K., Kilchert, C., Heo, D.-H., Kecman, T., Cramer, P., Grimes, J. M., Vasiljeva, L. (2017): The conserved protein Seb1 drives transcription termination by binding RNA polymerase II and nascent RNA. *Nature communications* 8, 14861.

Wolffe, A. P. (2001): Chromatin remodeling: why it is important in cancer. *Oncogene* 20, S. 2988–2990.

Xie, Y. and Ren, Y. (2019): Mechanisms of nuclear mRNA export: A structural perspective. *Traffic* 20, S. 829–840.

Xing, Z., Ma, W. K., Tran, E. J. (2019): The DDX5/Dbp2 subfamily of DEAD-box RNA helicases. *Wiley interdisciplinary reviews. RNA* 10.

Yamada, K., Hirota, K., Mizuno, K.-I., Shibata, T., Ohta, K. (2008): Essential roles of Snf21, a Swi2/Snf2 family chromatin remodeler, in fission yeast mitosis. *Genes & genetic systems* 83, S. 361–372.

Yan, Z., Cui, K., Murray, D. M., Ling, C., Xue, Y., Gerstein, A., Parsons, R., Zhao, K., Wang, W. (2005): PBAF chromatin-remodeling complex requires a novel specificity subunit, BAF200, to regulate expression of selective interferon-responsive genes. *Genes & development* 19, S. 1662–1667.

Yang, Y., Wu, W., Liu, T., Dong, L., Lei, H. (2021): A robust method for protein depletion based on gene editing. *Methods* 194, S. 3–11.

Ye, Y., Wu, H., Chen, K., Clapier, C. R., Verma, N., Zhang, W., Deng, H., Cairns, B. R., Gao, N., Chen, Z. (2019): Structure of the RSC complex bound to the nucleosome. *Science* 366, S. 838–843.

Yesbolatova A., Saito Y., Kitamoto N., Makino-Itou H., Ajima R., Nakano R., Nakaoka H., Fukui K., Gamo K., Tominari Y., Takeuchi H., Saga Y., Hayashi K. I., Kanemaki M. T. (2002): The auxin-inducible degron 2 technology provides sharp degradation control in yeast, mammalian cells, and mice*Nature communications* 11, 5701.

Yu, E. Y., Steinberg-Neifach, O., Dandjinou, A. T., Kang, F., Morrison, A. J., Shen, X., Lue, N. F. (2007): Regulation of telomere structure and functions by subunits of the INO80 chromatin remodeling complex. *Molecular and cellular biology* 27, S. 5639–5649.

Zhang, X.-R., Zhao, L., Suo, F., Gao, Y., Wu, Q., Qi, X., Du, L.-L. (2022): An improved auxin-inducible degron system for fission yeast. *G3* 12.

Zhang, Z., Wang, X., Xin, J., Ding, Z., Liu, S., Fang, Q., Yang, N., Xu, R.-M., Cai, G. (2018): Architecture of SWI/SNF chromatin remodeling complex. *Protein & Cell* 9, S. 1045–1049.

7 Supplements

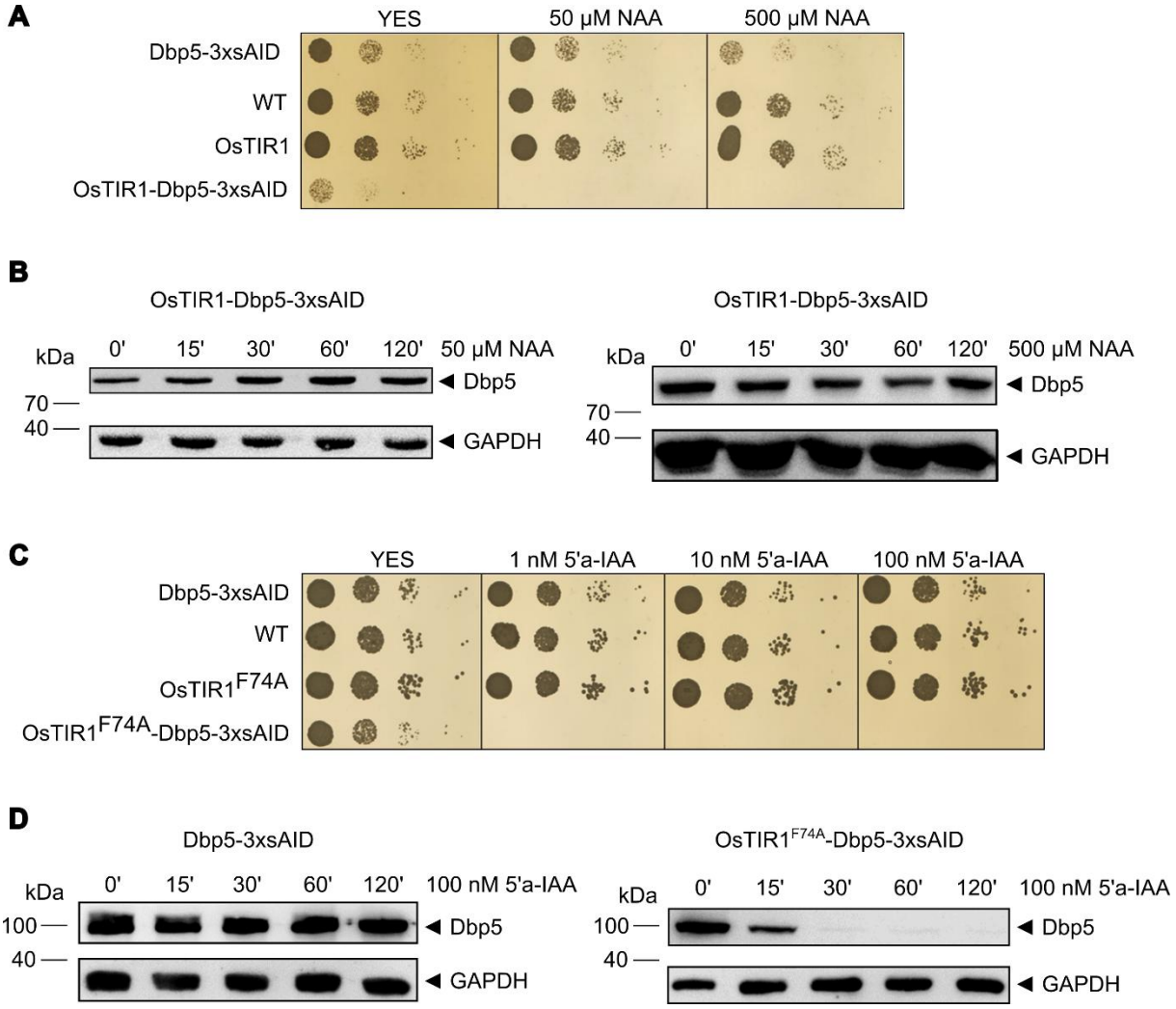

Supplement Figure 1 Successful Dbp5 depletion with 5'a-IAA, but not NAA. A Cells containing Dbp5-3xsAID in the OsTIR1 background were grown in YES overnight, serial dilutions were spotted on YES plates containing different concentrations of NAA and incubated at 30 °C. The depletion strain shows a growth defect after NAA addition. **B** Lysates of an NAA time course for OsTIR1-Dbp5-3xsAID were analyzed by SDS-PAGE and Western blot against AID and GAPDH as a loading control. The addition of NAA does not affect Dbp5 levels. **C** Cells containing Dbp5-3xsAID in the modified OsTIR1^{F74A} background were grown in YES overnight, serial dilutions were spotted on YES plates containing different concentrations of 5'a-IAA and incubated at 30 °C. The depletion strain shows a growth defect in the presence of 5'a-IAA. **D** Lysates of a 5'a-IAA time course for OsTIR1^{F74A}-Dbp5-3xsAID were analyzed by SDS-PAGE and Western blot against AID and GAPDH as a loading control. The addition of 100 nM 5'a-IAA leads to reduced Dbp5 levels within 15 min.

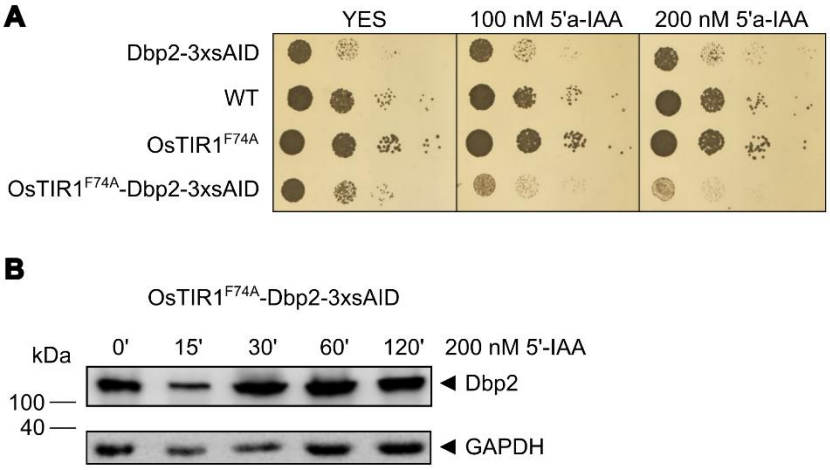

Supplement Figure 2 No evidence of Dbp2 depletion following 5'a-IAA treatment. A Cells containing Dbp2-3xsAID in the OsTIR1^{F74A} background were grown overnight, serial dilutions were spotted on YES plates containing different concentrations of 5'a-IAA and incubated at 30 °C. Strains that carry the Dbp2-3xsAID tag in either the wild-type or the OsTIR1^{F74A} background have a growth defect even in the absence of 5'a-IAA. **B** Lysates of a 5'a-IAA time course for OsTIR1^{F74A}-Dbp2-3xsAID were analyzed by SDS-PAGE and Western blot against AID and GAPDH as a loading control. Adding 200 nM 5'a-IAA has no effect on Dbp2-3xsAID levels after up to 2h.

List of figures

List of abbreviations

A	adenine
APS	ammonium persulfate
ATP	adenosine-5’-triphosphate
BSA	bovine serum albumin
C	cytosine
DAPI	4',6-Diamidino-2-phenylindole dihydrochloride
DMSO	dimethylsulfoxide
DNA	desoxyribonucleic acid
dNTPs	desoxynucleotide triphosphates
DTT	dithiothreitol
ECL	enhanced chemoluminescence
E. coli	*Escherichia coli*
EDTA	ethylenediaminetetraacetic acid
FACT	facilitates chromatin transcription
FISH	fluorescent in situ hybridization
G	guanine
g	gravitational acceleration constant
GFP	green fluorescent protein
HEPES	N-[2-Hydroxyethyl]piperazine-N‘-[2-ethanesulfonic acid]
HRP	horseradish peroxidase
Ino80	inositol requiring 80
IP	immunoprecipitation
kDa	kilodalton

LB	lysogeny broth
Mb	mega base pairs
mRNA	messenger RNA
mRNP	messenger RNA/protein containing complex
NDR	nucleosome depleted region
OD_{600}	optical density at 600 nm
ORF	open reading frame
PBS	phosphate-buffered saline
PCR	polymerase chain reaction
PMSF	phenylmethylsulfonylfluoride
qPCR	quantitative PCR
RNase	RNA-hydrolyzing enzyme
RSC	Remodeling the Structure of Chromatin
RT	room temperature
S. cerevisiae	*Saccharomyces cerevisiae*
SDS	sodium dodecyl sulfate
S. pombe	*Schizosaccharomyces pombe*
T	thymine
TBS	Tris-buffered saline
TEMED	N,N,N‘,N‘-Tetramethylethylenediamin
Tris	Tris(hydroxymethylaminomethane)
WT	wild-type
5'a-IAA	5'adamantyl-indole-3-acetic acid

Eidesstattliche Erklärung

Ich erkläre: Ich habe die vorgelegte Dissertation selbstständig und ohne unerlaubte fremde Hilfe und nur mit den Hilfen angefertigt, die ich in der Dissertation angegeben habe. Alle Textstellen, die wörtlich oder sinngemäß aus veröffentlichten Schriften entnommen sind, und alle Angaben, die auf mündlichen Auskünften beruhen, sind als solche kenntlich gemacht. Ich stimme einer evtl. Überprüfung meiner Dissertation durch eine Antiplagiat-Software zu. Bei den von mir durchgeführten und in der Dissertation erwähnten Untersuchungen habe ich die Grundsätze guter wissenschaftlicher Praxis, wie sie in der „Satzung der Justus-Liebig-Universität Gießen zur Sicherung guter wissenschaftlicher Praxis“ niedergelegt sind, eingehalten.

Angaben zu auf künstlicher Intelligenz (KI) basierender Hilfen wie ChatGPT oder SchulKI von OpenAI oder Gemini von Google zur Erstellung meiner Dissertation (Zutreffendes angekreuzt):

☐ Ich habe bei der Erstellung dieses Textes kein KI-Tool verwendet.

☒ Ich habe ein KI-Tool in den folgenden Bereichen eingesetzt (Mehrfachnennungen möglich):

- ☐ Ideen finden, meine Kreativität anregen
- ☐ Verstehen von Konzepten, Recherche von Fakten und Definitionen
- ☒ Optimierung eines von mir verfassten Textes
- ☐ Erstellen ganzer Textpassagen nach meinen Vorgaben

Folgende KI-Tools habe ich verwendet, damit aufgeführte Teile meines Textes von dem Tool wie folgt profitiert haben:

Zur Verbesserung von Lesbarkeit, Grammatik und Rechtschreibung wurden die KI-Tools „ChatGPT“ und „Grammarly“ eingesetzt. Alle Formulierungen der KI wurden anschließend kritisch geprüft, überarbeitet und in den wissenschaftlichen Kontext der Arbeit integriert.

Gießen, den: ..... Unterschrift: .....……....

(Vorname, Nachname)

Danksagung

Nach intensiven Jahren der Forschung ist nun der Moment gekommen, zurückzublicken. Die Promotion war eine prägende Zeit mit Erfolgen und Herausforderungen, die mich persönlich und fachlich weitergebracht haben. Mein aufrichtiger Dank gilt allen, die mich auf diesem Weg unterstützt haben.

Zunächst möchte ich mich ganz herzlich bei **Dr. Cornelia Kilchert** bedanken, die mir die Möglichkeit gegeben hat, dieses spannende und herausfordernde Thema in ihrem Labor zu bearbeiten. Ich bin dankbar für das Vertrauen, die fachliche Unterstützung, die wertvollen Anregungen und die stets offenen und konstruktiven Diskussionen, die wesentlich zum Erfolg dieser Arbeit beigetragen haben.

Mein besonderer Dank gilt außerdem meiner Zweitgutachterin **Apl. Prof. Dr. Elena Evguenieva-Hackenberg** für die Begutachtung meiner Arbeit sowie **Prof. Dr. Reinhard Dammann** und **Prof. Dr. Kai Thormann** für die investierte Zeit.

Ich danke **Prof. Dr. Andreas Diepold** (ehemals MPI Marburg) herzlich für die Möglichkeit, die FRAP-Experimente in seinem Labor durchzuführen, sowie für seine fachliche Unterstützung dabei.

Ein besonderer Dank gilt auch meiner **Arbeitsgruppe**, insbesondere Ebru, Philip, Nadine, Jan, Melanie und Silke. Die kollegiale Atmosphäre, die gegenseitige Hilfsbereitschaft und die gemeinsamen Diskussionen haben nicht nur zum Gelingen des Projekts beigetragen, sondern auch den Alltag im Labor bereichert. Darüber hinaus möchte ich auch den gesamten Mitarbeitern der Biochemie für die angenehme Arbeitsatmosphäre und die fachliche Unterstützung danken.

Ebenso möchte ich meinen **Freundinnen und Freunden** danken**.** Marie, Fabi, Nicole, Michel, Tessa und Lena danke ich dafür, dass ich mit ihnen die Studienzeit teilen durfte. Die gemeinsamen Stunden im Hörsaal und auch der Spaß neben dem Studium haben mir gezeigt, dass Wissenschaft nicht nur Arbeit, sondern auch Gemeinschaft bedeutet. Vielen Dank auch an Kirsten und Josef für die jahrelange Freundschaft und all die schönen Momente, die wir gemeinsam erleben.

Mein größter Dank gilt **meiner Familie**, insbesondere meinen Eltern und meinen Großeltern. Ohne eure bedingungslose Unterstützung, euren Zuspruch und euer Vertrauen hätte ich diesen Weg nicht so gehen können. Darüber hinaus danke ich **Tom**, der mich mit viel Geduld, Verständnis und tatkräftiger Unterstützung durch alle Höhen und Tiefen dieser Zeit begleitet hat. Ihr habt mir den Rückhalt gegeben, den ich gebraucht habe, um diese Arbeit zu Ende zu bringen.